Engineering Library PRR

Journal of Research

of the

National Bureau of Standards

JULY 1949

VOLUME 43 NUMBER 1

PERIODICALS OF THE NATIONAL BUREAU OF STANDARDS

Journal of Research

The National Bureau of Standards is the principal agency of the Federal Government for fundamental research in physics, chemistry, and engineering. It has the custody of the national standards of physical measurement in terms of which all working standards in research laboratories and industry are calibrated, and carries on necessary research leading to improvement in such standards and methods of measurement. It also has a general responsibility for basic research in physics, chemistry, and engineering, and for development of improved methods for testing materials and equipment. It determines physical constants and properties of materials, tests and calibrates standard measuring apparatus and reference standards, and studies technical processes. The results of the Bureau's research and investigations are published in the JOURNAL OF RESEARCH.

Research Papers

Reprints of individual articles appearing in the JOURNAL OF RESEARCH. They are made available to serve the needs of research workers, technical groups, and others for the separate papers relating to the special subjects in which they are interested.

Technical News Bulletin

Contains short but complete summaries of research, development, and testing in progress at the Bureau, accounts of the Bureau's national and international activities, scientific and technical announcements of new plans and programs, and a list of publications by members of the staff. It is a prompt and reliable source of official information of value to those who desire to keep in touch with the general activities of the Bureau.

Basic Radio Propagation Predictions

The CRPL-D series, Basic Radio Propagation Predictions, is issued as a monthly publication for those concerned with radio communication in determining the best sky-wave frequencies over any path at any time of day for average conditions for the month of prediction, which is made 3 months in advance. Charts of extraordinary-wave critical frequency for the F2 layer, of maximum usable frequency for a transmission distance of 4,000 km, and of percentage of time occurrence for transmission by sporadic E in excess of 15 Mc, for a distance of 2,000 km, are included.

ANNUAL SUBSCRIPTION Send order, with remittance, to Superintendent of Documents, U. S. Government Printing Office, Washington 25, D. C.	United States, Canada, Cuba, Mexico, Newfoundland, Republic of Panama	Other countries
JOURNAL OF RESEARCH of the National Bureau of Standards: 12 monthly issues (2 volumes), paper cover	$4.50	$5.50
Bound volume (½ year, 1 volume), blue buckram	3.00	3.50
RESEARCH PAPERS	(1)	(1)
TECHNICAL NEWS BULLETIN, 12 monthly issues	1.00	1.50
BASIC RADIO PROPAGATION PREDICTIONS, 12 monthly issues	1.00	1.25

The prices of the separate Research Papers appearing in this JOURNAL are given in the Contents. $1.00 or more copies of any separate are reduced, a discount of 25 percent is allowed. Please write direct to Superintendent of Documents, U. S. Government Printing Office, Washington 25, D. C. Give full name and address (number and street, city, State, and postal zone) and remittance (check, postal money order, or coupons) sufficient to cover the number of copies to be printed for sale. Research Papers are not printed here whenever and usually no more reprints exist than what are sold from the first and only printing by subscription.

The printing of this publication has been approved by the Director of the Bureau of the Budget, April 28, 1947

U. S. DEPARTMENT OF COMMERCE
Charles Sawyer, Secretary
NATIONAL BUREAU OF STANDARDS
E. U. Condon, Director

JULY 1949
VOLUME • 43
NUMBER 1

JOURNAL OF RESEARCH

of the

NATIONAL BUREAU OF STANDARDS

Contents

RP — Page

2000. Volume changes observed in small concrete cylinders during freezing and thawing with a mercury displacement dilatometer. Rudolph C. Valore. (Price 20 cents) 1

2001. Electrophoresis of modified collagen. James M. Cassel and Joseph R. Kanagy. (Price 10 cents) 29

2002. Infrared absorption spectra of cyclohydrocarbons. Earle K. Plyler and Nicolo Acquista. (Price 10 cents) 37

2003. Low-temperature performance of radiosonde electric hygrometer elements. Arnold Wexler. (Price 10 cents) 49

2004. Refractive index of natural rubber for different wavelengths. Lawrence A. Wood and Leroy W. Tilton (Price 10 cents) 57

2005. Metastable transitions in mass spectra of hydrocarbons. Evelyn G. Bloom, Fred L. Mohler, C. Edward Wise, and Edmunds J. Wells. (Price 10 cents) 65

2006. Impedance characteristics of some experimental broad-band antennas for vertical incidence ionosphere sounding. H. N. Cones. (Price 10 cents) 71

2007. Formulas for the percentage points of the distribution of the arithmetic mean in random samples from certain symmetrical universes. Uttam Chand. (Price 10 cents) 79

2008. Refractive indices of thallium bromide-iodide crystals for visible and infrared radiant energy. Leroy W. Tilton, Earle K. Plyler, and Robert E. Stephens. (Price 10 cents) 81

2009. Fundamental aspects of the reaction of oxygen with carbon adsorbents. William V. Loebenstein and Neil L. Pennington. (Price 10 cents) 87

For sale by the Superintendent of Documents, U. S. Government Printing Office, Washington 25, D. C. - Price 60¢
$4.50 per year on subscription

UNITED STATES GOVERNMENT PRINTING OFFICE, WASHINGTON : 1949

U. S. Department of Commerce
National Bureau of Standards

Research Paper RP2000
Volume 43, July 1949

Part of the Journal of Research of the National Bureau of Standards

Volume Changes Observed in Small Concrete Cylinders During Freezing and Thawing Using a Mercury Displacement Dilatometer

By Rudolph C. Valor, Jr.

A mercury-displacement dilatometer is described for continuously determining the changes in bulk volume of small concrete cylinders during freezing and thawing. Various types of freezing and thawing cycles were employed in which the 40° to −20° F range was covered at various rates. The results presented are representative volume-temperature relationships obtained for specimens tested in air-dry, partially saturated, and "vacuum-saturated" moisture conditions. Relationships for air-dry specimens yielded uniform thermal-expansion data, but those for partially saturated specimens showed departures from uniformity that are ascribed to the freezing and thawing of water in the pore structures of the specimens. Vacuum-saturated specimens showed much larger departures and failed as a result of a single cycle of freezing and thawing.

I. Introduction

Moist, porous building materials subjected to repeated alternate cycles of freezing and thawing usually show a progressive deterioration manifested by a softening, scaling, spalling, cracking, or loss of strength or elasticity. This deterioration has generally been ascribed to a repeated straining or distending of the material that may occur as a consequence of the conversion of water to ice within the pore system of the material.

The fact that water increases in volume as it freezes (approximately 9% at 32° F) has led various investigators to employ a dilatometric or displacement method for studying the volume–freezing-point relationships for a number of materials. The method has been employed by Anderson and Edlefson [1] [1] and others [2] in studies of soils, by Thomas [3] in England in a comprehensive study of the frost resistance of building stone, and by Powers and Brownyard [4] in a study of saturated, hardened portland cement pastes.

The present work is part of an investigation of the physical reactions occurring in concrete specimens of different degrees of moisture saturation during freezing and thawing. It was believed that the measurement of transient and residual changes in bulk volume (i. e., volume of solids plus volume of pores) occurring in specimens during, and as a result of, freezing and thawing cycles of various types might provide some desired information. To attain this end, the first objective was the development of a satisfactory dilatometer.

II. Scope

The initial problem in the development of a satisfactory dilatometer involved the choice of a suitable displacement medium. Liquids in the hydrocarbon group, such as toluene and kerosine, had been widely used as displacement media in previous dilatometer work and were found to be satisfactory where the detection of freezing points and measurement of volume changes in fully saturated samples were required. Thomas [3], however, using ligroine (petroleum ether), found the dilatometer unreliable for measuring changes in bulk volume in partially saturated specimens of building stone during freezing and thawing. It appeared that the physical properties of petroleum ether were such that the liquid readily entered, to an undetermined extent, those pore spaces not

[1] Figures in brackets indicate the literature references at the end of this paper.

filled with water. Thomas made his most satisfactory determinations by an optical-lever linear extensometer method.

For the present work, mercury was chosen as the displacement medium, because of several advantages it appeared to show over liquids in the hydrocarbon group within the desired working temperature range, 40° to −20° F. These advantages included (1) a uniform and relatively low coefficient of thermal expansion, (2) a relatively high coefficient of thermal conductivity, (3) a low specific heat, and (4) the nonwetting property. The high density of mercury allowed a high degree of precision in the various operations preparatory to and following the dilatometer tests, since very small volumes of mercury could be accurately determined by weighing.

Mercury, however, was found to penetrate to a slight but undesirable extent the surfaces of dry or partially saturated concrete specimens. It was found necessary to treat the specimens in such a way as to render the surfaces impermeable to mercury while not interfering with the free passage of air, water, and water vapor during drying and other curing operations. This was accomplished by rubbing a cement-fine-sand mortar into the surface of each specimen, effectively "sealing" the larger pore openings and surface voids. The weight of each specimen was increased by less than 0.5 percent by this treatment.

Of the many variables in specimen condition thought to affect the reaction to freezing and thawing, the moisture condition was chosen for greatest emphasis. Specimens were air-dried and "vacuum-saturated" before the testing to provide two extremes in moisture condition; and various curing procedures were employed to provide specimens in the more normal condition of partial saturation. The specimens did not have access to additional moisture during testing in the dilatometers, since they were completely immersed in mercury. Thus the "buildup" in saturation described by Kreuger [5] and observed by Tucker, Walker, and Swenson [6] did not occur and could not be studied.

The specimens were small cylinders cast from concrete of one-mix design (plain and modified by the addition of an air-entraining agent) made with one brand of normal portland cement and one type of aggregate.

Comparison of results obtained in laboratories using a wide variety of techniques in performing freezing and thawing testing of concrete indicated the rate of temperature change as a most significant variable. For this reason variations were made in rates of cooling and heating during the freezing and thawing cycles, and also in the length of periods at constant temperature during and between cycles. Volume-temperature relationships for the various types of cycles were obtained within a single temperature range, 40° to −20° F, which was sufficiently broad to permit the use of rather effective extremes in the rates of temperature change.

Most of the specimens tested were subjected to freezing and thawing cycles of several kinds. This was done in order that a comparison of the effects of various test procedures could be made upon a single specimen unobscured by the unpredictable dissimilarities that often occur in "duplicate" specimens.

In addition to the volume-temperature relationships, supplementary determinations were made for each specimen. The degree of saturation of a specimen was expressed as a percentage of "vacuum-saturation," based upon the weight of the specimen when oven dried, inasmuch as other means for evaluating the moisture condition were found to be less reliable. The effects of the various freezing and thawing treatments were evaluated in terms of changes in Young's modulus of elasticity (dynamic, flexural). The specimen could not conveniently be removed from the dilatometer during the progress of a cycle, or between cycles, so that normally only the total effect of a number of cycles was ascertained. This was done by obtaining the difference in Young's modulus, determined before and after the dilatometer tests.

Because of the exploratory nature of the work, the results obtained are not amenable to statistical treatment. Results presented are confined largely to figures portraying the volume-temperature behavior for approximately one-fourth of the more than 50 specimens tested. Nevertheless, certain patterns of behavior have been observed and are discussed. Such conclusions as may be implied in the discussion of results, however, apply only to the specimens tested in which the effects of brand of portland cement and type of aggregate were not included among the variables studied.

III. Dilatometers and Equipment

1. Construction of the Dilatometers

A drawing of the dilatometer is shown in figure 1. The vertical cylindrical chamber was constructed from 0.15-in.-thick seamless mild-steel tubing 2.05 in. in internal diameter and 7.25 in. in height. The top and bottom were formed from 1-in. steel plate. The bottom plate was machined to fit the tubing and then welded into place, as shown in the drawing. The steel cover was machined to fit the top of the cylinder, and the inner surface of the cover was funnel-shaped to facilitate the removal of air entrapped in the dilatometer during the liquid filling process. The apex of the inverted funnel opened into a $\frac{5}{8}$-in.-outside-diameter threaded steel tube, to the top end of which a glass burette assembly was attached. The cover was attached to the cylinder by means of four $\frac{1}{4}$-in. bolts, which extended through the bottom plate, and was secured by wing nuts. A compressible organic plastic gasket 0.002-in. thick was placed between the top of the cylinder and the cover to prevent the loss of mercury.

2. Burettes

Measuring pipettes were used as dilatometer burettes. The pipette tips were broken off and the straight-bore stems were cemented into short lengths of threaded steel tubing to form interchangeable, detachable burette assemblies. A thin, hard-rubber gasket separated the tubing at the bottom end of the burette from the tubing that formed a part of the dilatometer cover, as shown in figure 1. One-, two-, and five-ml-capacity pipettes were used. For most tests, the 1-ml size was satisfactory, but for tests of vacuum-saturated specimens it was necessary to use the 5-ml size.

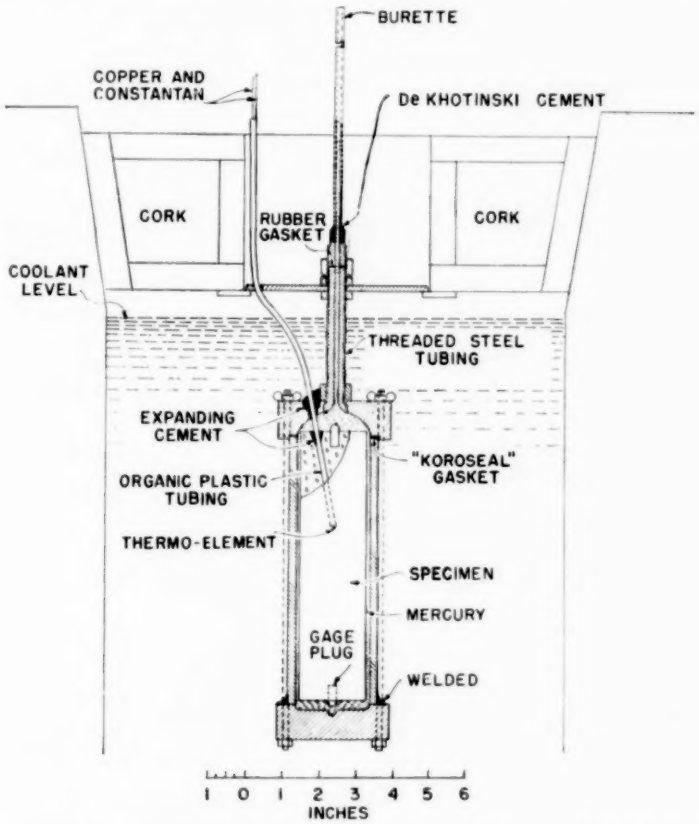

FIGURE 1. *Vertical section of mercury-displacement dilatometer containing a cylindrical concrete test specimen.*

The pipettes were calibrated by the Metrology Division of the National Bureau of Standards. Only those pipettes for which the mean error of marking was less than 1 percent were used. Readings were estimated to 0.001 ml for the 1- and 2-ml pipettes. Therefore, changes in volume as small as 0.0003 percent could be discerned for specimens with bulk volumes ranging between 335 and 340 ml.

3. Calibration of the Dilatometer Assemblies

The dilatometer calibration consisted in obtaining a value for the thermal coefficient of volume change for the dilatometer chamber. This value was calculated as the volume change per degree per milliliter capacity. The capacity was the volume at 40° F when the dilatometer was filled to the chosen burette level. The use of a solid steel cylinder having dimensions similar to those of the concrete specimens to be described in a following section facilitated the determination.

The calibration was performed in several steps. First, the thermal coefficient of linear expansion for the steel calibration "specimen" was computed from thermal extensions and contractions, as observed by means of a Tuckerman optical-lever extensometer and autocollimator [7].[2] The specimen was placed in a controlled temperature, thermally insulated air chamber, and gage readings were observed when the system attained temperature equilibrium. The gages used were 6 in. long and were calibrated relative to a standard steel bar for which the thermal coefficient of linear expansion had been determined by the Metrology Division. The gage readings represented changes in length of the test objects relative to changes in length of the gages. The test chamber was taken through two complete cycles of temperature change so that four determinations were made. The mean value obtained for the thermal coefficient of linear expansion for the steel specimen was 6.3×10^{-6} per degree Fahrenheit, as shown in table 1. This value was multiplied by 3 to obtain the coefficient of cubical expansion.

TABLE 1. *Thermal coefficient of linear expansion of steel calibration specimen, determined by means of Tuckerman optical lever extensometer*

Temperature		Thermal coefficient of linear expansion per degree Fahrenheit
Initial	Final	
° F	° F	
66.9	22.6	6.33×10^{-6}
22.6	70.2	6.25
70.2	30.2	6.25
30.2	68.0	6.28
		Mean.....6.3×10^{-6}

The second step in the calibration consisted in determining the burette reading change per degree Fahrenheit when the dilatometer contained the steel specimen and mercury. To obtain these data, the loaded dilatometer was immersed suc-

[2] A complete description of the apparatus is given in The thermal expansion of clay building bricks, by C. W. Ross [8].

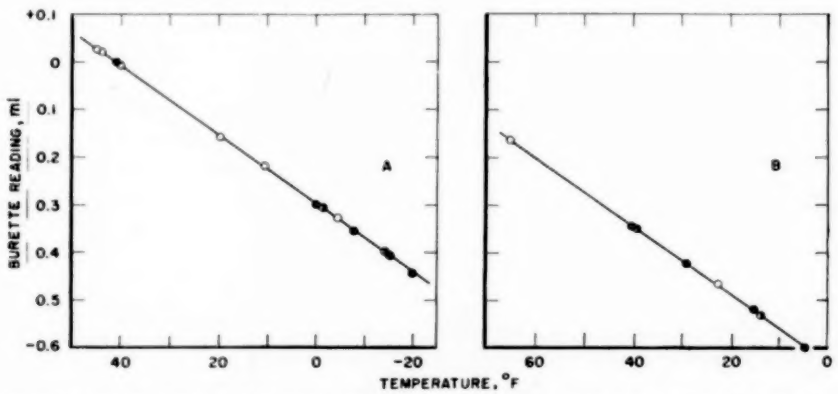

FIGURE 2. *Changes in burette reading with temperature for dilatometer 1 containing a steel calibration specimen surrounded by mercury.*

Two burette sizes were used A, 2-ml burette; B, 1-ml burette; ●, cooling; ○, heating.

cessively in a number of constant-temperature baths between 40° and −20° F and held at each temperature until equilibrium was reached. Figure 2, A, shows the burette readings plotted against temperature for one of the dilatometers with a 2-ml burette attachment. In figure 2, B, similar data are shown for the same dilatometer with a 1-ml burette and for a somewhat different temperature range. Values for the slopes were computed by the method of least squares and represent the burette reading changes per degree Fahrenheit. The total volume change per degree for the dilatometer chamber was simply the burette reading change per degree subtracted from the computed volume change per degree for the steel specimen and the mercury. The value used for the thermal coefficient of cubical expansion of mercury, 100.7×10^{-6} per degree Fahrenheit was derived from data on the specific volume over the range +40° to −20° F [9].

The following is a sample calculation for the thermal coefficient of volume change per degree Fahrenheit per milliliter capacity of dilatometer 1 with 2-ml burette attachment:

Volume of steel specimen at 40° F	341.0 ml
Volume of mercury in dilatometer at 40° F	87.9 ml
Capacity of dilatometer chamber at 40° F	428.9 ml
Volume change of steel specimen per degree Fahrenheit equals $341.0\times6.3\times10^{-6}\times3$	0.0064 ml
Volume change of mercury per degree Fahrenheit equals $87.9\times100.7\times10^{-6}$	.0089 ml
Total volume change, steel specimen and mercury, per degree Fahrenheit	.0153 ml
Burette reading change per degree Fahrenheit	.0072 ml
Volume change of dilatometer chamber, per degree Fahrenheit	.0081 ml
Volume change of dilatometer chamber per degree Fahrenheit per milliliter capacity	19.0×10^{-6}ml
Thermal coefficient of linear expansion for steel dilatometer chamber (computed as one-third of volume change per degree Fahrenheit per milliliter capacity)	6.3×10^{-6}

The results of the determination of the coefficients of cubical and linear expansion for the chamber of dilatometer 1 are shown in table 2.

To provide an approximate but independent check on the calibration of the dilatometer, the thermal coefficient of linear expansion for the cylindrical portion alone of dilatometer 1 was determined by means of the optical lever extensometer [7], previously mentioned. These results are shown in table 3. The mean value for the thermal coefficient of linear expansion, 6.45×10^{-6} per degree Fahrenheit, obtained by the extensometer method was less than 3 percent higher than the mean value, 6.3×10^{-6} per degree Fahrenheit, obtained by the volumetric method. The value accepted for the thermal coefficient of volume change for the entire dilatometer chamber was the one calculated from the volumetric determinations, as it was obtained under conditions most nearly simulating the method actually used for testing the concrete specimens.

TABLE 2. *Thermal coefficients of cubical and linear expansion for dilatometer chamber 1.*

Burette capacity	Slope of line of regression [1] (milliliters per degree Fahrenheit)	Thermal coefficient of expansion per degree Fahrenheit	
		Cubical [2]	Linear [3]
ml			
2	−0.00716	19.0×10^{-6}	6.3×10^{-6}
2	−.00724	18.6	6.2
1	−.00713	18.8	6.3
	Mean	18.8×10^{-6}	6.3×10^{-6}

[1] Computed by the method of least squares; 2 of the 3 determinations are shown in figure 2.
[2] Volume change of dilatometer chamber per milliliter of capacity per degree Fahrenheit.
[3] Computed as one-third of cubical coefficient.

TABLE 3. *Thermal coefficient of linear expansion for the cylindrical portion of dilatometer (No. 1), as determined by means of the Tuckerman optical-lever extensometer*

Temperature		Thermal coefficient of linear expansion per degree Fahrenheit
Initial	Final	
° F	° F	
66.9	22.6	6.45×10^{-6}
22.6	70.2	6.45
70.2	30.2	6.46
30.2	68.0	6.44
		Mean... 6.45×10^{-6}

The thermal coefficient of volume change for a second dilatometer was also determined by the methods outlined above. The calibration gave a mean value identical with that obtained for the first dilatometer. The volume change of a concrete specimen tested in a dilatometer was equal to the burette reading change, plus the volume

change of the dilatometer chamber, minus the volume change of the mercury.

4. Refrigerated Baths

Concrete freezing-and-thawing test equipment, in which the coolant was an ethylene glycol-water mixture, was adapted to accommodate the dilatometers. The dilatometers were suspended from wells in the covers, so that the chamber of the dilatometer was completely immersed in the coolant. The burettes extended some 4 or 5 in. above the top of the well. Since all tests and the volumetric calibration of the dilatometers were made with the dilatometers suspended identically, burette stem corrections were obviated.

Five controlled temperature baths were available for the tests. The temperature of the baths was generally controlled to within 1 deg F of the desired temperature within the 40° to −20° F range. In addition, the temperature of each bath could be varied within this range in steps as small as 2 deg F. In operation one bath was maintained continuously at 40° F ± 1° F and another near −20° F. In a third bath the temperature could be lowered stepwise from 40° to −20° F in a minimum time of about 8 hrs, and the temperature could be increased in this range at a comparable rate. More rapid cooling or heating rates were obtained by transferring dilatometers to the appropriate bath.

5. Temperature Measurements

All temperature measurements were made by using calibrated copper-constantan thermocouples. For the purposes of this study, equilibrium conditions were assumed to exist when the temperature difference between the center of the specimen and the bath was 0.5 deg F or less.

IV. Preparation of Test Specimens

1. Materials

A portland cement was used that complied with the requirements of Federal Specification SS–C–191b [10]. The chemical analysis and calculated compound composition of this cement are shown in table 4.

Siliceous sand and ¾-in. gravel of Potomac River origin were used as aggregate. The percentage absorption by weight was 1.0 for the sand and 1.3 for the gravel. The sieve analyses for these materials, made with United States Standard Sieves, are listed in table 5.

TABLE 4. *Chemical analysis and calculated compound composition of the portland cement*

Component	Percentage	Component	Percentage
SiO_2	22.0	Ignition loss	0.8
Fe_2O_3	2.5	Insoluble residue	.1
Al_2O_3	5.7	$CHCl_3$ solubility	.004
CaO	64.7		
MgO	1.6	$3CaO.Al_2O_3$	11
SO_3	1.7	$2\ CaO.SiO_2$	26
K_2O	.72	$3CaO.SiO_2$	49
Na_2O	.18		

TABLE 5. *Sieve analyses of aggregates*

Sand			Gravel	
Sieve	Percentage retained	Cumulative percentage retained	Sieve	Percentage retained
No. 8	15.8	15.8	¾ inch	4.5
No. 16	17.8	33.6	No. 4	95.5
No. 30	31.0	64.6	.....	.....
No. 50	23.1	87.7	.....	.....
No. 100	9.8	97.5	.....	.....
Pan	2.5	.....	.....	.....
Total	100.0	[a] 299.2	Total	100.0

[a] This value gives a fineness modulus of 2.99.

2. Fabrication of the Test Specimens

Specimens were cast from a concrete mix designed to a cement factor of six bags per cubic yard of concrete. Half of the specimens were prepared from a plain mix and half from a mix modified by the addition of an air-entraining agent. A slight adjustment in the proportion of sand was required in the modified mix to maintain the cement factor constant. The basic mix proportions were, by weight, 1 cement: 2.8 sand: 2.5 gravel, on the basis of a saturated, surface-dry condition for the aggregates. Actually, dry aggregates were used and corrections for water absorption were made in determining batch weights. The quantity of mixing water was adjusted for each batch to give a consistency on the flow table within the range of 100 to 115 percent, as determined in accordance with Federal Specification SS–C–158b [11]. A water-cement weight ratio of 0.56 produced the desired flow in the plain mixes,

whereas 0.53 was sufficient for the aerated batches, that contained 0.01 percent by weight of cement of a proprietary resin added in neutralized solution.

The total weight of each batch of materials was approximately 2,800 g and was sufficient for casting three specimens. Batches were hand-mixed for 3 min, allowed to stand for 2 min, and remixed for a 2-min period.

Air in the plastic mixes was determined gravimetrically by the method described in Federal Specification SS–C–158b, [11]. The plain mixes contained 2.5 ±0.5 percent of air, by volume, which is a relatively large amount for a nonaerated mix, and the aerated mixes contained 5.3 ±0.6 percent of air. The plain mix appeared coarse and harsh in contrast to the plasticity and cohesiveness of the aerated mix, as judged by the relative ease of mixing.

Immediately following the mixing, the test specimens (1.92 ±0.01 in. in diameter and 7.20 ±0.10 in. in height) were molded. The cylindrical molds were filled vertically in three layers, and each layer was rodded with a bullet-nosed ¼-in. diameter metal rod. The bottom and top ends of the molds were closed with wooden plugs; gage points were held in place in holes in the centers of the plugs. (The gage points were available for use in determining residual length changes; only in the case of the vacuum saturated specimens were these data significant). The bottom plug also held a ⅛-in. diameter metal rod, one end of which extended 2½ in. into the specimen to a point at the center of the circular cross section. A cellophane tape sleeve was fitted on the metal rod so that when the specimen was removed from the mold the rod could be easily extracted, leaving a hole for the insertion of the thermoelement (figs. 1 and 3). The top plus was fitted into the mold after most of the bleeding had occurred. The specimens remained in the molds for 24 hr before removal.

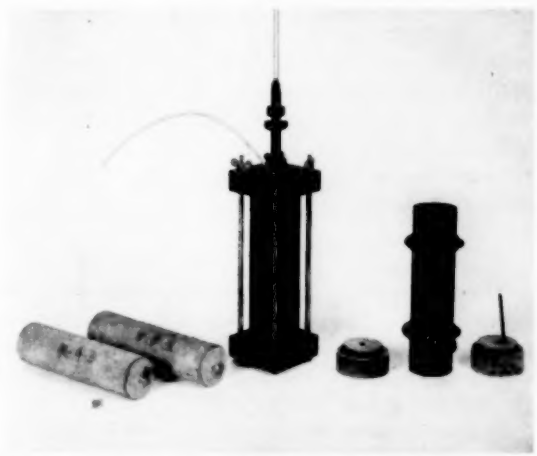

FIGURE 3. *Typical concrete test specimens, mercury-displacement dilatometer, and specimen mold with top and bottom plugs.*

3. Surface Treatment of the Specimens

Preliminary experiments indicated the necessity for surface treatment of the specimen to prevent the penetration of mercury during the testing. A 1:1 cement-sand mortar of putty-like consistency was rubbed into the surface of each specimen upon its removal from the mold, in such a way as to fill all surface voids and larger pores. The mortar was made with the same cement used for the specimen and with sand passing a No. 50 sieve.

All specimens were subsequently stored in a fog room, maintained at 70° ±2° F and between 95- and 100-percent relative humidity, until they were 28 days old, after which the curing procedures varied.

V. Procedures

1. Preparation for the Dilatometer Tests

The copper-constantan thermoelement and lead wires were sealed into the ⅛-in.-outside-diameter organic plastic tubing so that the element barely protruded from one end of the tubing. The element and end of the tubing were coated with an organic plastic cement; after the cement had dried, the unit was inserted into the hole provided in the specimen so that the coated thermoelement was in contact with the concrete. The unit was sealed in place by tamping "iron" cement paste of dry consistency between the flared opening at the top of the specimen and the plastic tubing (fig. 1). The cement was of a quick-setting, expanding type and constricted the tubing when set.

The specimen was placed in the dilatometer after being quickly wiped with a dry cloth when necessary, and the cover was then bolted securely to the dilatometer chamber. The dilatometer was next filled with sufficient mercury to cover the specimen.

It was found that the entrapping of air upon the

839743—49——2

inner walls of the dilatometer and upon the surface of the specimen could be largely avoided by introducing the mercury into the dilatometer in small drops. Therefore, the mercury was poured into the dilatometer through a fine capillary that formed the stem of a glass funnel. The time required for filling was about 15 min. The specimen did not appear to lose an appreciable amount of moisture during this period, as judged by the weight of the specimen before and after testing.

It was next necessary to seal the tubing containing the thermoelement leads at the point where it passed through the dilatometer cover. The iron cement paste was tamped between the tubing and the flared hole in the dilatometer cover. After the iron cement had set, it was coated with the organic plastic cement to protect it from the coolant liquid of the refrigerated baths.

To complete the dilatometer-specimen assembly, the burette was attached to the dilatometer and sufficient mercury was added so that the meniscus was visible in the burette. Even with careful filling it was necessary in some cases to agitate the dilatometer occasionally over a 24-hr period, in order to remove all of the entrapped air. A simple test for determining the approximate volume of entrapped air remaining in the dilatometer consisted in applying a small amount of pressure through the open end of the burette. The amount of entrapped air was indicated by the displacement of the mercury meniscus. When this air had been removed, the mercury meniscus was adjusted to the zero reference level at 40° F. Testing was not begun until the burette reading remained unchanged over a 24-hr period.

2. Determination of the Degree of Saturation

After considerable preliminary investigation, it was decided that the moisture condition of a specimen could be described best in terms of the amount of water in the specimen evaporable at 230° F, relative to the amount of water that the specimen could contain when saturated in vacuum. This evaluation of moisture condition is termed "percentage of vacuum saturation" and was determined in the following way:

Immediately following the dilatometer tests each specimen was removed from the dilatometer and weighed. It was then heated in an oven at 230° F for a period of 24 hr, and weighed again. The specimen was next placed in a container and covered with a bell jar, which was then evacuated at about 4 mm of mercury for a period of 24 hr. At the end of this time, and while the specimen was still under vacuum, a sufficient amount of freshly distilled water was drawn into the container under the bell jar to cover the specimen. Twenty-four hours later the vacuum was released. After the specimen had remained immersed for an additional 6 days, it was removed from the container, wiped, and weighed. The percentage of vacuum saturation was then equal to:

$$\frac{W_i - W_o}{W_s - W_o} \times 100,$$

where W_i is the initial weight, W_o is the oven-dry weight, and W_s is the vacuum saturation weight. These weights were determined to the nearest 0.01 g.

The percentage of vacuum saturation as herein defined is not presumed to represent an absolute value for the degree of saturation, inasmuch as the oven-dry basis for these determinations is subject to question. The alternative, however, of drying in a constant temperature, constant humidity room required an inconveniently long period of time. Nevertheless, a limited number of specimens was dried at 70° ±2° F and 50 ±5-percent relative humidity for a period of 6 weeks or longer. The calculated percentage of vacuum saturation on the air-dry basis was about 5 percent lower than on the oven-dry basis, in the range 65 to 80 percent of vacuum saturation. The values given in this report for the percentage of vacuum saturation represent, for each specimen, the upper limit for the true percentage of saturation. Obviously the percentage of vacuum saturation is the true percentage of saturation only if the vacuum-saturation procedure completely fills all pores with water.

3. Methods of curing

The various specimen moisture conditions were brought about and maintained by several curing procedures. Following the initial fog-room curing common to all specimens to the age of 28 days, the storage was as follows:

1. Specimens to be tested in an air-dry condition were stored at 70° ±2° F and 50 ±5-percent relative humidity for periods of from 60 to 120 days prior to testing.

2. Specimens to be tested in the vacuum-saturated condition were stored at 70° ±2° F and 50 ±5-percent relative humidity for periods up to 250 days and then vacuum saturated, as described in the preceding section of this paper. The specimens were then maintained wholly immersed for as long as 1 yr before testing them.

3. Specimens to be tested in a partially saturated condition were subjected to either of two types of curing treatment:

(a) Continuous immersion in water at 70° ±2° F until the time of test, for periods of from 1 to 12 weeks.

(b) Storage in air at 70° ±2° F and 50 ±5-percent relative humidity for at least 45 days, followed by immersion at 70° ±2° F for periods of from 1 week to 1 year.

The values for the percentage of vacuum saturation calculated for the partially saturated specimens ranged from 75 to 85 percent for the plain specimens and from 65 to 75 percent for the aerated specimens.

4. Types of Freezing and Thawing Treatments

Freezing and thawing cycles of several types were obtained, within the 40° to −20° F range, in the following ways:

1. Slow cycle (32 hr or longer). The temperature of the bath in which the dilatometer-specimen assembly was immersed was lowered stepwise from 40° to −20° F in approximately 8 hr, held constant at −20° F for 16 hr or longer, and raised stepwise to 40° F in approximately 8 hr.

2. Fast cycles. In the 1-hr fast cycle the dilatometer-specimen assembly, initially at 40° F, was transferred to and allowed to remain in the −20° F bath for a period of 30 min. It was then retransferred to the 40° F bath, where it remained for an additional 30-min period. Figure 4 shows that 30 min was sufficient time for a partially saturated specimen to attain temperature equilibrium with the bath.

The interrupted fast cycle was similar to the 1-hr fast cycle, except that the dilatometer-specimen assembly remained in the −20° F bath for 16 hr or longer, between the 30-min cooling and heating periods.

3. Combined cycles. These cycles were obtained by combining a fast cooling with a slow heating, or a slow cooling with a fast heating.

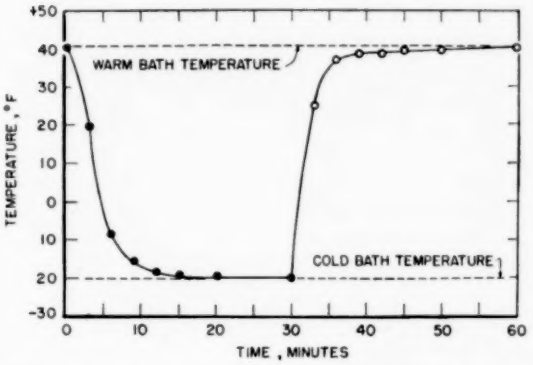

FIGURE 4. *Time-temperature relationship for a complete 1-hour fast cycle.*

Temperature is that indicated at center of cross section of a partially saturated specimen. ●, cooling; ○, heating.

Another type of combination treatment was employed in which a portion of the temperature range was traversed at one rate of cooling or heating and the remaining portion at a different rate.

Other types of treatment employed, but which will not be discussed in the present report, consisted of moderate cycles in which the cooling or heating was done in two or more equal temperature steps by the successive transfer of the dilatometers into a series of baths at appropriate temperatures. These cycles were used in the exploratory phases of the study that resulted in the selection of the slow cycle for special emphasis. The reasons for this emphasis will appear in the discussion in which the effects of various types of treatment are compared.

Some of the partially saturated specimens tested were subjected to all of the types of treatment described above, and others received a number of cycles of one type of treatment only.

VI. Results and Discussion

1. Air-Dry Specimens

Volume-temperature relationships obtained in dilatometer tests of a plain and an aerated air-dry specimen are shown in figure 5, for successive slow and fast cycles. The moisture condition of these air-dry specimens was determined to be approximately 15 percent of vacuum saturation. The relationships are uniformly linear and not significantly different in slope for the fast and slow

cooling or heating. In tests of other air-dry specimens, similar results were obtained.

The values for thermal coefficients of expansion obtained by this method for four air-dry specimens, are shown in table 6. The present dilatometric method provided the conditions stated by Meyers [12] as necessary for valid determinations of the thermal coefficients of expansion of portland cement pastes, mortars, and concretes. These conditions require that "the specimens must be either in an atmosphere of controlled humidity or enclosed in airtight containers that do not restrict the movements of the specimens."

2. Partially Saturated Specimens

About three-quarters of the more than 50 specimens tested were in a partially saturated condition. The data for four of these specimens, which were subjected to various types of freezing and thawing cycles, are presented in figures 6 to 9. Each graph gives the volume-temperature relationship obtained for a single cycle.[3]

Partial or complete results for four additional partially saturated specimens are presented in figures 10, 12, and 14, in which only one type of cycle is presented in each figure. Figures 11, 13, and 15 illustrate similarities, differences, or trends in the volume-temperature behavior of specimens subjected to similar treatments; these data are taken from their contexts in figures 6 to 9.

(a) General

The data plotted in figures 6 through 9 show that in most cases, cooling caused the partially saturated specimens to contract, and heating caused them to expand. In contrast to the uniformity in results obtained for the air-dry specimens, these curves show discontinuities, points of inflection, and changes in slope in the volume-temperature behavior of the specimens during the progress of the various cycles.

In addition, for most of the cycles shown, the volume of a specimen was greater at the end than at the beginning of a cycle, indicating a "residual" expansion. These residual expansions are observed to be cumulative when the volume-temperature curves are examined in relation to the zero ordinate on each graph, which represents the volume of the specimen at 40° F. at the start of the first cycle. The cumulative effect is evident in a vertical displacement of the starting points for the succeeding cycles away from the zero

[3] The sequence of cycles is designated by circled numerals. Cycles not discussed are omitted.

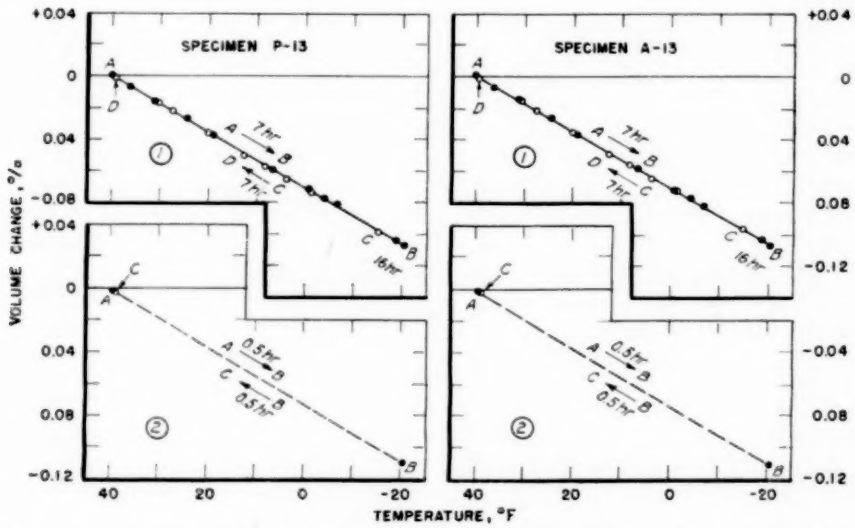

FIGURE 5. *Volume-temperature relationships for a slow and a fast cycle for two air-dry specimens, P–13 (plain) and A–13 (aerated).*

The thermal coefficient of linear expansion computed from these data was about 5.9×10^{-6} per °F (table 6). Both specimens were 155 days old at the beginning of the first cycle and had been stored at 70° F and 50-percent relative humidity for 125 days following the initial fog-room storage. After testing, the moisture condition of these specimens was determined to be 15 percent of vacuum saturation. ●, Cooling; ○, heating.

TABLE 6. *Thermal coefficients of cubical and linear expansion calculated from results of dilatometer tests of air-dry specimens*

Specimen	Date	Temperature range	Time required to cover range	Specimen volume change per degree Fahrenheit	Volume of specimen	Thermal coefficient of expansion per degree Fahrenheit	
						Cubical	Linear [a]
		°F.	*min*	*ml*	*ml*		
P-13 [b]	6/8	40.2 to −20.3	430	[c] 0.005595	336.4	17.7×10^{-6}	5.9×10^{-6}
	6/9	−14.8 to 39.5	425	.00602	.....	17.9	6.0
	6/9	39.5 to −20.3	30	.00607	.....	18.1	6.0
	6/9	−20.3 to 39.0	30	.00592	.....	17.6	5.9
	7/12	40.7 to −16.0	30	.00606	.....	18.0	6.0
	7/12	−16.0 to 40.3	30	.00610	.....	18.1	6.0
	7/13	40.0 to −19.1	90	.00598	.....	17.8	5.9
	7/13	−19.1 to 40.0	30	.00598	.....	17.8	5.9
A-13 [b]	6/8	40.2 to −20.3	430	[c] .00583	335.3	17.7	5.9
	6/9	−14.8 to 39.5	425	.00600	.....	17.9	6.0
	6/9	39.5 to −20.3	30	.00602	.....	17.9	6.0
	6/9	−20.3 to 39.0	30	.00597	.....	17.8	5.9
	7/12	40.7 to −16.0	30	.00601	.....	18.0	6.0
	7/12	−16.0 to 40.3	30	.00601	.....	18.0	6.0
	7/13	40.0 to −19.1	90	.00587	.....	17.5	5.8
	7/13	−19.1 to 40.0	30	.00579	.....	17.3	5.8
P-24 [d]	11/12	71.0 to 3.3	465	.00596	334.0	17.9	6.0
	11/13	5.3 to 52.0	20	.00590	.....	17.7	5.9
	11/13	52.0 to 6.7	30	.00584	.....	17.5	5.8
	11/13	6.7 to 70.2	410	.00593	.....	17.8	5.9
A-24 [d]	11/12	71.0 to 3.3	465	.00601	336.1	17.9	6.0
	11/13	5.3 to 52.0	20	.00595	.....	17.7	5.9
	11/13	52.0 to 6.7	30	.00594	.....	17.7	5.9
	11/13	6.7 to 70.2	410	.00596	.....	17.7	5.9

[a] Computed as one-third of cubical coefficient.

[b] 155 days old at start of tests; stored at 70°±2°F and 50±5 percent relative humidity for 125 days prior to test.

[c] First four determinations computed from data shown in figure 5.

[d] 640 days old at start of tests; stored in fog room at 70°±2°F for 80 days from time of fabrication, totally immersed for 160 days at 70°±2°F, and then stored at 70°±2°F and 50±5 percent relative humidity for 400 days.

ordinate. The total residual volume change for all specimens discussed are shown in table 7.

(b) Description of the Volume-Temperature Relationships for the Various Types of Cycles

Slow cycle. As shown in figures 6 to 9, tests of partially saturated specimens subjected to various types of cycles were started with a slow cycle. The general characteristics of the volume-temperature relationships for this type of cycle are shown in figure 10 for the initial slow cycle given to two partially saturated specimens. These specimens were approximately the same in degree of moisture saturation but differed widely in age and curing.

The specimens contracted uniformly during cooling at the start of the initial slow cycle to temperatures as low as 21.5° F. This cooling and supercooling,[4] is indicated by the line *AB* in figure 10, A and B. At point *B* an abrupt increase in the temperature and volume of each specimen occurred, presumably as water within the pore structure began to freeze. Maximum values for volume and temperature (point *C*) were attained within a few seconds. The bath, dilatometer, and mercury surrounding the specimen remained at the temperature to which the system had been cooled when freezing occurred, or slightly lower, so that *C* was a point of nonequilibrium. Usually within 15 min the temperature of the specimen returned to equilibrium with the bath, and during this period the volume of the specimen decreased, as indicated in figure 10, by the location of point *D*. Cooling was resumed when point *D* had been observed, and

[4] Supercooling as herein used is defined as cooling of a specimen below the freezing point of water without thereby inducing freezing of the water within the pore structure of the specimen, as indicated by volume changes.

TABLE 7. *Effect of freezing and thawing cycles upon volume and elasticity of specimens for which volume-temperature relationships are presented in figures 5 to 16*

Specimen [a]	Age	Condition	Percentage of vacuum saturation	Number of cycles	Total residual volume change	Change in Young's modulus (dynamic) [b]	Figure in text
	Days				*Percent*	*Percent*	
P-13	155	Air-dry	15	5	0	−4	5
A-13	155	do	15	5	0	−4	5
P-27	90	Partially saturated	75	15	+0.100	−27	6, 11, 13, 15
A-27	90	do	67	15	+.040	−11	7, 11, 13, 15
P-23	80	do	85	11	+.135	−34	8, 11, 13, 15
A-19	95	do	65	17	+.065	−13	9, 11, 13
P-11	360	do	78	8	+.085	−37	[c] 10
P-26	37	do	77	18	+.085	−19	[c] 10
P-29	120	do	81	7	+.040	−17	12
P-30	120	do	78	7	+.060	−13	14
P-13	650	Vacuum saturated	100	1	+.400	−65	16
A-13	650	do	100	1	+.310	−60	16

[a] The specimens are listed in the order in which they appear in the discussion. The plain specimens are designated by the letter P, and the aerated specimens by the letter A.

[b] Changes were computed from determinations made prior to the start and 48 hr after the completion of the dilatometer tests, except for specimens P-13 and A-13. For these specimens the second determination was made 1 week after the completion of the dilatometer tests.

[c] Figure 10 shows only the first cycle.

was continued to the −20° F end point, except for necessary interruptions to obtain a sufficient number of burette and equilibrium temperature readings to establish the nature of the volume-temperature curve.

Holding the system at or near −20° F overnight (16 hr) usually produced no appreciable further change in the volume of the specimen. In many cases −20° F could not be reached during the first 8 hr of the test because of mechanical difficulties. However, it was found that the temperature gradually decreased to −20° F. during the night, and the volume indication obtained 24 hr after the start of the cycle produced a continuation of the curve obtained during the first 8 hr.

Heating was begun about 24 hr after the start of the cycle. Figure 10 shows that the specimens increased uniformly in volume as the temperature was raised, and also that the volume at any given temperature up to about +20° F was somewhat greater during heating than it had been during cooling. A change in slope occurred in the heating curve above +20° F. A comparison of the relationships presented in figures 10, A and B (and also those shown for the initial cycles in figures 6 through 9) shows that the manner in which the slope changed varied. In the curve shown in figure 10, A, the change in slope was sufficient to produce a sharp point of inflection, and at about 30° F the volume of the specimen decreased as the temperature increased. A minimum value for the volume of the specimen in this region occurred between 31° and 32° F when all ice within the pore structure had presumably melted, following which the specimen again increased in volume as the temperature was raised to 40° F. The relationship in figure 10, B, showed only a gradual decrease in slope above +20° F. Between 32° and 40° F the slope of the heating curve for each specimen was essentially the same as that of the initial cooling curves. In both instances the distance AF is a measure of the residual expansion.

Thermal contraction and "shrinkage" during slow cooling. An obvious difference between figure 10, A and B, appears in the nature of the cooling curves at temperatures below that of the discontinuity attributed to initial freezing at point C. In figure 10, A, the volume-temperature relationships preceding and following the discontinuity are nearly parallel. Such relationships may be said to represent an idealized or expected behavior of moist porous materials during freezing.

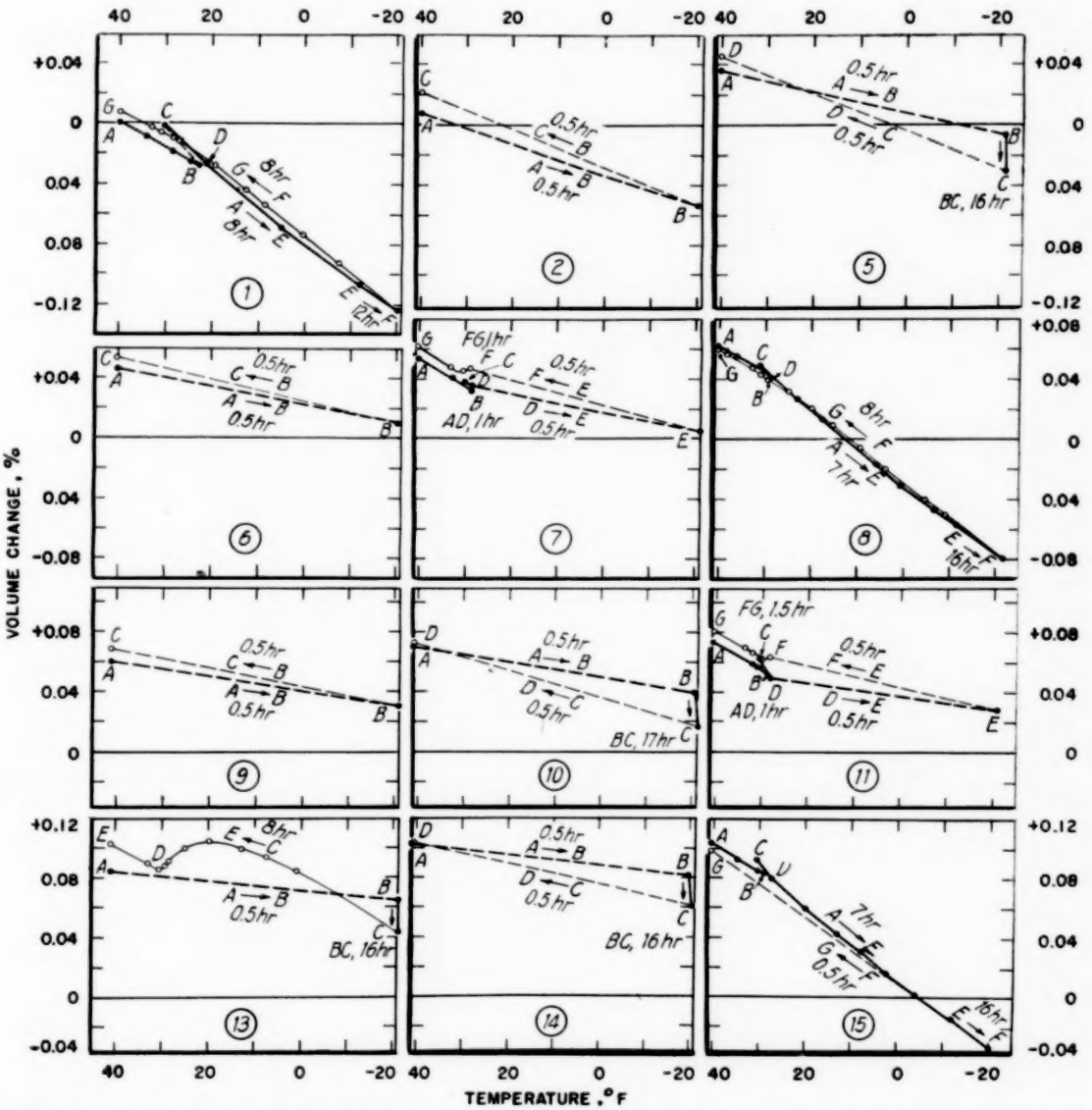

FIGURE 6. *Volume-temperature relationships for 12 freezing and thawing cycles of various types as obtained for the plain partially saturated specimen P–27.*

Cycles 1 and 8 were slow cycles; 2, 5, 6, 9, 10, and 14 were 1-hour and interrupted fast cycles; 7, 11, 13, and 15 were combined cycles of several kinds; and 3, 4, and 12, of a type not discussed, are omitted. The specimen was 90 days old at the beginning of the first cycle, and had been immersed in water at 70° F for 60 days following the initial fog-room storage. The moisture condition was determined to be 75 percent of vacuum saturation. This specimen decreased 27 percent in Young's modulus (dynamic, flexural) during the testing. ●, Cooling; ○, heating.

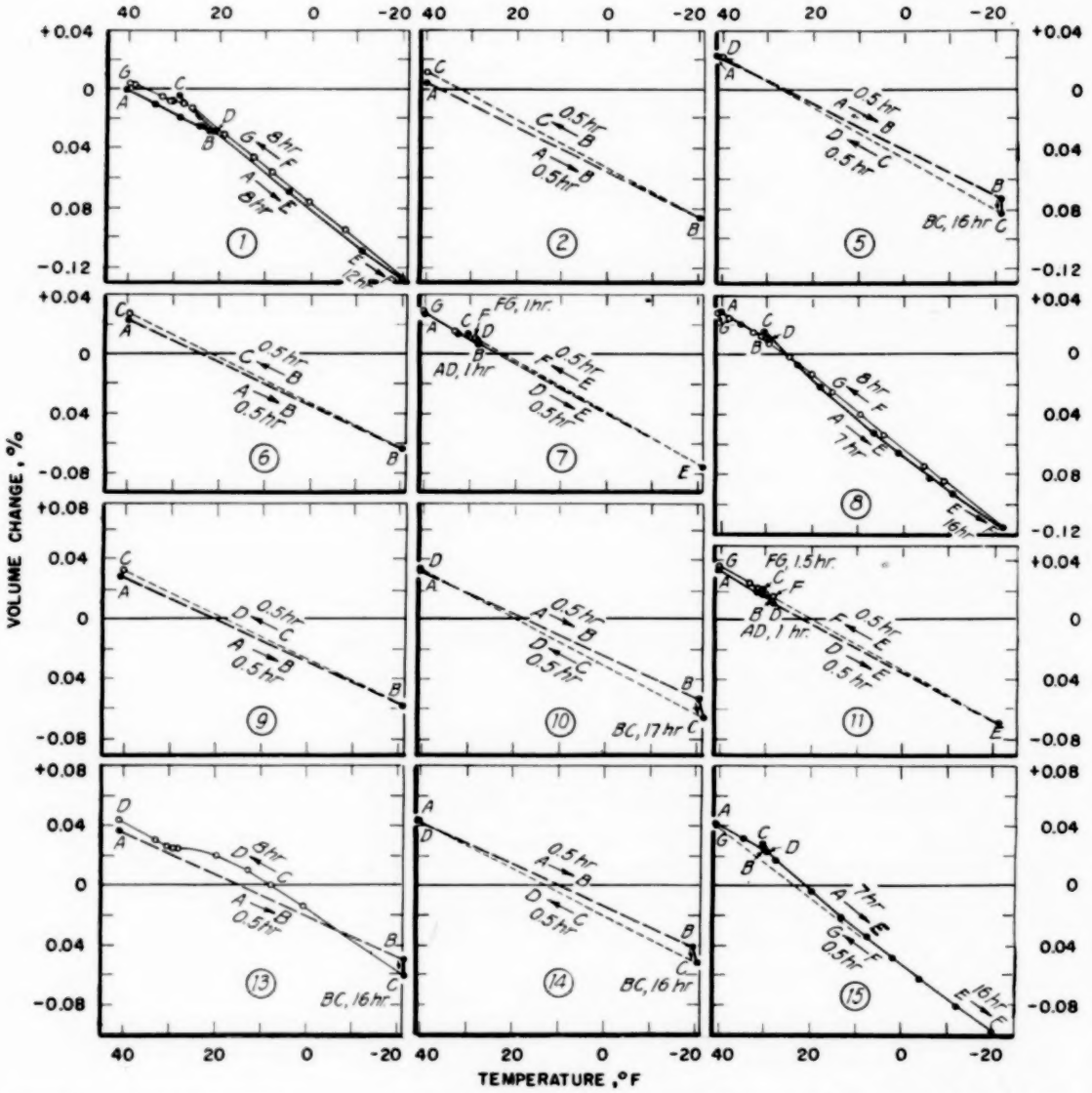

FIGURE 7. *Volume-temperature relationships for 12 freezing and thawing cycles of various types as obtained for the aerated partially saturated specimen A–27.*

Cycles 1 and 8 were slow cycles; 2, 5, 6, 9, 10, and 14 were 1-hour and interrupted fast cycles; 7, 11, 13, and 15 were combined cycles of several kinds; and 3, 4, and 12 of a type not discussed, are omitted. The specimen was 90 days old at the beginning of the first cycle, and had been immersed in water at 70° F for 60 days following the initial fog-room storage. The moisture condition was determined to be 67 percent of vacuum saturation. This specimen decreased 11 percent in Young's modulus (dynamic, flexural) during the testing. ●, Cooling; ○, heating.

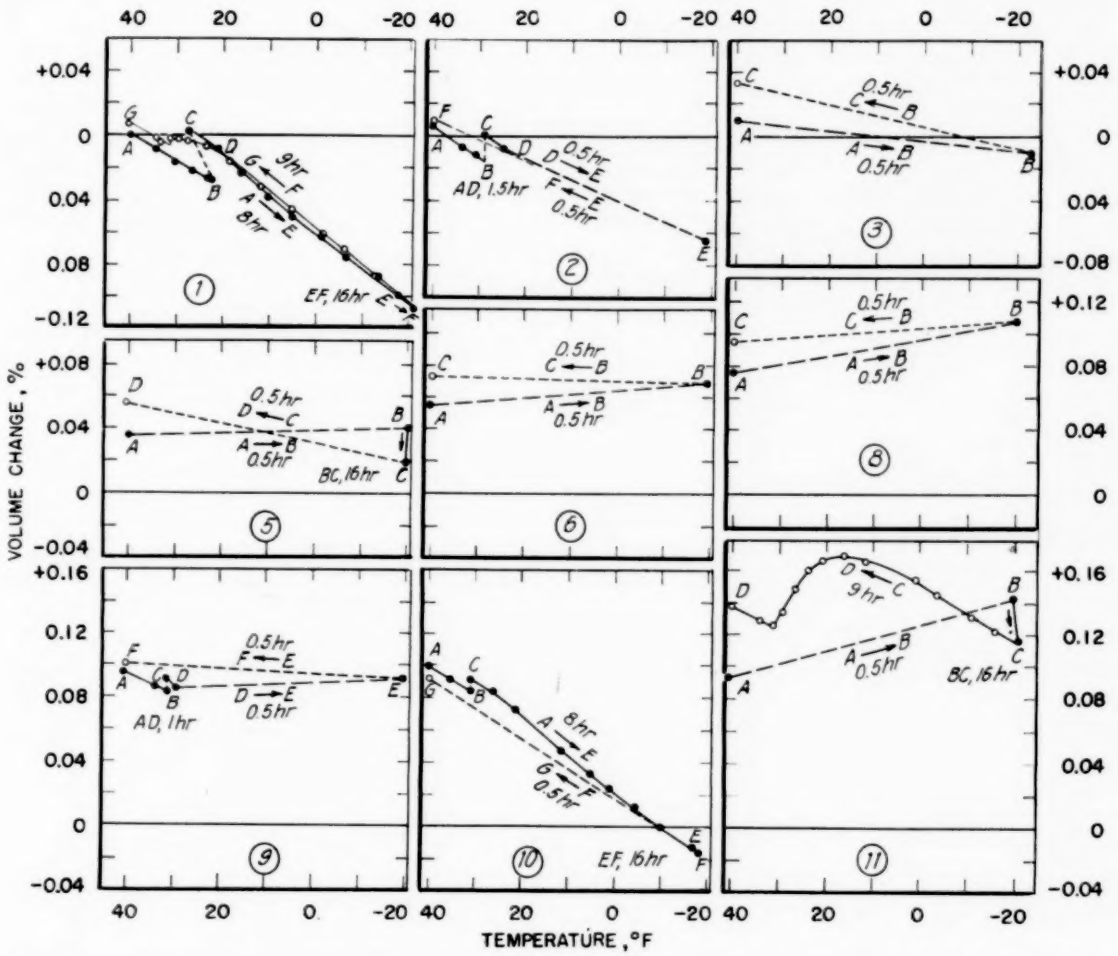

FIGURE 8. *Volume-temperature relationships for nine freezing and thawing cycles of various types as obtained for the plain partially saturated specimen P–23.*

Cycle 1 was a slow cycle; 3, 5, 6, and 8, were 1-hour and interrupted fast cycles; 2, 9, 10, and 11, were combined cycles of several kinds; and 4 and 7, of a type not discussed, are omitted. The specimen was 80 days old at the beginning of the first cycle, and had been immersed in water for 49 days at 70° F following the initial fog-room storage. The moisture condition was determined to be 85 percent of vacuum saturation. This specimen decreased 34 percent in Young's modulus (dynamic, flexural) during the testing and was found to be one of the least resistant among the specimens tested. ●, Cooling; ○, heating.

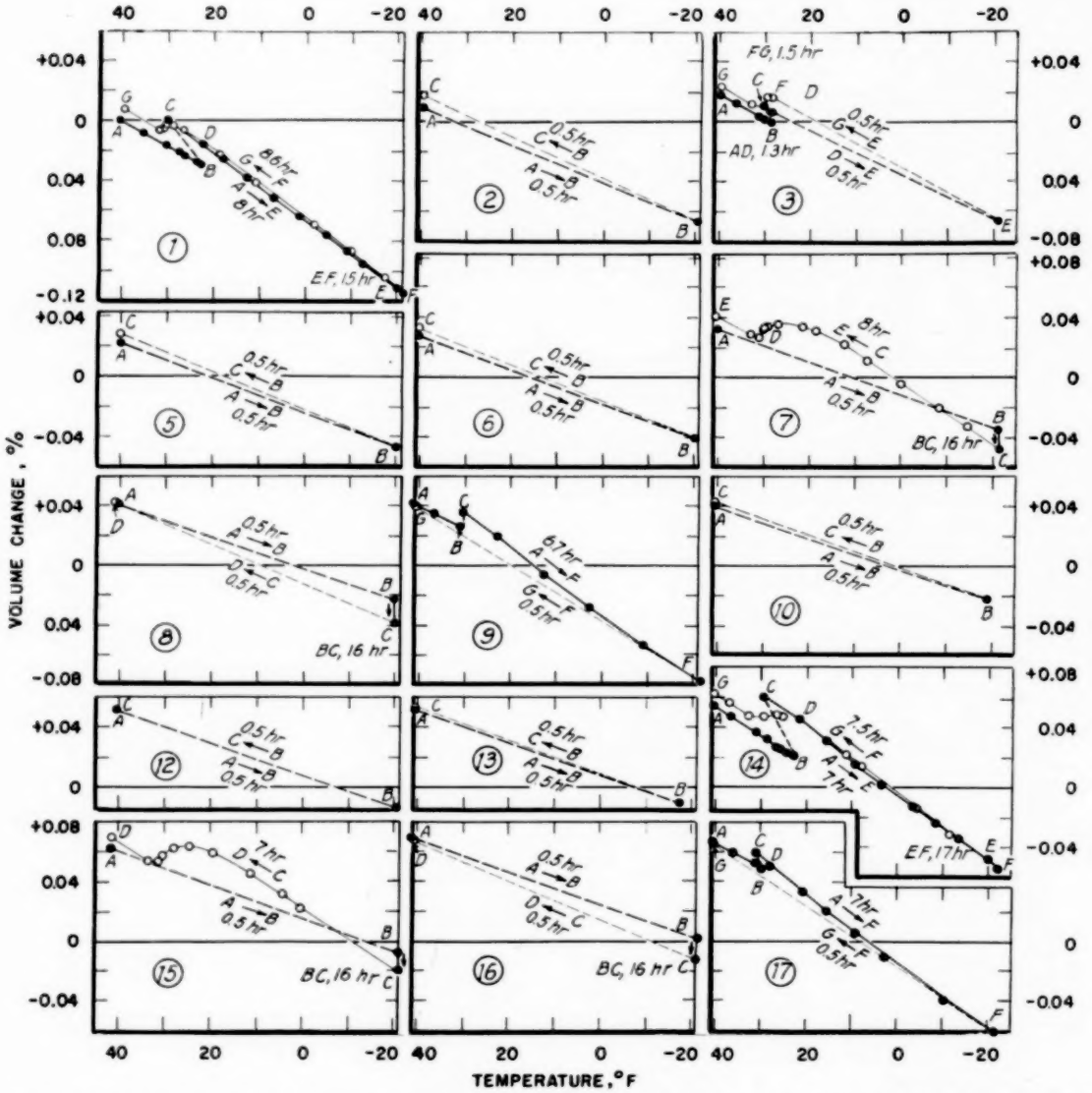

FIGURE 9. *Volume-temperature relationships for 15 freezing and thawing cycles of various types as obtained for the aerated partially saturated specimen A–19.*

Cycles 1 and 14 were slow cycles; 2, 5, 6, 8, 10, 12, 13, and 16 were 1-hour and interrupted fast cycles; 3, 7, 9, 15, and 17 were combined cycles of several kinds; and 4 and 11, of a type not discussed, are omitted. The specimen was 93 days old at the beginning of the first cycle. It had been stored at 70° F and 50-percent relative humidity for 45 days following the initial fog-room storage and had then been immersed in water at 70° F for 20 days before testing. The moisture condition was determined to be 65 percent of vacuum saturation. This specimen decreased 13 percent in Young's modulus (dynamic, flexural) during the testing. ●, Cooling; ○, heating.

Relationships of the type shown in figure 10, B, however, were obtained for most of the partially saturated specimens. Here the volume-temperature relationships preceding and following the initial freezing were notably different in slope. In the figures the linear relationship AB, obtained during the initial cooling, has been extrapolated to B'. It may be assumed that the line AB' represents the volume-temperature behavior of the specimen when freezing does not occur, or when a temperature range that does not include the freezing point of water is employed. Hence, the slope of line AB' represents the thermal coefficient of cubical expansion of the specimen. The relationship actually obtained, CE, however, intersects and descends below the extrapolated line, and the total contraction during cooling from +40° to −20° F appears to be *greater* than it would have been had freezing not occurred. Thus, the total volume change during cooling appeared to consist not only of the normal thermal contraction, upon which the abrupt expansion caused by freezing (point C) is superimposed, but also of a "shrinkage" factor. This factor appears to occur solely as an effect of freezing, since it was absent in the results obtained for the air-dry specimens. The term *shrinkage* is used here to distinguish the effect from the purely thermal contraction, and not to imply that the mechanism by which it occurs is known. Thomas has [3] ascribed extra-thermal length contractions, observed during the freezing of partially saturated sandstones and other materials, to internal "drying" that resulted when water was, in effect, "removed" by its conversion to ice.

Volume-temperature relationships for repeated slow cycles.—In figure 11, the volume-temperature relationships for repetitions of the slow cooling are abstracted from their contexts in figures 6 to 9. Also shown are the slow cooling relationships for some of the "combined" cycles. The most obvious point of variation among the relationships obtained for each specimen is in the temperature to which the specimen was cooled before the initial freezing occurred. For slow coolings following the first, it is seen that the amount of supercooling was notably reduced, i. e., freezing was apparently initiated at a higher temperature than in the first cycle. An exception is noted for the fourteenth cycle shown in figure 9 for specimen A–19 and, more clearly, in figure 11. During the fourteenth cycle for this specimen, the amount of supercooling was as much as during the first cycle. In all previous testing schedules the specimen-dilatometer assembly was maintained at 40° F between successive cycles, and the period of such storage never exceeded 72 hr. In this case, however, a period of 5 days at 40° F intervened be-

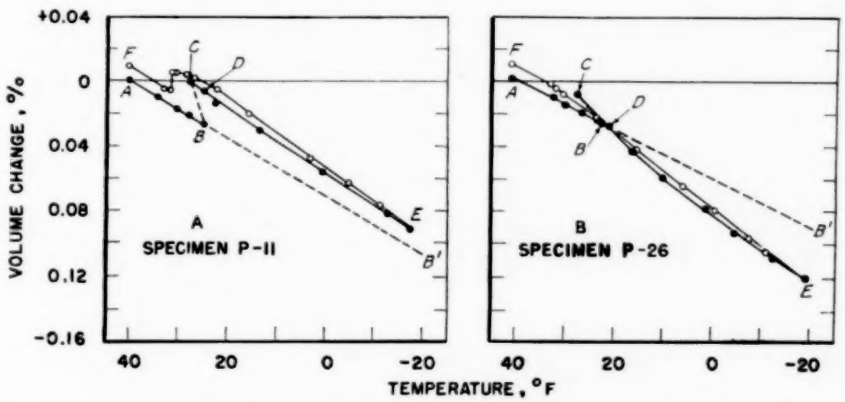

FIGURE 10. *Volume-temperature relationships for a slow cycle as obtained for two plain partially saturated virgin specimens of similar degree of saturation, but of considerably different ages and curing histories.*

Specimen P-11, which was 1 year old at the time of the test, had been stored at 70° F and 50-percent relative humidity for 60 days following the initial fog-room storage, and had been immersed in water at 70° F for 270 days before testing. The moisture condition was determined to be 78 percent of vacuum saturation. Specimen P-26, which was 37 days old at the time of test, had been immersed for 7 days at 70° F following the initial fog-room storage. The moisture condition was determined to be 77 percent of vacuum saturation. Specimen P-11, which decreased 37 percent in Young's modulus (dynamic, flexural) during eight cycles, was regarded as one of the least resistant of all the specimens tested. Specimen P-26 decreased only 19 percent during 18 cycles of similar types. ●, Cooling; ○, heating.

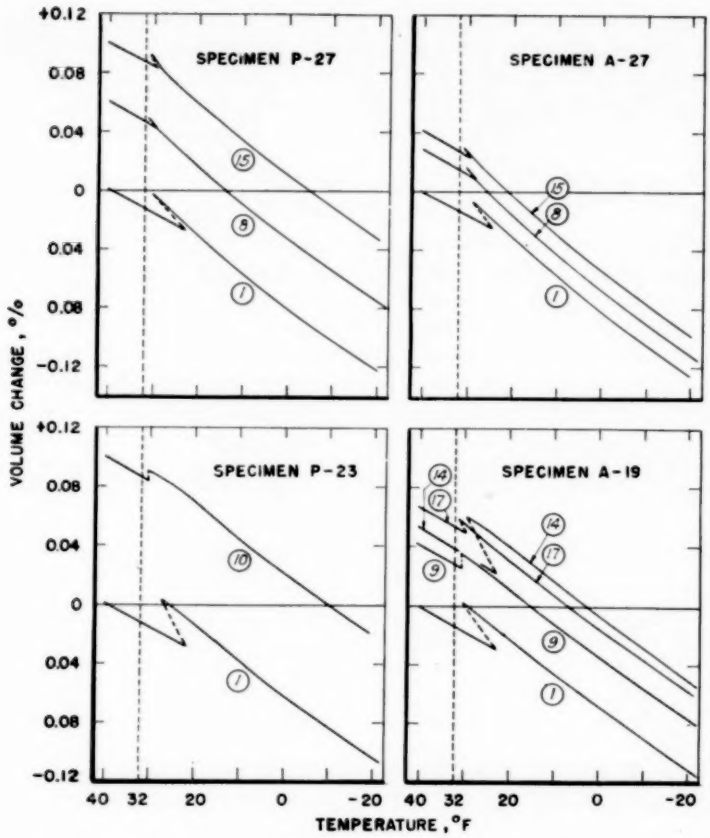

FIGURE 11. *Volume-temperature relationships for four partially saturated specimens during slow cooling.*

The volume-temperature relationships are removed from their contexts in figures 6 to 9 and plotted to a common origin for each specimen. The number of the cycle appears with each curve. The relative extent of super-cooling may be noted with reference to the broken line, which is the 32° abscissa.

tween the thirteenth and fourteenth cycles. Otherwise, the cycle was no different from preceding slow cycles.

Volume-temperature relationships are presented in figure 12 for specimen P–29, which was subjected to seven successive slow cycles. The periods of storage at 40° F between cycles, or the "recovery times," were varied. The recovery times and temperatures to which each specimen was supercooled are shown in table 8 for the partially saturated specimens discussed in this report, including specimen P–29. About 100 hr appeared to be a "critical" duration of recovery time for all specimens tested. When this time was less than 100 hr, supercooling of from 1° to 5° F occurred during the next cooling; when this time exceeded 100 hr, supercooling was increased to from 7° to 10.5° F during the next cooling. The critical duration was exceeded, among the specimens listed in table 8, only for the specimens A–19, P–11, P–26, and P–29. Variations in the degree of supercooling, other than those appearing to occur in relation to the critical recovery time, appeared to depend upon unknown factors, but not upon how greatly the recovery time exceeded or fell short of 100 hr.

Fast cycles. During the 1-hr fast cycle only three burette readings were obtained. The first and third readings were observed at 40° F at the start and completion of the cycle, and the difference between them was the residual volume change. The intermediate reading was observed

TABLE 8. *Effect of "recovery time" upon supercooling during slow and slow-fast cooling in partially saturated specimens* [a]

Specimen	Cycle [b]	Cooling	Recovery time	Supercooled to—
			hr	*°F*
P–27	1	Slow	.....	23.0
	7	Slow-fast	3.0	28.5
	8	Slow	17.0	29.0
	11	Slow-fast	0.5	28.5
	15	Slow	70.5	28.5
A–27	1	Slow	.....	22.5
	7	Slow-fast	3.0	28.5
	8	Slow	17.0	29.0
	11	Slow-fast	0.5	28.5
	15	Slow	70.5	29.5
P–23	1	Slow	.....	22.0
	2	Slow-fast	38.0	30.0
	9	do	0.5	30.5
	11	Slow	7.0	30.5
A–19	1	Slow	.....	23.0
	3	Slow-fast	3.0	28.5
	9	Slow	2.0	30.0
	14	do	140.0	22.5
	17	do	1.0	29.5
P–11	1	Slow	.....	24.5
	5	Slow-fast	0.5	30.0
	6	Slow	470.0	24.5
	7	do	1140.0	23.0
P–26	1	Slow	.....	22.5
	4	Slow-fast	4.0	27.0
	6	Slow	1.0	27.5
	7	do	45.0	27.0
	10	do	460.0	22.5
	13	do	70.0	28.0
P–29	1	Slow	.....	22.0
	2	do	111.0	21.5
	3	do	16.0	30.0
	4	do	112.0	24.0
	5	do	17.0	29.0
	6	do	16.0	28.5
	7	do	136.0	22.5

[a] The specimens are listed in the order in which they are discussed in the text.

[b] The cycles omitted from this table were those in which the cooling was fast or moderate, and in which supercooling could not be detected.

at −20° F, 30 min after the transfer of the dilatometer from the 40° F bath. The data given in figures 6 to 9 show rather significant differences in the amount of contraction during the fast cooling, not only among the various specimens, but also, for specimens P–27 and P–23, among the several fast cycles administered to each specimen. This is shown more clearly in figure 13, where data for the fast coolings only are plotted. Specimens A–27 and A–19 show only a slight change in slope with repetitions of the fast cooling, whereas specimen P–27 and particularly, specimen P–23, show a marked change in slope.

The interrupted fast cycle differed from the 1-hr fast cycle only in the prolonging of immersion of the dilatometer in the −20° F bath for 16 hr or longer before retransfer of the dilatometer to the 40° F bath. At least one interrupted fast cycle was given to each of the specimens for which data are shown in figures 6 to 9. The data show that the specimens decreased in volume during the prolonged immersion at approximately −20° F. The decrease in volume was found to continue at a gradually diminishing rate for several days for some specimens allowed to remain at −20° F for that length of time.

Combined cycles. Data are presented in figure 14 for a specimen subjected to seven successive fast cooling-slow heating cycles. These data show the previously described contraction at −20° F following the fast cooling, and the volume-temperature relationship for the slow heating. The heating curve for each cycle shows a change in slope beginning at a lower temperature than was indicated during the complete slow cycles shown for other specimens. This is indicated in figures 6 to 9 for specimens receiving both types of cycles. Compare heating curves for cycles 1 and 8 with that for cycle 13 in figures 6 and 7; note also cycle 11, figure 8, and cycles 7 and 15, figure 9.

Volume-temperature relationships for a type of combined cycle in which the combination was reversed from that described in the preceding paragraph, i. e., a slow cooling-fast heating cycle, are also shown. Note cycle 15 in figures 6 and 7, cycle 10 in figure 8, and cycles 9 and 17 in figure 9. In each case there was a residual contraction at the completion of the cycle, in contrast to the residual expansions shown for most of the other types of cycles.

Also shown in figures 6 to 9 are volume-temperature relationships for cycles in which "slow-fast" cooling was employed. The initial, slow-cooling portion of the relationship includes the discontinuity attributed to freezing and is, to this point, the same as the previously described slow cooling. This may be seen, for example, in cycles 7 and 11 in figures 6 and 7. After the specimen returned to equilibrium following the discontinuity at point *C*, it was cooled in the remaining portion of the 40° to −20° F range in one step, indicated by the broken lines *DE*. The similarity between this

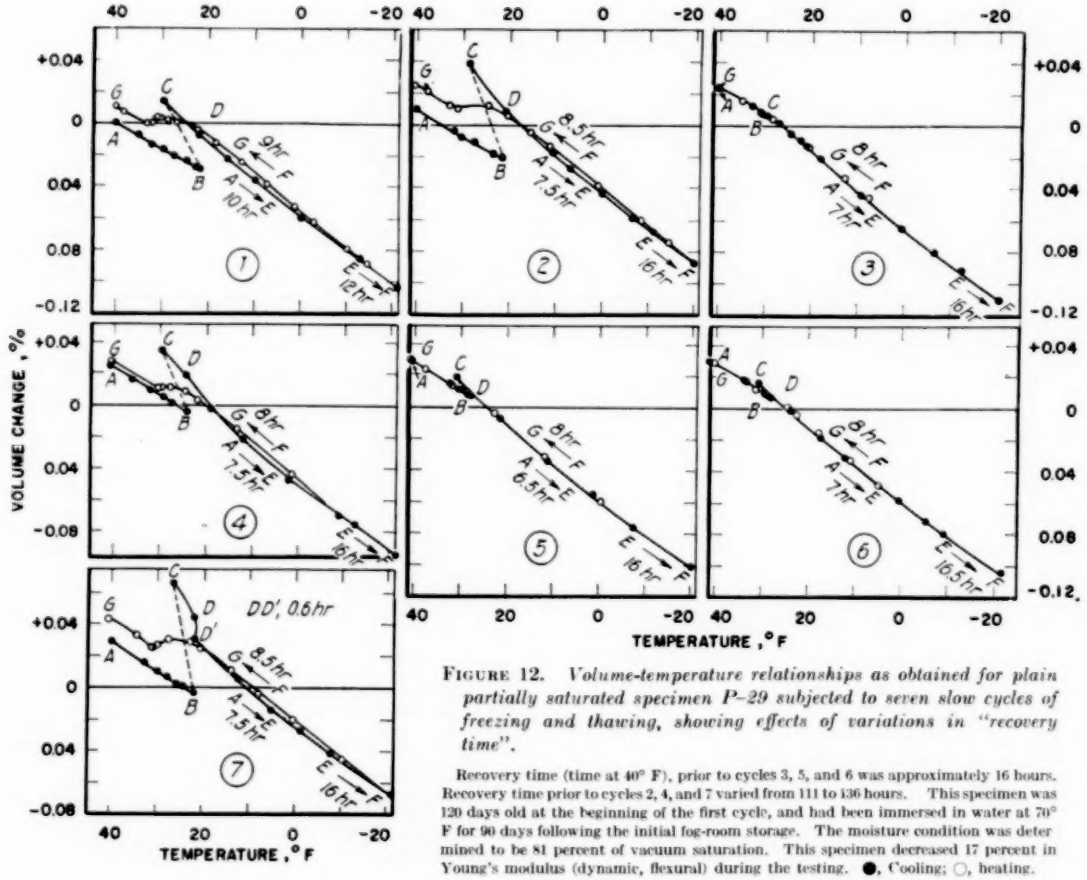

FIGURE 12. *Volume-temperature relationships as obtained for plain partially saturated specimen P–29 subjected to seven slow cycles of freezing and thawing, showing effects of variations in "recovery time".*

Recovery time (time at 40° F), prior to cycles 3, 5, and 6 was approximately 16 hours. Recovery time prior to cycles 2, 4, and 7 varied from 111 to 136 hours. This specimen was 120 days old at the beginning of the first cycle, and had been immersed in water at 70° F for 90 days following the initial fog-room storage. The moisture condition was determined to be 81 percent of vacuum saturation. This specimen decreased 17 percent in Young's modulus (dynamic, flexural) during the testing. ●, Cooling; ○, heating.

fast cooling portion of the cycle and the cooling during a fast cycle for each specimen is obvious. To interpret the relationships obtained, it appears that some of the water in the pore structures of the specimens froze at point *C* and then additional water froze during the subsequent fast cooling. That all freezable water in a porous material does not freeze at the same temperature has been pointed out by a number of other investigators [3, 4, 14].

Comparison of various types of freezing and thawing cycles. The data presented in figure 15 show differences in volume behavior of three specimens when subjected to a sequence of different types of cooling. These data are taken from figures 6, 7, and 8. In figure 15 the starting point for each curve (40° F) is drawn to coincide with an arbitrary "0" reference ordinate. The sequence of treatments as given was fast, slow-fast, slow, and fast for each specimen. The slow and slow-fast coolings were accompanied by a minimum of supercooling.

The relationships exhibit a pattern common to all partially saturated specimens subjected to successive cycles of different kinds. In each case the slow cooling (maximum rate of temperature drop 10° F/hr) produced the largest contraction, and the fast cooling (maximum rate of temperature drop 10° F/min at the center of a specimen) produced the smallest contraction.

Although the volume behavior during repeated slow coolings showed no systematic variation when supercooling was a minimum (fig. 11), repeated fast coolings produced progressively smaller contractions in all but a few, aerated, specimens (fig. 13).

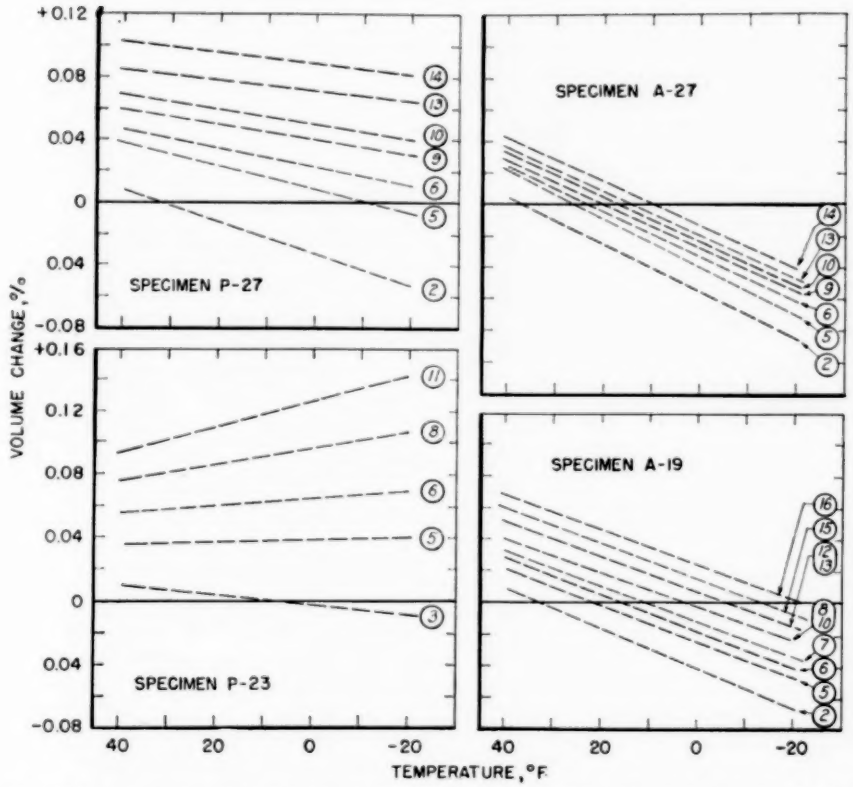

FIGURE 13. *Volume-temperature relationships for four partially saturated specimens during repeated fast coolings.*

The volume-temperature relationships are removed from their contexts in figures 6 to 9 and plotted to a common origin for each specimen. The number of the cycle is designated by a numeral. Specimens P-27 and A-27, which were identical in age and curing history, were tested simultaneously in two dilatometers and followed identical testing schedules.

That the gradual change in the condition of each specimen, reflected by the decrease in contraction with repeated fast coolings, did not distort the pattern shown is indicated in figure 15. The sequence of treatments started and ended with identical fast coolings. In each case the differences in contraction for these two fast coolings were small in comparison with the indicated differences between successive treatments of different kinds. An examination of table 7 shows that the specimens for which data are shown in figure 15 are representative of the range in degree of saturation, and resistance to freezing and thawing as indicated by the decrease in dynamic Young's modulus.

There are indications in figures 6 to 9 and 12 that, at least between 0° and −20° F, the volume of each specimen at a given temperature during a slow cooling was an irreducible minimum. The final temperature decrement, *EF*, occurring in most cases over a period of approximately 16 hr, produced a continuation of the volume-temperature relationship without a significant change in slope. In contrast the specimens were shown to contract at constant temperature (−20° F) following a fast cooling. This contraction may have been similar to the shrinkage effect (discussed on page 17) observed in some of the partially saturated specimens during a slow cooling. That the shrinkage during slow cooling was not simply a decrease in strain, is indicated by the magnitude of the effect, which greatly exceeded the maximum strain discerned in the discontinuity following supercooling. It was not possible, however, to distinguish between shrinkage and a decrease in strain in the fast cycle,

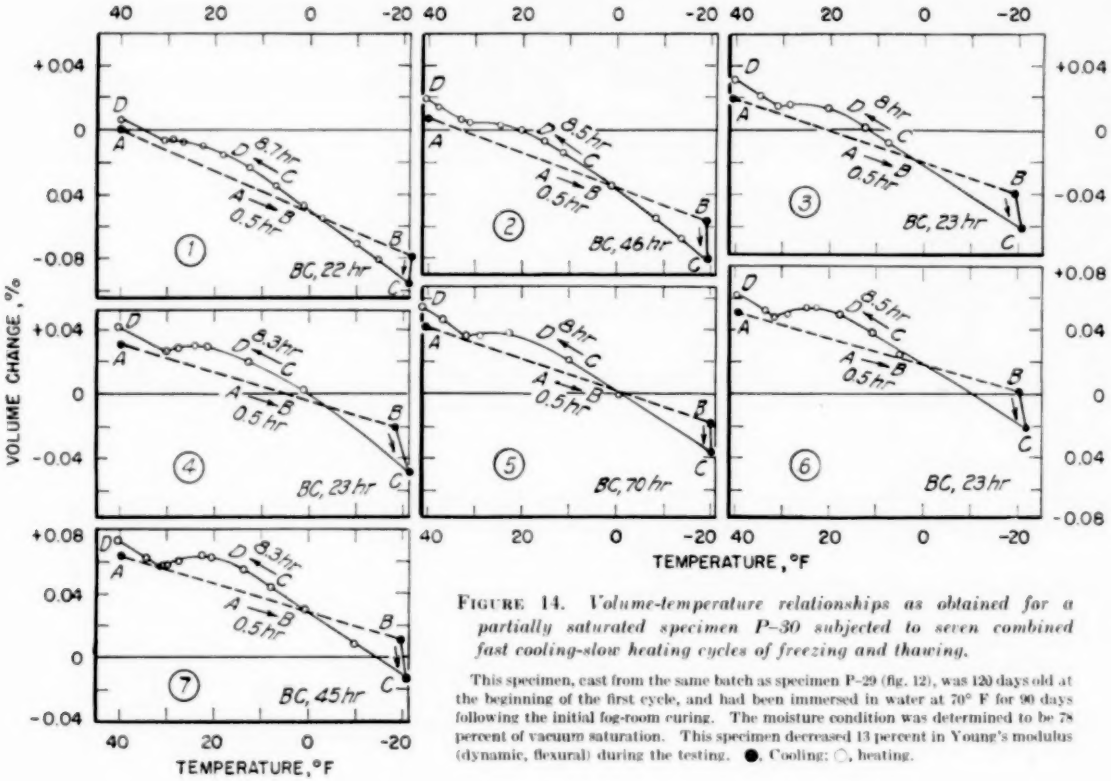

FIGURE 14. *Volume-temperature relationships as obtained for a partially saturated specimen P–30 subjected to seven combined fast cooling-slow heating cycles of freezing and thawing.*

This specimen, cast from the same batch as specimen P–29 (fig. 12), was 120 days old at the beginning of the first cycle, and had been immersed in water at 70° F for 90 days following the initial fog-room curing. The moisture condition was determined to be 78 percent of vacuum saturation. This specimen decreased 13 percent in Young's modulus (dynamic, flexural) during the testing. ●, Cooling; ○, heating.

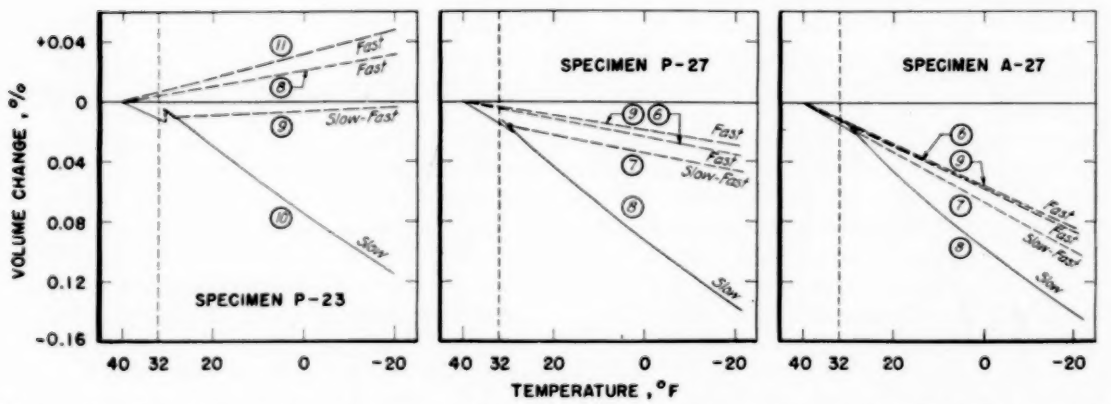

FIGURE 15. *Comparison of volume-temperature relationships for three types of cooling as obtained for three partially saturated specimens during successive cycles of freezing and thawing.*

The relationships are removed from their contexts in figures 6, 7, and 8, and drawn with starting points coinciding with an arbitrary origin. In each case the cycles were administered in the order fast, slow-fast, slow, and fast.

because observations were made only for the extremes of the +40° to −20° F temperature range. A decrease in strain or relaxation phenomenon should be expected according to the hydraulic pressure hypotheses of Thomas [3], Kennedy [13], and Powers [14]. These hypotheses attribute the disruptive force of freezing in porous materials to a hydraulic pressure produced by a movement of water ahead of the "ice front" and generated by the expansion accompanying the freezing of water rather than to pressure developed directly from the growth of ice crystals. The occurrence of stress relaxation, however, would not preclude the occurrence of the shrinkage effect during a fast cooling.

The observed differences in contraction of a given specimen when cooled in different ways were considered to be a measure of differences in strain. Considering the treatments that produced the least contraction as most severe, the various types of cooling would rank, in the order of decreasing severity, fast, slow-fast, and slow.

Although comparisons of cooling effects could be made by examining transient volume behavior, the effects of varying the rate of heating could not be similarly analyzed. The end of the heating period, which completed a cycle, usually resulted in a residual volume change, measurable at 40° F. The residual changes (normally expansions) were usually small in comparison with the strains observed at −20° F, and reflected the effects of the complete cycle, i. e., the effects of cooling as well as heating. Although the effects of varying the rate of heating were not investigated as extensively as the rate of cooling, comparison of the slow and fast heating indicated that the slower treatment produced greater positive residual volume changes, other things being equal. Examples of this may be found in cycles 13 and 14, figures 6 and 7; the only difference between the treatments given occurs, in each case, in the rate of heating. Similar illustrations are cycles 7 and 8, and cycles 15 and 16 in figure 9.

Examination of figures 6 to 9 indicates that appreciable residual contractions resulted only from the combination of the slow cooling (minimum supercooling) and the fast heating. The need for further study, to evaluate properly the relative effects of variations in the rate of heating is recognized. However, a tentative rating of the complete cycles, arranged in the order of increasing residual expansions, is as follows:

1. Slow cooling [5]-fast heating.
2. Slow cooling [5]-slow heating.
3. Fast cooling-fast heating.
4. Fast cooling-slow heating.

Wide variations in the magnitude of residual expansions during repeated slow cycles appeared to be related to the previously discussed variations in supercooling. A slow cooling with a maximum of supercooling produced a larger residual expansion in a given specimen than a slow cooling in which supercooling was reduced to a minimum, other things being equal. In the fast cooling, however, the large initial temperature gradient probably prevented the appearance of the effects of supercooling. No general comparison, applicable to all specimens, of the effects of the fast coolings and the slow cooling with a maximum of supercooling, may be made. Among the specimens more susceptible to damage by freezing and thawing, the fast cooling produced the larger residual expansions, whereas among less susceptible specimens the reverse was often true. In many cases, a slow cycle with a maximum degree of supercooling produced about the same residual expansion as a fast cycle.

It is recognized that a "swelling" as a result of thawing, corresponding to the shrinkage effect during freezing, may have confused the observations. Such a swelling, resulting from one cycle, may have continued into a succeeding cycle. It is believed, however, that such effects were not sufficiently large to vitiate the observed pattern of volume behavior.

(c) Differences Among Specimens

Differences between plain and aerated specimens. The nondestructive dynamic determination of Young's modulus of elasticity, which is widely used in freezing and thawing studies, was used as a criterion of the relative "soundness" condition of specimens subjected to the dilatometer tests. The moduli were computed from values for the resonant frequency of flexural vibration, determined prior to, and following the dilatometer tests. A specimen showing a decrease in dynamic

[5] Supercooling absent or reduced to a minimum.

E of 25 to 30 percent was considered to have "failed."

Most of the partially saturated specimens were tested in pairs (one plain and one aerated), in which both specimens received identical treatments. The different pairs of specimens, however, did not all receive similar treatment, and therefore only a composite analysis of specimen moisture condition and of the effects of the freezing and thawing treatments may be given.

	Plain	Aerated
Average percentage of vacuum saturation (10 pairs of specimens)	78	69
Average percentage change in dynamic E	−22	−13
Average percentage total residual volume change	+0.092	+0.043

For each pair of specimens, the plain specimen was of a higher degree of saturation, decreased more in dynamic E, and increased more in volume than the aerated specimen.

Effect of degree of saturation and type of curing upon volume-temperature behavior. The differences in behavior between plain and aerated specimens of comparable age and curing were believed to be related to differences in degree of saturation. The values obtained for the percentage of vacuum saturation ranged from 75 to 85 percent for the plain specimens, and from 65 to 75 percent for the aerated specimens. In general, there was a difference of 10 percent of vacuum saturation between plain and aerated specimens cured and tested in pairs. The four specimens for which data are presented in figures 6 to 9 are representative of specimens in the range 65 to 85 percent of vacuum saturation.

As seen in these figures, differences in the initial slow cycle volume temperature relationships among different specimens did not appear to be related to differences in the degree of saturation. For example, there is little difference between the initial slow cycle relationships for specimens P–27 and A–27 (figs. 6, 7, and 11) despite the 8-percent difference in the degree of saturation. In contrast, the slow-cycle relationships shown in figure 10 for specimens P–11 and P–26 were notably different, but the specimens were of approximately the same degree of saturation. An examination of the data shows no great differences in residual volume changes resulting from slow cycles given specimens of different degrees of saturation. Results of the type presented in figure 13 for the fast cycles, however, show rather large differences among specimens differing in percentage of vacuum saturation. These specimens were of comparable ages, but the curing of specimen A–19 included a drying period, whereas the others were continuously wet prior to testing. Specimen P–23 not only showed the least contraction during the initial fast cooling, but also showed the greatest change in the amount of contraction during repeated fast coolings. A relatively large expansion occurred during the fast cooling for the 11th and final cycle. The volume-temperature relationships for the last two cycles, as seen in figure 8, may be of interest in that they show the transient volume changes in a specimen definitely failing. This specimen decreased 34 percent in dynamic E during 11 cycles of freezing and thawing.

An insufficient amount of data was obtained to allow a study of the effect of type of curing on the transient and residual volume changes to be made. It can only be stated that type of curing and age of specimen appear to affect these changes for some of the types of cycles.

3. Vacuum-Saturated Specimens

Two specimens, P–13 and A–13, which were first tested in the air-dry condition (fig. 5), were then vacuum-saturated and immersed in water for 1 yr. The vacuum-saturation procedure described previously was used to provide specimens for test with a maximum degree of moisture saturation. Figure 16 shows the volume-temperature relationships obtained for these specimens during one slow cycle of freezing and thawing.

The specimens decreased in volume uniformly as the temperature was lowered to approximately +25° F. Near this temperature, expansion, which was attributed to the beginning of freezing of water in the pores of the specimens, began and continued for about 30 min as the temperature of the bath was held at 25° F. During this time the temperature at the centers of the specimens first increased to about 31° F and then returned to equilibrium with the bath. When both the volume and the temperature of the specimens became stable, point C was observed. When cooling was resumed the

specimens showed additional increases in volume and at −25° F had not begun to contract. Such behavior indicated that not all of the freezable water in the specimen had been frozen at −25° F.

The specimens showed additional increases in volume during heating to a temperature of approximately +16° F, after which, with continued heating, they decreased in volume until point *F*, at 31° F, was reached. Further heating produced increases in volume to point *G*.

The volume-temperature relationships in figure 16 are remarkable in indicating maximum transient increases in volume at −25° F of approximately 0.80 percent for the plain, and 0.75 percent for the aerated specimen. Residual expansions were considerably smaller; 0.40 percent for the plain, and 0.30 percent for the aerated specimen. Residual linear expansions, determined by means of a length comparator, were 0.12 percent for the plain and 0.11 percent for the aerated specimen, and

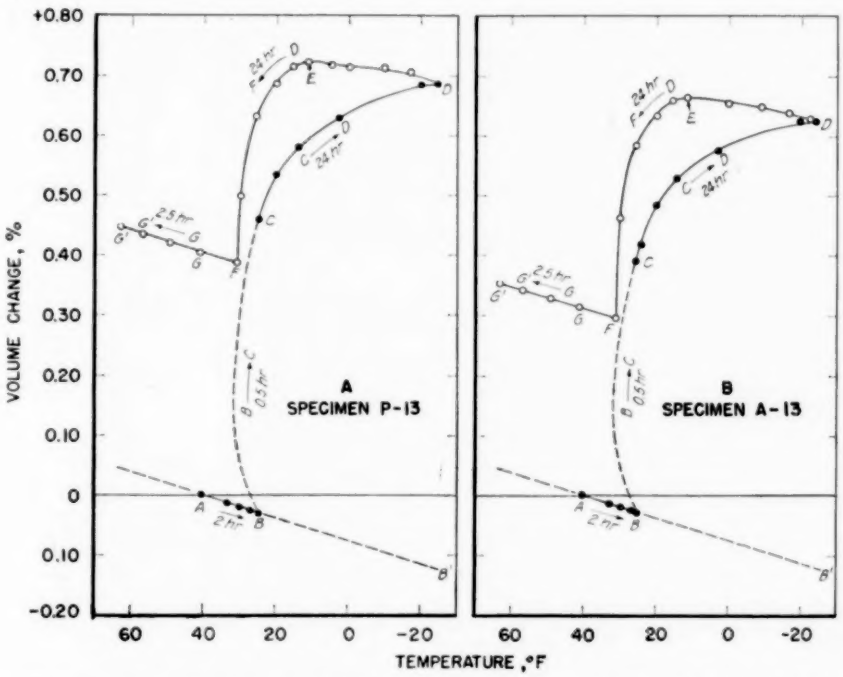

FIGURE 16. *Volume-temperature relationships as obtained for specimens P–13 (plain) and A–13 (aerated), both vacuum saturated, subjected to a single slow cycle of freezing and thawing.*

These specimens were 650 days old at the time of testing and had been tested in the air-dry condition at age 155 days (fig. 5). These specimens were in the dilatometers for 35 days following the air-dry storage and were then returned to air-dry storage for an additional 70 days before being vacuum-saturated. They were then kept immersed in water at 70° F for 1 year before testing in the vacuum saturated condition. Specimen P-13 showed a decrease in Young's modulus (dynamic, flexural) of 65 percent 1 week after the completion of the cycle, and specimen A-13 showed a decrease of 60 percent ●, Cooling; ○, heating.

After completion of the tests it was found that mercury had penetrated the specimens to a limited extent, through several small spalls or "popouts." A portion of the heating curves *FG* has therefore been corrected in each case by an amount equal to the volume of mercury which had entered the specimens.

agreed quite well with values obtained by dividing the indicated residual volume expansions by three. Several other specimens tested in the vacuum-saturated condition gave results of similar magnitude.

Other than the few spalls or popouts, there were no visible signs of disintegration in the specimens.

Determinations of Young's modulus of elasticity, before and after testing, however, showed the following changes:

	Specimen P–13	Specimen A–13
Dynamic E, before testing	6.3×10^6 psi	6.3×10^6 psi
Dynamic E, 1 week after testing.	2.2×10^6 psi	2.5×10^6 psi
Change in dynamic E, 1 week after testing.	−65%	−60%
Dynamic E, 1 year after testing.	5.5×10^6 psi	5.2×10^6 psi
Change in dynamic E from initial value, 1 year after testing.	−13%	−17%

Had the dynamic E determinations been made immediately following the completion of the freezing and thawing cycle, the decrease may have exceeded 90 percent, on the basis of previous experience in the "recovery" in dynamic E in specimens subjected to freezing and thawing treatments [15]. Thus the vacuum saturated specimens were, for practical purposes, destroyed by a single cycle of freezing and thawing. In this connection it may be pointed out that the moisture condition is one not normally attained in laboratory specimens or in masses of concrete exposed to natural freezing and thawing. However, a fairly complete saturation may occur in top layers of horizontally exposed concrete surfaces. Under these conditions volume changes, as shown in figure 16, would occur in the surface layers and thus account for the familiar type of deterioration known as scaling.

VII. Summary

A detailed description has been presented of a mercury-displacement dilatometer for observing volume changes in moist, porous building materials during freezing and thawing.

Results presented have been confined to representative volume-temperature relationships for small cylindrical specimens cast from a concrete of one-mix design (plain and modified by the addition of an air-entraining agent) and made with one brand of normal portland cement and Potomac River aggregate.

The moisture condition of the specimens ranged from air-dry to vacuum-saturated. Most tests were performed upon specimens in a state of partial saturation, attained during various curing periods. These specimens, when tested, contained from 65 to more than 85 percent of the total water that they were made to contain upon being oven-dried, evacuated, and resaturated following the freezing and thawing tests.

The types of freezing and thawing cycles employed varied in rates of cooling and heating within the $+40°$ to $-20°$ F range. These cycles included a slow cycle, which required 32 hr, and a fast cycle, which required 1 hr for completion.

The volume changes for all specimens tested in the air-dry condition were directly proportional to changes in temperature and independent of the rate of temperature change. The slopes of the volume-temperature relationships obtained were measures of the thermal coefficients of expansion.

The volume changes for the partially saturated specimens were generally not independent of the rate of temperature change, and showed departures from a uniform volume-temperature relationship such as that described for the air-dry specimens. These departures were believed to be effects of the conversion of water to ice (or ice to water) within the pore structures of the specimens.

The immediate effect of the freezing of water was a distension, which appeared to be directly related to the rate of cooling in those cases in which supercooling was minimized or absent.

Secondary effects of freezing were shrinkage and relaxation phenomena, which consisted of contractions in addition to the normal thermal contraction of the solid volume of a specimen.

The specimens usually showed a permanent "set" or residual expansion at the completion of a cycle. The residual expansions for repeated cycles were cumulative.

During slow cooling the pore water in a virgin specimen was apparently supercooled before it froze. The amount of supercooling diminished in succeeding repetitions of the slow cycle, except that when the specimen was maintained unfrozen for a sufficient time after any cycle, supercooling in the following slow cycle was again pronounced. There was no evidence of supercooling during the fast cycle.

Vacuum-saturated specimens subjected to one slow cycle showed distensions upon freezing, and residual expansions at the end of the cycle, more

than 30 times as great as the corresponding volume changes in partially saturated specimens similarly tested. According to accepted criteria for soundness, these specimens definitely would have failed during one cycle of freezing and thawing.

Appreciation is expressed to P. H. Bates, former chief of the Clay and Silicate Products Division, at whose suggestion the study was initiated; to J. Tucker, Jr., who designed the concrete mixes; and to F. B. Hornibrook, P. H. Petersen, R. L. Blaine, N. Ernest Dorsey, and the late Phillip Turner, all of whose interest in the study was especially helpful.

Appreciation is also due Gerald Pickett of Kansas State College, Manhattan, Kans., and T. C. Powers of the Portland Cement Association, Chicago, Ill., for helpful discussion and comments during the progress of the study.

IX. References

[1] A. B. C. Anderson and N. E. Edlefson, Soil Sci. **54,** 221 to 232 (1942).

[2] G. J. Bouyoucos, J. Agr. Research **8,** 195 to 197 (1917).

[3] W. N. Thomas, Dept. Sci. Ind. Research (Great Britain) Building Research Technical Paper No. 17 (1938).

[4] T. C. Powers and T. L. Brownyard, J. Am. Concrete Inst. **18,** 933 to 969 (1947).

[5] H. Kreuger, Transactions of the Royal Swedish Institute for Scientific-Industrial Research, No. 24, Stockholm (1923).

[6] John Tucker, Jr., G. W. Walker, and J. Arthur Swenson, BS J. Research **7,** 1067 (1931) RP389.

[7] L. B. Tuckerman, Proc. Am. Soc. Testing Materials **23,** part 2, 602 (1923).

[8] Culbertson W. Ross, J. Research NBS **27,** 197 (1941) RP1414.

[9] International Critical Tables **II,** 457–8 (1927).

[10] Federal Specification SS–C–191b for Cements; Portland (April 29, 1941).

[11] Federal Specification SS–C–158b for Cements, Hydraulic; General Specifications (Methods for Sampling, Inspection, and Testing) (May 20, 1946).

[12] S. L. Meyers, Ind. Eng. Chem. **32,** 1107 (1940).

[13] Henry L. Kennedy, Proc. Am. Soc. Testing Materials **44,** 821, (1944).

[14] T. C. Powers, J. Am. Concrete Inst. **16,** 245 to 272 (1945).

[15] M. O. Withey, Proc. Highway Research Board **24,** 174 to 202 (1944).

Washington, February 1, 1949.

U. S. Department of Commerce
National Bureau of Standards

Research Paper RP2001
Volume 43, July 1949

Part of the Journal of Research of the National Bureau of Standards

Electrophoresis of Modified Collagen

By James M. Cassel and Joseph R. Kanagy

Electrophoretic studies were made on collagen samples that were modified by a variety of treatments. The isoelectric point of collagen heated at 140° C in air is pH 5.3, and that of collagen shrunken by heating in water is pH 5.2, as compared with pH 7.0 for the untreated collagen. Deaminized collagen was isoelectric at pH 4.6.

The isoelectric point of purified collagen was lowered by tanning with basic chromium sulfate solutions. Samples were tanned to contain 0.6-, 1.0-, 1.8-, and 2.5-percent of chromium expressed as chromic oxide. A maximum shift in isoelectric point was observed with a sample in which 1.8-percent of chromic oxide was fixed. Chrome tanning a deaminized collagen sample had only a small effect on the isoelectric point. A vegetable-tanned leather and vegetable-tanned collagen were isoelectric at pH 3.2. Chrome retanning a vegetable-tanned collagen did not affect its isoelectric point.

The electrophoretic behavior of tanned collagen is compared with that of unstretched nylon.

I. Introduction

Electrophoretic techniques have been frequently used to investigate the properties of protein surfaces. Excellent discussions and reviews of the general subject have been presented by Abramson [1],[1] by Abramson, Moyer, and Gorin [2], and by Moyer [3].

Collagen contains a number of reactive groups capable of fixing acid and base. Undoubtedly these reactive groups play an important role not only in combining with acid or base but also in the combination that occurs with formaldehyde, tannins, and dyes. It was believed that some fundamental information in regard to the mechanism of these reactions might be obtained from an electrophoretic study. In a publication now in press [4] the authors have described the electric mobility measurements made on collagen samples prepared in various ways. It is the purpose of this paper to present similar measurements on collagen samples that have been modified by heating, water shrinking, deaminizing, protracted ball mill grinding, and by several tanning processes. The tanning processes included vegetable, chrome, formaldehyde, and vegetable followed by chrome.

[1] Figures in brackets indicate the literature references at the end of this paper.

II. Materials

It was believed that a better understanding of the tanning mechanism could be obtained by tanning a material that had not been degraded and that contained for the most part pure collagen. For this reason collagen purified as recommended by Highberger [5] rather than commercial hide powder was used as a standard from which changes in electrophoretic characteristics could be estimated. With one exception the modified collagen samples were prepared from this purified collagen. The exception was a sample of vegetable-tanned leather.

III. Preparation of Modified Collagens

Chrome-tanned samples were prepared by tanning collagen in solutions of several concentrations of basic chromium sulfate. Previous to tannage, the collagen was ground to a uniform particle size in a Wiley mill. Approximately 20 g was then added to cold distilled water in a glass-stoppered bottle and allowed to soak overnight. The tan liquor was prepared by leaching a weighed

amount of the crude commercial form of basic chromium sulfate in water and filtering off the insoluble material. This liquor was transferred to the bottle containing collagen and water, and the chromic salt-collagen mixture was agitated for 24 to 30 hr, during which time no adjustment of pH was made. The tanned sample was thoroughly washed in changes of distilled water, dehydrated in successive changes of alcohol and ether, and air-dried. Chromium was determined on the air-dried material by the perchloric acid method.

A portion of deaminized collagen, prepared by the method of Thomas and Foster [6], was treated in the same manner as collagen with a basic chrome tanning solution. A determination of chromium by the perchloric acid method showed that deaminized collagen fixed 83 percent as much chromium as did collagen when treated under the same conditions.

Two types of vegetable-tanned materials were studied. These were commercially tanned leather and laboratory tanned collagen samples. The commercial leather was ground in a Wiley mill, degreased in petroleum ether, air-dried, and reground in the Wiley mill to pass a 60-mesh screen. In the laboratory tannage, collagen was treated with two concentrations of chestnut tannin. Two 20-g portions of collagen were soaked overnight in cold water contained in glass stoppered bottles. The chestnut extracts containing 20 and 40 g of tannin per 350 ml of water were added to the collagen water mixtures, and the contents were agitated 24 to 30 hr on a shaker. The materials were then thoroughly washed in distilled water and dehydrated in successive changes of alcohol and ether. They were then reground in a Wiley mill to pass the 60-mesh screen.

A vegetable-chrome tanned sample was prepared by treating a portion of the vegetable-tanned collagen with chrome-tanning solution according to the method previously described. The sample fixed 0.5-percent chromium expressed as chromic oxide.

Formaldehyde-tanned collagen samples were prepared by the method suggested by Highberger and Retzsch [7], with the exception that the material was washed thoroughly in changes of 0.1 *M* phosphate buffer before washing in several changes of distilled water. It was then dehydrated in alcohol and ethyl ether.

To determine whether the grinding action of a ball mill had any effect on collagen, a sample (previously ground in a Wiley mill) was pulverized to a fine powder in the ball mill. At various intervals, specimens were removed from the mill for mobility measurements.

Water-shrunken samples were obtained by heating collagen powder for 5 min in water at 65° C. The material was dried by successive alcohol and ether extractions and then reground in the Wiley mill to pass the 60-mesh screen.

The effect of exposing collagen to moderately high temperatures was studied by drying collagen samples in a Brabender moisture apparatus at 140° C for 1 day and 4 days, respectively. The loss in moisture was followed with the built-in weighing mechanism of the oven.

IV. Determination of Electrical Mobilities

The electrophoresis cell employed in this work is the horizontal microelectrophoresis cell like the one used by Abramson [8]. A description of the technique to be used with this type of cell is given by Moyer [9]. With the exception of the samples used in the study of the effect of the ball mill, the modified collagens were ground in a Wiley mill until the powder formed passed through a 60-mesh sieve. The powder was agitated in a buffer by using a Waring blendor, and after the large particles were allowed to settle to the bottom, the upper portion was decanted. The finer particles remained suspended in the liquid for several hours.

The ionic strength of all buffers was 0.005. The buffer mixtures used were as follows: pH 2.4 to 3.6, potassium chloride-hydrochloric acid; pH 4.0 to 5.6, sodium acetate-acetic acid; pH 6.0 to 7.8 disodium phosphate-dihydrogen phosphate; pH 8.0 to 9.2 boric acid-borax; pH 10.0 sodium hydroxide-boric acid-potassium chloride. The specific resistance of solutions introduced into the cell was determined with a pipette conductivity cell and a conductivity bridge [9]. Two or three groups of measurements, each consisting of at least ten measurements of the velocities of the particles, were made at each selected pH.

All mobility measurements were made in a room at approximately 23° C, and the values were corrected to 25° C by applying a factor of 2 percent per degree [9].

V. Results and Discussion

The results obtained by determining the pH-mobility curves for the collagens modified in several ways are presented, and their significance is discussed.

1. Effect of Chrome Tanning

The change in the isoelectric point of collagen caused by chrome tannage has been followed by Gustavson [10] and Theis [11]. In both investigations additional ions were introduced into the medium with the formation of a more complicated system than is expedient for such a study. In the present work collagen samples were tanned to contain 0.6-, 1.0-, 1.8-, and 2.5-percent chromium expressed as chromic oxide, and the tanning was done with no extraneous ions present. The pH-mobility curves are shown in figure 1 for the tanned and untanned materials.

The isoelectric point of the untanned material is higher than the isoelectric point of any of the tanned samples. There are several possible mechanisms that would explain such a difference in isoelectric point. If the amino groups of the collagen were inactivated through combination with the complex chromium ions, the effect would be to make the net charge of the collagen more negative and result in a lowering of the isoelectric point. There is also the possibility that the complex chromium ions combine with the collagen in some other way so that highly negative charges are imparted to the protein surface with the net result that the isoelectric point of the product is lowered.

In addition to these two possible mechanisms, a third has been suggested that proposes that the chromium combines with both amino and carboxyl groups [11]. Equivalent inactivation of both groups would lower the isoelectric point since the basic groups of the protein are supposedly stronger [12]. Although such a mechanism would lower the isoelectric point, there is some doubt that it would cause the large shift from pH 7.0 to pH 4.2.

The results shown in figure 1 indicate that a maximum shift in isoelectric point occurred with a sample that contained 1.8-percent chromium expressed as chromic oxide. It is possible that the initial take-up of chromium (up to 1.8%) represents a different process than that which occurs in the pick-up of additional chromium.

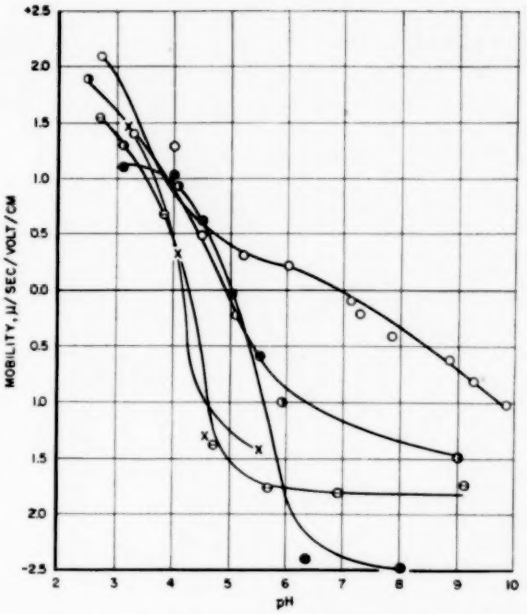

FIGURE 1. *Effect of chrome tanning on the* pH-*mobility curve of collagen.*

○, 0.0-percent Cr_2O_3; ◑, 0.6-percent Cr_2O_3; ⊖, 1.0-percent Cr_2O_3; ×, 1.8-percent Cr_2O_3; ●, 2.5-percent Cr_2O_3.

It may be that initially the complex chromium ions, which theoretically are present in both anionic and cationic form, combine predominantly with the amino groups of the collagen. After approximately 1.8-percent chromic oxide has been fixed, combination with the carboxyl groups of the collagen begins to play a more important part. Such a mechanism of tanning would result in a minimum isoelectric point with a certain content of fixed chromic oxide. It may be pointed out that if initial combination does occur between the complex chromium ions and the amino groups, then fixation of 1.8-percent chromic oxide would mean that two equivalents of chromium are combined with one equivalent of amino nitrogen.

Other results that have a bearing on the theory of chrome tanning are discussed later in this paper.

2. Effect of Deaminization

If a portion of the basic groups of collagen is removed by deaminization, the collagen should show a different and more acid isoelectric point. In figure 2 the pH-mobility curve of the deami-

839743—49——3

nized material is compared with that of the untreated collagen.

The shift in isoelectric point to a lower pH (7.0 to 4.6) is quite pronounced. These results support the theory that deamination removes a portion of the basic groups of collagen.

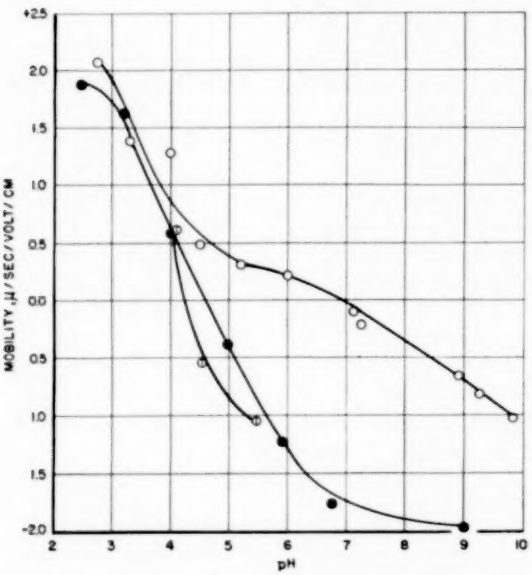

FIGURE 2. *Effect of deamination on the* pH-*mobility curve of collagen.*

○, Untreated; ●, deaminized; ①, deaminized-chrome tanned.

Thomas and Foster [6] located the isoelectric point of deaminized hide powder by the dye technique between pH 3.7 and 4.2, which is a shift from the isoelectric point of 5.0 that they found for hide powder. Page and Holland [13] found that deaminized vegetable-tanned hide powder contained considerably less alkali resistant tannin, and they reasoned that it was the uncharged amino groups that were removed by deamination.

Stiasny [14] has suggested that the change in hide substance upon deamination is not due to purely chemical modifications but may be attributed to a change in its structure whereby the active surface has been decreased. However, in figure 2 that sharp slope of the pH-mobility curve in the isoelectric region indicates that the deaminized material is as reactive as the untreated collagen, if not more reactive.

3. Deamination Followed by Chrome Tanning

In 1926, Thomas and Kelly [15] suggested that if the basic groups of collagen play a role in chrome tanning, their removal by deamination should markedly affect the fixation of chrome. By deaminizing hide powder and then retanning with basic chromium sulfate solutions, they found considerably less chromium fixed by the deaminized hide powder than by the untreated hide powder, and they concluded that the basic groups of collagen played a significant role in chrome tanning. Gustavson [16] carried out similar studies and stated that the diminished acid-combining capacity of the structurally altered hide powder was responsible for the inhibition of cationic chrome fixation by deaminized hide powder. In the present study it was found that deaminized collagen fixed 83 percent as much chromium as did the untreated collagen.

In figure 2 the pH-mobility curves of deaminized and chrome-tanned deaminized collagen are compared with the mobility curve of untreated collagen. Treating the deaminized collagen with basic chrome tanning solution has resulted in a very slight change in isoelectric point from pH 4.6 to 4.3. Comparing the data of figures 1 and 2, it will be observed that either deaminized collagen or untreated collagen, when treated to contain 1.5-percent chromic oxide, is isoelectric at pH 4.3.

In figure 2 the very slight shift in isoelectric point caused by chrome tanning of deaminized collagen indicates that the charge of the chrome complex does not influence to any great extent the electrophoretic characteristics of the sample. This result greatly weakens the theory discussed in regard to the data of figure 1, which suggested that chrome tanning imparts highly negative charges to the collagen surface with the net result that the isoelectric point of the product is lowered. On the other hand the theory is strengthened that proposes that inactivation of the basic groups of collagen by the chrome-tanning solution is responsible for the large shifts in isoelectric point observed in figure 1.

4. Effect of Vegetable Tanning

In figure 3 the pH-mobility curves are shown for collagen tanned with two concentrations of chestnut tannin, and for vegetable-tanned leather that had been degreased.

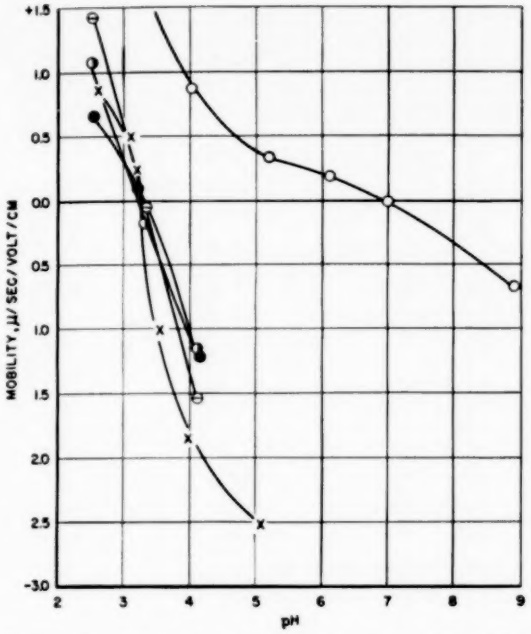

FIGURE 3. *Effect of vegetable tanning on the* pH-*mobility curve of collagen.*

○, Untanned collagen; ⊖, vegetable-tanned collagen (1 g of collagen per 1 g of tannin); ◑, vegetable-tanned collagen (1 g of collagen per 2 g of tannin); ×, vegetable-tanned leather; ●, vegetable-chrome tanned collagen.

The very close agreement in isoelectric point of the three samples leads one to believe that the dominant factor affecting the isoelectric point of vegetable-tanned material is the vegetable tannin itself. This would be in agreement with the theory that from pH 2.5 to 14.0 the vegetable tannin particles are negatively charged [17]. Adsorption of the vegetable tannin by the collagen would then produce a surface dominated by the negative charges of the tanning material. One would not expect much change in the surface by doubling the concentration of tanning material. This theory of the tanning mechanism does not rule out chemical combination between the amino groups of collagen and the negatively charged tannin particles. Rather, it is believed that this does occur, but the adsorption phenomenon overshadows this specific reaction.

In attempting to retan vegetable-tanned collagen with basic chromium sulfate, only 0.5-percent chromic oxide was fixed. The results in figure 3 show that this fixation of chromium had no effect on the isoelectric point of the vegetable-tanned collagen. The pick-up of the chromium has diminished the net charge on the surface in the extreme acid region. This again would indicate a surface that is predominantly that exhibited by vegetable tannin particles but which is altered slightly by the addition of the chrome-tanning material.

5. Effect of Formaldehyde Tanning

Tanning with 1-percent formaldehyde at pH 7.8 lowered the isoelectric point of collagen from pH 7.0 to pH 4.6 (see fig. 4).

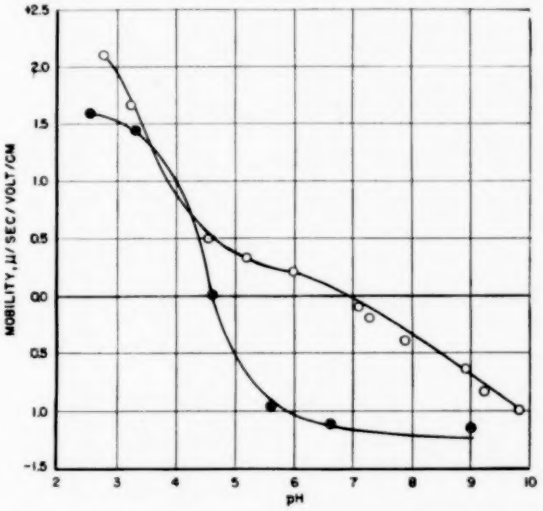

FIGURE 4. *Effect of formaldehyde tanning on the* pH-*mobility curve of collagen.*

○, Untanned; ●, formaldehyde tanned.

Since there is no reason to suspect, as in the case of chrome tanning, that the formaldehyde molecules would contribute to the net charge of the tanned product, we can be reasonably sure that the change in isoelectric point is due to inactivation of ionizable protein groups. In this instance, since the isoelectric point has been lowered, the amino groups of collagen must be involved in the tanning action. This would agree with the majority of work that has been done on this subject [18], [19].

6. Effect of Protracted Ball Mill Grinding

Curves 1 and 3 of figure 5 represent the pH-mobility data for two samples of hide collagen

that had been ground in a Wiley mill until the material could be sifted through a 60-mesh screen.

The difference in isoelectric point of the materials is attributed to the methods of preparation [4]. Curves 2 and 4 are for the two samples after they were powdered in a ball mill. The difference in the magnitude of the shifts of isoelectric point for the samples is probably due to the differences in time that the materials were ground in the ball mill (30 hr vs. 15 hr).

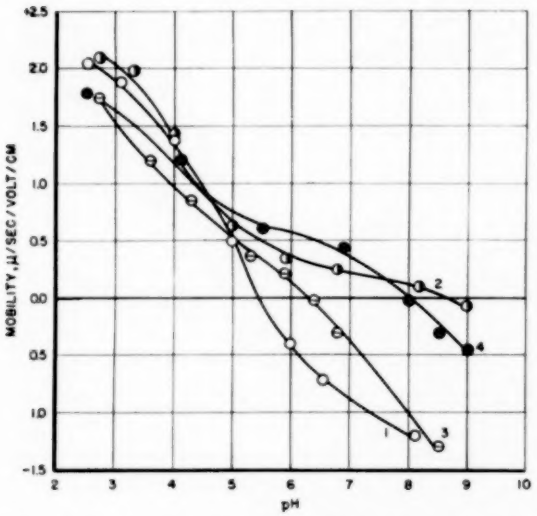

FIGURE 5. *Comparison of the* pH-*mobility curves of collagens ground in the ball mill and in the Wiley mill.*

Curve 1, sample A ground in Wiley mill; curve 2, sample A ground in ball mill for 30 hr; curve 3, sample B ground in Wiley mill; curve 4, sample B ground in ball mill for 15 hr.

A similar shift in isoelectric point to a higher pH is shown in figure 6, which represents data obtained by determining the mobilities of samples ground for different periods of time in a ball mill.

Prior to pulverization in the ball mill, the collagen (ash content 0.1%) was isoelectric at pH 6.3. The ash contents of the specimens removed from the ball mill after 4, 12, and 27 hr of milling were 1.8, 3.9, and 4.2 percent, respectively. The results of figure 6 show that the latter two specimens of high ash content were isoelectric at a more alkaline pH than either the unpulverized collagen or that milled for 4 hr.

Cohen [20] has shown that dry grinding of numerous proteins produces definite irreversible changes in protein molecules. He found that

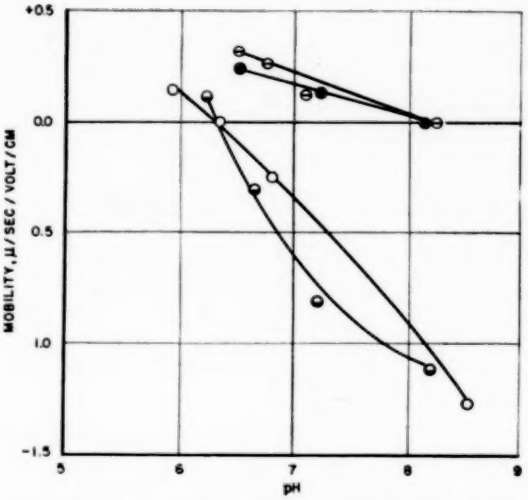

FIGURE 6. *Comparison of the* pH-*mobility curves of collagens ground for different periods of time in the ball mill.*

○, Untreated; ◒, 4 hr; ⊖, 12 hr; ●, 27 hr.

collagen yielded some water soluble protein after having been ground in a ball mill, and he concluded that dry grinding is a physical agent that produces changes that are associated with denaturation. Routh [21] has pointed out that at the point of contact of the balls a large amount of energy as heat may be liberated and that this may be one of the factors influencing the changes produced in proteins ground in this fashion. It has been shown that heat denaturation of soluble proteins, such as albumin, causes a shift in isoelectric point of these substances to a more alkaline pH [2]. In contrast to the shift in isoelectric point to higher pH observed with soluble protein, work reported later in this paper shows that exposure of collagen to rather high temperature actually lowers the isoelectric point. However, it is believed that some heat denaturation of the collagen occurs but that this denaturating effect is compensated for by another factor, namely that due to the presence of mineral ash.

The increase in ash content of the collagen upon grinding in the ball mill is the result of a breakdown in the surface of the porcelain mill. The ash adsorbed by the collagen is siliceous matter containing potassium, aluminum, and magnesium. Adsorption of these basic ions would shift the isoelectric point to a more alkaline pH. It is believed that the collagen sample ground 4 hr was de-

natured but adsorbed sufficient ash to compensate, and no change was produced in the electrophoretic characteristics of the product. As the grinding period is extended, the effect on the electrophoretic characteristics, due to the increased ash content, overbalances the effect due to denaturation, and the isoelectric point is shifted to a more alkaline region.

7. Effect of Heating

In figure 7 the pH-mobility curves of collagen samples that have been heated in air and water are compared with the mobility curve of untreated collagen.

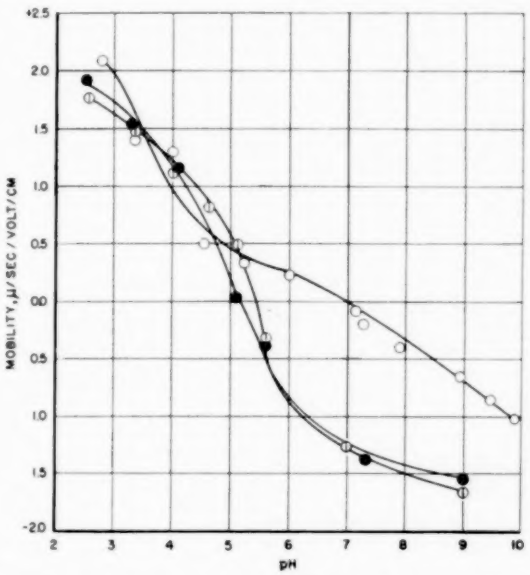

FIGURE 7. *Comparison of the* pH-*mobility curves of untreated, water shrunken, and dry heated collagen.*

○, Untreated; ◐, dry heated; ●, water shrunken.

From the results of Weir's work on the shrinkage of kangaroo tendon [22], it was estimated that collagen powder would be completely shrunken after 5 minutes' exposure to water at 65° C. Astbury [23] has postulated that the thermal contraction of collagen is an example of the capacity of polypeptide chains to shorten by intramolecular folding. This collapsing of the chains upon themselves produces a change in the surface of the material. It is this change of purely a physical nature that is believed to be responsible for the shift in isoelectric point observed in figure 7. Abramson, Moyer, and Gorin [2] have pointed out that changes of a physical nature in a substance may lead to a decrease or increase in the adsorption of ions from a buffer medium and thus result in a marked shift in isoelectric point. It should be observed that the surface of the shrunken collagen is apparently very similar to that of gelatin, for the isoelectric point of gelatin made from purified collagen by heating in water at a high temperature is at pH 5.0 [24].

In figure 7 the mobility curve of dry heated collagen represents data obtained from a sample heated 1 day at 140° C. A portion of this sample was heated an additional 3 days at the same temperature, but no change in the electrophoretic characteristics of the material was observed. The weight loss of the collagen per 1 and 4 days was 19.0 and 19.6 percent, respectively. This loss in weight would indicate that more than moisture had been removed and that an actual breakdown of the sample had begun [25]. It is believed that the lower isoelectric point of the treated sample is the result of local shrinkage and that the surface of these collagen fibers resembles a great deal the surface of the collagen fibers that have been shrunken in water.

VI. Comparison of Tanned Collagen and Nylon

One pertinent fact obtained by viewing the data is that the isoelectric point of many of the altered collagens was between pH 4.2 and 5.0. The fairly consistent change in isoelectric point to this pH region may be in some manner related to the structure of the collagen. Harris and Sookne [26] showed that the polyamide nylon, which has the following type of structure:

$$-CO-R-CO-NH-R^1-NH-CO-R-CO-NH-R^1-NH-,$$

where R and R^1 may represent 4 and 6 methylene ($-CH_2-$) groups, had an isoelectric point at pH 4.0. Nylon does not contain side chains with active basic or acidic groups. The amphoteric character of the polymer is attributed to what Harris and Sookne called amide groups but which are also known as peptide groups. If, during tanning, the free acid and basic groups of collagen were inactivated, the structure that remains is essentially similar to that of nylon, and such a material would be isoelectric near pH 4.0. Appar-

ently in the case of vegetable tanning, fixation of tannin particles builds up a high negatively charged surface with the result that the isoelectric point is even lower than that shown by the nylon type structure.

VII. References

[1] H. A. Abramson, Cold Springs Harbor Symposia, Quant. Biol. **1,** 39 (1933).

[2] H. A. Abramson, L. S. Moyer, and M. H. Gorin, Electrophoresis of proteins (Rheinhold Publishing Corp., New York, N. Y., 1942).

[3] L. A. Moyer, Cold Springs Harbor Symposia, Quant. Biol. **6,** 228 (1938).

[4] J. M. Cassel, J. R. Kanagy, J. Research NBS **42,** (1949) RP1992.

[5] J. H. Highberger, J. Am. Leather Chem. Assn. **31,** 93 (1936).

[6] A. W. Thomas and S. B. Foster, J. Am. Chem. Soc. **48,** 489 (1926).

[7] J. H. Highberger and C. E. Retzsch, J. Am. Leather Chem. Assn. **34,** 131 (1936).

[8] H. A. Abramson, Electrokinetic phenomena (Chemical Catalog Co., Inc., New York, N. Y., 1934).

[9] L. S. Moyer, J. Bact. **31,** 531 (1936).

[10] K. H. Gustavson, Discussed in Stiasny's "Gerbereichemie" (Theodore Steinkopff, Dresden, 1931).

[11] E. R. Theis, J. Am. Leather Chem. Assn. **36,** 459 (1941).

[12] W. E. Braybrooks, J. Int. Soc. Leather Trades Chem. **23,** 73 (1939).

[13] R. O. Page and H. C. Holland, J. Am. Leather Chem. Assn. **32,** 78 (1937).

[14] E. J. Stiasny, Gerbereichemie (Theodore Steinkopff, Dresden, 1931).

[15] A. W. Thomas and M. W. Kelly, J. Am. Chem. Soc. **48,** 1312 (1926).

[16] K. H. Gustavson, J. Am. Leather Chem. Assn. **22,** 236 (1927).

[17] A. W. Thomas and S. B. Foster, Ind. Eng. Chem. **15,** 707 (1923).

[18] G. D. McLaughlin and E. R. Theis, the chemistry of leather manufacture. (Rheinhold Publishing Corp., New York, N. Y., 1945).

[19] O. Gerngross and S. Bach, Collegium No. **631,** 350 (1922); No. **644,** 377 (1923).

[20] H. R. Cohen, Arch. Biochem. **2,** 1 to 8 (1943).

[21] J. I. Routh, J. Biol. Chem. **135,** 175 (1940).

[22] C. E. Weir, J. Research NBS **42,** 17 (1949) RP 1947.

[23] W. T. Astbury. J. Int. Soc. Leather Trades Chem. **24,** 69 (1940).

[24] J. Beek and A. Sookne, J. Research NBS **23,** 271 (1939) RP1230; J. Am. Leather Chem. Assn. **34,** 641 (1939).

[25] J. R. Kanagy, J. Am. Leather Chem. Assn. **35,** 632 (1940); J. Research NBS **25,** 149 (1940) RP1319.

[26] M. Harris and A. Sookne, J. Research NBS **26,** 289 (1941) RP1376.

WASHINGTON, December 9, 1948.

U. S. Department of Commerce
National Bureau of Standards

Research Paper RP2002
Volume 43, July 1949

Part of the Journal of Research of the National Bureau of Standards

Infrared Absorption Spectra of Cyclo-Hydrocarbons

By Earle K. Plyler and Nicolo Acquista

The infrared absorption spectra of 19 hydrocarbons have been measured in the 3.4-micron region, and the location of the two CH_2 vibrations has been determined. The vibrations occur at 2,854 and 2,927 cm^{-1} for the methylcyclohexane and 2,866 and 2,952 cm^{-1} for the methylcyclopentane. For cyclohexene the wave numbers of the bands are 2,845 and 2,934 cm^{-1}, and for cyclopentene they occur at 2,853 and 2,959 cm^{-1}.

The region from 2 to 4 microns has been measured for methylcyclohexane, ethylcyclohexane, *cis*-1,2-dimethylcyclohexane, *trans*-1,2-dimethylcyclohexane, and the corresponding cyclopentanes. Also, the spectra of cyclohexene and cyclopentene have been measured from 2 to 4 microns. The near infrared bands of methylcyclohexane, methylcyclopentane, and ethylcyclopentane have been classified as fundamentals and as combinations of long wavelength bands.

I. Introduction

The infrared absorption spectra of hydrocarbons have been measured for the purpose of identification by means of characteristic bands. Also, such data are useful as a measure of the purity of compounds. There have been some investigations in narrow regions of the spectrum, for example from 1 to 2 μ, to see if the differences in the spectra of various types of hydrocarbons were sufficient for identification. Liddel and Kasper [1] [1] were able to show certain changes in the spectra of groups such as the aromatic and aliphatic compounds in the regions of 1.1 and 1.7 μ. They found that primary, secondary, and tertiary linkages seemed to change the position of certain bands. There was some indication in their studies that the manner in which the CH_2 and CH_3 groups were arranged could be ascertained from the spectra. Rose [2] measured the absorption of 19 hydrocarbons in the near infrared, 9 of low molecular weight (C_5 to C_{10}) and 10 of high molecular weight (C_{24} to C_{32}). It was assumed by Rose that each CH, CH_2, and CH_3 group in the molecule would make a fixed contribution to the absorption in a band. By measuring the amount of absorption for a given hydrocarbon, the number of groups in each configuration could be determined. Experimentally he found that isomers did not have the same amount of absorption in the 1.7-μ region and that the assumption was not valid. Although the absorption of the 1.7-μ band, which is the harmonic of the CH stretching vibration at 3.4 μ, may roughly be considered independent of the molecule as a whole, the position and intensity of this band is somewhat influenced by the structure of the entire molecule.

Fox and Martin [3] investigated the absorption of several hydrocarbons in the region of the 3.4 μ. They were interested in the absorption of the CH_2 groups in different types of molecules such as benzyl alcohol, dioxane, and cyclohexane. The results showed that the CH_2 groups usually give rise to two bands in the 3.4-μ region and the CH groups produce one band. However, in some molecules, for example dioxane, there was an interaction between groups that gave rise to several bands. Fox and Martin also studied ethylene and showed that the CH_2 groups in that molecule had absorption bands in the 3.4-μ region that were similar to the bands of the larger molecules containing CH_2 groups. In molecules that have only CH_2 groups, the two bands were produced by the CH valence vibration with the hydrogens in and

[1] Figures in brackets indicate the literature references at the end of this paper.

out of phase. In cyclohexane, which has several CH_2 groups, the number of bands observed at 3.4 μ may be greater than two on account of interactions between the groups. The way in which the CH_2 group is linked in the molecule may produce changes in the location of the band. However, the mass of the other part of the molecule has small effect on the position of the two bands of the group. Molecules, which are not hydrocarbons but contain the CH_2 group, also have two bands in 3.4-μ region. The formaldehyde molecule has vibrations with smaller wave numbers than those found for CH_2 groups in hydrocarbons, but in fluorene, ($C_{13}H_{10}$), the wave numbers for the CH_2 groups are larger. This indicates that the binding forces in neighboring groups of the molecules have some effect on the vibrations observed in the 3.4-μ region.

The results that have just been described do not take into consideration the contribution of harmonic and overtone bands in the region of 3.4 μ. By measuring the region from 2 to 4.5 μ with good resolution, many bands of low intensity may be observed. The spectrum in this region may be sufficient for identification of the hydrocarbon, because some of the overtone bands will include the long wavelength bands that are commonly used for distinguishing one hydrocarbon from another.

The present investigation is primarily concerned with the absorption spectra of some cyclopentanes and cyclohexanes in the 3.4-μ region. The spectra of cyclopentene, cyclohexene, and some benzene derivatives have been measured for comparison with the other hydrocarbons. Two isomers, *cis*-1,2-dimethylcyclohexane and *trans*-1,2-dimethylcyclohexane have been studied in the region from 2 to 4 μ.

II. Experimental Results

A Perkin-Elmer infrared spectrometer with an LiF prism was used for the resolving instrument. All the substances measured were standard samples of the National Bureau of Standards. Two cells, 0.05 and 0.2 mm in thickness, were used for measuring the liquids. For the region of 3.4 μ, the hydrocarbons were diluted in CCl_4 so that an equivalent cell thickness of 0.0017 mm was obtained. Preliminary experiments showed that this was a suitable thickness of the material for resolving the main components of the band. It was also of importance to check whether any changes were brought about by the measurement of the hydrocarbons in solution rather than in the pure state. In order to make this comparison a small amount of the liquid was put in a cell, and then the cell was tipped so that the liquid formed a film over the inside surfaces of the cell. As the cell was of the closed type, the film did not evaporate rapidly, and the region from 3.3 to 3.6 μ could be measured under fairly constant conditions. The cell was only 0.05 mm in thickness, and the saturated vapor would contribute very little to the total absorption.

In figure 1, a is shown the absorption bands of diluted methylcyclohexane and in figure 1, b the absorption bands of a film of liquid methylcyclohexane. The comparison of a film of the liquid with a dilute solution of the same substance was made for several compounds. It was found that the wavelengths of the two major compounds checked in the two cases to better than 0.01 μ.

The spectra of methylcyclohexane and ethylcyclohexane are shown in figure 2. The two main components of the band at 3.415 and 3.508 μ check closely in position for these compounds, but there is a difference in intensity. The region from 2.5 to 2.85 μ is represented by a broken line. On account of the water vapor in the air path and an absorption band in the prism at 2.78 μ, bands of low intensity could not be accurately measured in this region. The presence of the methyl group in one molecule and the ethyl group in the other molecule produces changes in the spectra of the 2- to 4-μ region. This makes it possible to readily distinguish these two compounds from each other. The wavelengths of the observed bands are given in table 1.

TABLE 1. *Location of infrared absorption bands in the region from 2.2 to 4.2 microns*

Wavelength	Wave number	Wavelength	Wave number
Methylcyclopentane			
μ	cm^{-1}	μ	cm^{-1}
2.287	4,373	*3.387	2,952
2.305	4,338	*3.489	2,866
2.327	4,297	3.663	2,730
2.416	4,139	3.707	2,698
2.454	4,075	3.807	2,627
3.060	3,268	3.857	2,593
3.140	3,185	4.070	2,457

TABLE 1. *Location of infrared absorption bands in the region from 2.2 to 4.2 microns*—Continued

Wavelength	Wave number	Wavelength	Wave number
Ethylcyclopentane			
μ	cm^{-1}	μ	cm^{-1}
2.292	4,363	* 3.383	2,956
2.331	4,290	* 3.489	2,866
2.422	4,129	3.655	2,736
2.456	4,072	3.778	2,647
3.000	3,333	3.816	2,621
3.158	3,167	4.038	2,476
***cis*-1,2-Dimethylcyclopentane**			
2.268	4,409	* 3.487	2,868
2.297	4,354	3.655	2,736
2.317	4,316	3.678	2,719
2.397	4,172	3.725	2,685
2.451	4,080	3.768	2,654
3.031	3,299	3.814	2,622
3.143	3,182	3.853	2,595
* 3.382	2,957	4.032	2,480
.....	.....	4.132	2,420
Cyclopentene			
2.284	4,380	* 3.450	2,903
2.322	4,306	* 3.505	2,853
3.031	3,299	3.615	2,766
3.096	3,229	3.665	2,728
* 3.290	3,067	3.795	2,635
* 3.380	2,959	3.895	2,567
* 3.415	2,928	.....	.....
***trans*-1,2-Dimethylcyclopentane**			
2.268	4,409	* 3.145	3,180
2.303	4,342	* 3.387	2,952
2.326	4,299	3.489	2,866
2.346	4,263	3.617	2,765
2.397	4,172	3.664	2,729
2.454	4,075	3.704	2,700
2.486	4,023	3.805	2,628
3.006	3,327	3.873	2,582
3.039	3,291	4.078	2,452
.....	.....	4.156	2,406
Methylcyclohexane			
2.300	4,348	* 3.504	2,854
2.337	4,279	3.579	2,794
2.390	4,184	3.669	2,726
2.422	4,129	3.696	2,706
2.454	4,075	3.751	2,667
2.483	4,027	3.778	2,647
2.887	3,464	3.839	2,605
2.987	3,348	3.889	2,571
3.057	3,271	3.920	2,551
3.078	3,249	3.986	2,509
3.162	3,163	4.027	2,483
3.240	3,085	4.054	2,468
* 3.416	2,927	4.122	2,426
.....	.....	4.170	2,398

TABLE 1. *Location of infrared absorption bands in the region from 2.2 to 4.2 microns*—Continued

Wavelength	Wave number	Wavelength	Wave number
Ethylcyclohexane			
μ	cm^{-1}	μ	cm^{-1}
2.300	4,348	* 3.420	2,924
2.341	4,272	* 3.482	2,872
2.394	4,177	* 3.509	2,850
2.426	4,122	3.668	2,726
2.443	4,093	3.746	2,670
2.486	4,023	3.839	2,605
2.895	3,454	3.880	2,577
2.949	3,391	3.940	2,538
2.979	3,357	4.029	2,482
* 3.170	3,155	4.126	2,424
* 3.575	2,667	4.174	2,396
* 3.377	2,961	.....	.....
Cyclohexene			
2.300	4,348	* 3.500	2,857
2.317	4,316	* 3.515	2,845
2.334	4,284	3.595	2,782
2.381	4,199	3.635	2,751
2.422	4,128	3.657	2,734
2.486	4,023	3.680	2,717
2.527	3,957	3.720	2,688
2.952	3,388	3.751	2,665
3.021	3,310	3.778	2,647
3.109	3,216	3.819	2,619
3.258	3,069	3.873	2,581
* 3.295	3,035	3.946	2,534
* 3.408	2,934	3.978	2,514
* 3.452	2,897	4.034	2,478
***cis*-1,2-Dimethylcyclohexane**			
2.268	4,409	3.639	2,748
2.298	4,352	3.667	2,727
2.336	4,281	3.714	2,693
2.390	4,184	3.753	2,665
2.445	4,090	3.839	2,605
2.480	4,032	3.845	2,601
3.034	3,296	3.907	2,560
3.083	3,244	3.944	2,535
* 3.380	2,959	3.995	2,503
* 3.418	2,926	4.048	2,470
* 3.485	2,869	4.107	2,435
* 3.504	2,854	.....	.....
***trans*-1,2-Dimethylcyclohexane**			
2.294	4,359	3.632	2,753
2.337	4,279	3.649	2,740
2.387	4,189	3.663	2,730
2.406	4,156	3.684	2,714
2.429	4,117	3.702	2,701
2.453	4,077	3.738	2,675
2.477	4,037	3.803	2,630
2.874	3,479	3.839	2,605
2.963	3,375	3.851	2,597
3.075	3,252	3.907	2,560
3.160	3,165	3.957	2,527
3.203	3,122	3.977	2,514
* 3.387	2,952	4.062	2,462
* 3.422	2,922	4.138	2,417
* 3.486	2,869	4.170	2,398
* 3.506	2,852	.....	.....

* Values determined from observation in CCl_4.

839743—49——4

In figure 3 the spectra of two isomers, *cis*-1,2-dimethylcyclohexane and *trans*-1,2-dimethylcyclohexane are shown. The spectral region from 3.0 to 4.2 μ is sufficient to show differences in the combination bands of these materials. However, the spectra from 3.35 to 3.55 μ, curve a, are almost alike. These compounds have been measured [4] with a rock-salt prism from 2 to 15 μ, and several of the bands in the 7- to 15-μ region may be used for identification. With the lower resolution of the rock-salt prism in the 3-μ region, many of the low intensity bands are not observed. The results obtained with an LiF prism are more accurate in near infrared region.

In figure 4 the comparison of the spectra of methylcyclopentane and ethylcyclopentane is shown. The two CH_2 vibrations are well defined at 3.38 and 3.49 μ, and the vibration with greater wave number has a greater intensity. The two insert curves, a, from the two compounds are similar. The CH_2 vibrations in the cyclopentanes are located at shorter wavelengths than are observed in the cyclohexanes. The change in wavelength, about 0.03 μ, is sufficient to distinguish between these groups of compounds. The general pattern of the spectra from 2 to 4.2 μ is the same for methylcyclopentane and ethylcyclopentane, but a difference in the position of the small bands can be observed. The list of the bands observed for these two compounds is given in table 1.

The spectra of *cis*-1,2-dimethylcyclopentane and *trans*-1,2-dimethylcyclopentane are shown in figure 5. The spectra of the two dimethylcyclopentanes are different from each other and from the methylcyclopentane. The two CH_2 bands in the region of 3.4 μ overlap the two stretching vibrations of the methyl groups, and these bands cannot be resolved as was done in the spectra of the methylcyclohexanes. The two CH_2 vibrations have wave numbers of 2,957 and 2,868 cm^{-1} for the *cis* compound, and 2,952 and 2,866 cm^{-1} for the *trans* compound. The locations of the bands in the 2- to 4-μ region are listed in table 1.

In figure 6 the spectra are shown of cyclohexene and cyclopentene. The absorption bands are listed in table 1. These molecules have one CC double bond and two CH groups. The CH vibrations produce the strong band at 3.26 μ in the spectrum of cyclopentene. In figure 7 the 3.4-μ region is shown in greater detail, and the CH vibration for cyclohexene falls at 3.30 μ. The CH_2 vibrations of cyclohexene occur at longer wavelengths than the vibrations of cyclopentene. Cyclohexene vapor shows intense bands at 3.42 and 3.52 μ. These values correspond closely with the wavelengths observed for the solution. Almost all of the bands observed in the vapor have *P*, *Q*, and *R* branches, and with low resolution it is difficult to determine the center of the band.

In figure 8 a comparison is made of the absorption spectra of methylcyclopentane, *trans*-1,2-dimethylcyclopentane, and *cis*, *cis*, *trans*-1,2,4-trimethylcyclopentane. The two main bands at 3.385 and 3.49 μ occur nearly in the same position for the three compounds, but the small bands between these two become more pronounced as the number of methyl groups increases.

In figure 9 the observations for the 3.4-μ region are represented for eight hydrocarbons. The spectrum of isopropylcyclopentane does not show the small bands that are present in isopropylcyclohexane. This is caused by the overlapping of the CH_2 bands, which occur at shorter wavelengths in cyclopentanes. The other six hydrocarbons show the contrast between benzene

TABLE 2. *Location of infrared absorption bands in the region from 3.2 to 3.6 microns*

(Values determined from observations in CCl_4)

Wavelength	Wave number	Wavelength	Wave number	Wavelength	Wave number
Isopropylcyclopentane		*n*-Butylcyclohexane		*ter*-Butylbenzene	
μ	cm^{-1}	μ	cm^{-1}	μ	cm^{-1}
3.387	2,952	3.384	2,955	3.265	3,063
3.490	2,865	3.423	2,921	3.303	3,028
		3.488	2,867	3.374	2,964
Isopropylcyclohexane		3.509	2,850	3.411	2,932
				3.495	2,861
3.384	2,955	*sec*-Butylbenzene			
3.422	2,922			*ter*-Butylcyclohexane	
3.456	2,894				
3.510	2,849	3.302	3,028	3.412	2,931
		3.376	2,962	3.410	2,849
n-Butylbenzene		3.418	2,926		
		3.484	2,870	*cis-cis-trans*-1,2,4-Trimethylcyclopentane	
3.242	3,084	*sec*-Butylcyclohexane			
3.264	3,064				
3.304	3,027	3.378	2,960		
3.382	2,957	3.419	2,925	3.386	2,953
3.416	2,927	3.484	2,870	3.418	2,926
3.488	2,868	3.508	2,851	3.450	2,899
3.503	2,855			3.489	2,866

derivatives and cyclohexane derivatives. The three cyclohexanes, *n*-butyl, *sec*-butyl, and *tert*-butyl are much alike in their spectra. The three butyl benzenes show marked contrasts in their spectra. The benzenes are less absorbing in this region than the cyclohexanes, and it is possible to see the effect of the butyl compounds more readily. The band at 3.30 μ is characteristic of the CH vibration and does not appear in the cyclohexane derivatives. The positions of these bands are listed in table 2.

III. Discussion of Results

The experimental results that have been obtained show that the wavelengths of the two CH_2 stretching vibrations are influenced by the type of the molecule in which they are included. For example, in methylcyclohexane the two bands are located with wave numbers 2,854 and 2,927 cm^{-1}, whereas the corresponding bands for methylcyclopentane have values 2,866 and 2,952 cm^{-1}.

These changes in the positions of the bands in the cyclopentanes and cyclohexanes are produced by differences in the skeletal structure. Eight cyclohexanes have been measured in the 3,200-cm^{-1} region, and the positions of the two bands vary about 4 cm^{-1} or less from each other. This is almost within experimental error, which is about 2 cm^{-1}. With higher resolution, no doubt, changes in their positions could be detected, but with a prism instrument it would not be feasible to use these bands as a method of distinguishing one cyclohexane from another.

Six cyclopentanes have been measured, and the values for the two CH_2 vibrations fall at about 2,866 and 2,952 cm^{-1}. There is little variation from these values by any of the compounds. Because of the presence of CH_3 groups, there are other bands in the 3.4-μ region. In some cases the CH_3 bands may fall on the side of the CH_2 bands and cause a slight change in their position. The CH_2 vibrations in the cyclohexanes occur at longer wavelengths than in the cyclopentanes. The CH_3 bands are not entirely overlapped in methylcyclohexane and can be observed at 2,952 and 2,872 cm^{-1}.

In addition to CH, CH_2, and CH_3 stretching vibrations, which occur in the 3.4-μ region, there are combination bands that are located in this region. Twenty-seven bands have been observed in the spectrum of methylcyclohexane in the region from 2.25 to 4.50 μ. In the region of 3.4 μ the intense bands probably mask low intensity bands. The classification of the bands in this region has been made by the use of the observed wavelengths of the methylcyclohexane spectrum [4]. The results are tabulated in table 3. Several strong

TABLE 3. *Combination bands in the near infrared of methylcyclohexane*

Term	Wave number		Wave length observed
	Calculated	Observed	
	cm^{-1}	cm^{-1}	μ
ν_1	.....	442	22.60
ν_2	.....	547	18.29
ν_3	.....	607	16.48
ν_4	.....	843	11.86
ν_5	.....	872	11.47
ν_6	.....	910	10.99
ν_7	.....	967	10.34
ν_8	.....	1,093	9.15
$\nu_1+\nu_3$	1,049	1,033	9.68
ν_9	.....	1,167	8.57
ν_{10}	.....	1,248	8.01
$\nu_1+\nu_4$	1,285	1,263	7.92
$\nu_1+\nu_5$	1,314	1,305	7.66
$\nu_1+\nu_6$	1,352	1,346	7.43
$\nu_2+\nu_4$	1,390	1,364	7.33
ν_{11}	.....	1,376	7.27
ν_{12}	.....	1,458	6.86
$2\nu_6$	1,820	1,799	5.56
$\nu_1+\nu_{11}$	1,818	.....	.....
$\nu_2+\nu_{11}$	1,923	1,901	5.26
$\nu_1+\nu_1+\nu_3$	1,921	.....	.....
$\nu_3+\nu_9$	2,039	2,016	4.96
$\nu_7+\nu_9$	2,134	2,123	4.71
$\nu_1+\nu_4+\nu_6$	2,195	2,174	4.60
$\nu_9+\nu_{11}$	2,286	2,268	4.41
$\nu_1+\nu_3+\nu_7$	2,281	.....	.....
$\nu_7+\nu_{12}$	2,425	2,398	4.170
$\nu_1+\nu_2\nu_{11}$	2,425	.....	.....
$\nu_1+\nu_6+\nu_8$	2,445	2,426	4.122
$2\nu_{10}$	2,496	2,483	4.027
$\nu_9+\nu_{12}$	2,625	2,605	3.839
$\nu_{10}+\nu_{11}$	2,624	.....	.....
$\nu_1+\nu_3+\nu_7$	2,682	2,667	3.751
$\nu_1+\nu_8+\nu_7$	2,720	2,705	3.696
$2\nu_{11}$	2,752	2,726	3.669
$\nu_1+\nu_9+\nu_{12}$	2,810	2,794	3.579
ν_{13}	.....	2,854	3.504
ν_{14}	.....	2,927	3.416
$\nu_1+2\nu_{11}$	3,194	3,163	3.162
$\nu_1+\nu_{13}$	3,296	3,271	3.057
$\nu_2+2\nu_{11}$	3,299	.....	.....
$\nu_1+\nu_{14}$	3,369	3,348	2.987
$\nu_2+\nu_{14}$	3,474	3,464	2.887
$\nu_1+\nu_3+\nu_7+\nu_{11}$	4,058	4,029	2.483
$\nu_9+\nu_{14}$	4,094	4,075	2.454
$2\nu_{11}+\nu_{12}$	4,210	4,184	2.390
$\nu_{11}+\nu_{14}$	4,303	4,279	2.337
$\nu_{12}+\nu_{14}$	4,385	4,348	2.300

fundamental bands of methylcyclohexane, such as ν_6, ν_7, ν_9, and ν_{11} were found to give combination wave numbers that agreed well with observed bands. In each case the experimental value was about 25 cm^{-1} less than the calculated value. Because of higher order terms, the combination bands occur at longer wavelengths than would be expected by considering the position of the band to be the sum of the wave numbers of two fundamental bands. By the use of several of the more intense bands, it was found that the calculated values would be in error by about 25 cm^{-1} because of neglecting the anharmonicity of the combination bands. In assigning the weaker bands the agreement was considered good when the calculated values were greater than the observed values by 15 to 35 cm^{-1}.

The spectra of methylcyclopentane and ethylcyclopentane contain a number of bands in the 2- to 4-μ region, but the number is not as great as found for methylcyclohexane. Some of these bands have been classified, and the results are tabulated in tables 4 and 5. The wave numbers of the fundamental bands are taken from previous measurements [4, 5]. The long wavelength fundamental bands are not known, but they are usually of low intensity and do not produce strong bands in combination.

Two compounds, cyclohexene and cyclopentene, contain CH_2 groups and have a skeletal structure similar to that of the cyclohexanes and cyclopentanes respectively. The observed spectra show three strong bands with several weaker bands for each substance. In the spectrum of cyclohexene the band at 3,035 cm^{-1} arises from the CH vibration, and the corresponding vibration in cyclopentene is at 3,067 cm^{-1}. The CH_2 vibrations are somewhat modified by the CC double bond. The two bands are observed at 2,845 and 2,934 cm^{-1} in cyclohexene and 2,853 and 2,959 cm^{-1} in cyclopentene. The two components of the CH_2 vibrations of cyclohexene are separated by 89 cm^{-1}, and the separation is 73 cm^{-1} for the two bands in the cyclohexanes. The separation for the corresponding bands in cyclopentene and the cyclopentanes is 107 and 87 cm^{-1}, respectively.

The position of the CH_2 vibrations is dependent on the skeletal structure of the molecule. This can be seen more readily by comparing CH_2 bands in other compounds that have different molecular structures. The compounds included in addition to those reported in this paper are formaldehyde [6] ketene [7, 8], cyclohexane [6], cyclopropane [6], and propylene [6]. The antisymmetrical vibration of the CH_2 group, occurring when the two hydrogens are out of phase, has a larger wave number for all these compounds. In table 6 is given the value for the two CH_2 bands of these substances and the difference in wave numbers between the two modes of vibration of each substance. From this table it is seen that the vibra-

TABLE 4. *Combination bands in the near infrared of methylcyclopentane*

Term	Wave number		Wavelength observed	Term	Wave number		Wavelength observed
	Calculated	Observed			Calculated	Observed	
	cm^{-1}	cm^{-1}	μ		cm^{-1}	cm^{-1}	μ
ν_1	...	431	23.22	$2\nu_5$	2,702	2,698	3.707
$2\nu_{11}$	862	842	11.87	$2\nu_6$	2,754	2,730	3.663
ν_2	...	902	11.09	$\nu_4+\nu_7$	2,753	...	....
ν_3	...	1,139	8.78	ν_8	...	2,866	3.489
ν_4	...	1,295	7.72	ν_9	...	2,952	3.387
ν_5	...	1,351	7.40	$\nu_1+\nu_8$	3,297	3,268	3.060
ν_6	...	1,377	7.26	$\nu_2+\nu_9$	3,383	3,356	2.979
ν_7	...	1,458	6.86	$\nu_3+\nu_9$	4,091	4,075	2.454
$\nu_2+\nu_{11}$	2,197	2,179	4.59				
				$\nu_4+\nu_8$	4,161	4,139	2.416
				$\nu_7+\nu_8$	4,324	4,297	2.327
$\nu_3+\nu_{11}$	2,490	2,457	4.070	$\nu_6+\nu_9$	4,329	...	....
$\nu_4+\nu_{11}$	2,646	2,627	3.807	.....	...	...	....

TABLE 5. *Combination bands in the near infrared of ethylcyclopentane*

Term	Wave number		Wavelength observed	Term	Wave number		Wavelength observed
	Calculated	Observed			Calculated	Observed	
	cm^{-1}	cm^{-1}	μ		cm^{-1}	cm^{-1}	μ
ν_1	...	768	13.02	$\nu_5+\nu_7$	2,667	2,647	3.778
ν_2	...	931	10.74	$2\nu_7$	2,666	....	....
ν_3	....	1,020	9.80	$\nu_3+\nu_9$	2,750	2,736	3.655
ν_4	....	1,131	8.84	$2\nu_8$	2,754	....	....
ν_5	...	1,290	7.75	ν_{10}	....	2,866	3.489
ν_6	....	1,313	7.61	ν_{11}	....	2,956	3.383
ν_7	....	1,333	7.50	$\nu_1+\nu_{11}$	4,087	4,072	2.456
ν_8	....	1,377	7.26	$\nu_2+\nu_{10}$	4,156	4,129	2.422
ν_9	....	1,460	6.85	$\nu_9+\nu_{10}$	4,326	4,280	2.331
$\nu_1+\nu_9$	2,081	2,066	4.84	.....	....	....	....
				.....	....	....	....
$\nu_2+\nu_9$	2,244	2,227	4.49	.....	....	....	....
$\nu_3+\nu_9$	2,480	2,476	4.038	.....	....	....	....
$2\nu_9$	2,626	2,621	3.816	.....	....	....	....

tions of the CH_2 groups are not fixed values but vary with the type of the molecule.

In *n*-butylbenzene the three CH_2 groups have bands at 3.42 μ and 3.50 μ, which are close to the positions for the bands in *n*-butylcyclohexane. These two bands become of low intensity in the spectrum of *sec*-butylbenzene. The band at 3.30 μ is produced by the CH vibration of the benzene ring. This band checks closely in position with the CH band in cyclohexene.

TABLE 6. *Location of* CH_2 *vibrational bands for different types of molecules*

Compound	CH_2 bands in infrared	Difference
	cm^{-1}	
Formaldehyde	2,874	94
	2,780	
Ketene	3,162	96
	3,066	
Cyclopropane	3,103	79
	3,024	
Propylene	3,081	109
	2,972	
Cyclohexane	2,927	76
	2,851	
Cyclohexane (derivatives of)	2,927	73
	2,854	
Cyclopentane (derivatives of)	2,952	86
	2,866	
Cyclohexene (derivatives of)	2,934	89
	2,845	
Cyclopentene (derivatives of)	2,959	106
	2,853	

Many of these compounds that have been studied in the 3.4-μ region have been measured previously in the region of 1.15 and 1.7 μ by Lidell and Kasper [1] and by Rose [2]. The fundamental band and the harmonics should be related by the equation $\nu_n = \nu_o n(1+nx)$, where n is the number of the harmonic and x is the anharmonic correction factor. It was found that considerable differences in the value of ν_o and x, were obtained, depending on which two of the observed bands were used in the equation. The discrepancy in the constants was produced by experimental error in the observations. For an error of 0.01 μ the wave number error would be 75 cm^{-1} at 1.15 μ, 35 cm^{-1} at 1.70 μ, and 9 cm^{-1} at 3.40 μ. Because the uncertainty of the wave numbers in the 3.4-μ region is much smaller than in the 1.15- and 1.7-μ regions, and with the high resolution of LiF prism, this region is the best suited for the observation of the CH_2 valence vibrations.

Fox and Martin [3] used a grating spectrometer, with good resolving power, to investigate a group of hydrocarbons in the 3.4-μ region. Cyclopentene and some of the cyclohexanes were included in their work, and the positions of the bands observed by us check to 0.01 μ or better with their values. The present work includes a wider region of the spectrum than that used by previous authors. For ten of the hydrocarbons, the region from 2 to 4 μ has been included in order to show that many combination bands overlap the 3.4-μ region. Consequently, the intensities of fundamental bands could not be used for quantitative determination of the number of CH, CH_2, and CH_3 groups. By reducing the temperature of the samples, the band widths can be decreased and the chance of overlapping by combination bands becomes less likely. The cooling method offers some promise of providing a new technique for quantitative analysis in the region of the fundamental vibration.

In conclusion it should be pointed out that the region from 7 to 15 μ is better suited for infrared analysis than the detailed study of the 3.4-μ region. However, the measurement of the CH_2 vibrations in different molecules reveals the presence of different force constants for the various types of skeletal structures.

IV. References

[1] U. Liddel and C. Kasper, BS J. Research **11,** 599 (1933) RP 610.

[2] F. W. Rose, Jr., J. Research NBS **19,** 143 (1937) RP1017.

[3] J. J. Fox and A. E. Martin, Proc. Roy. Soc. (London) [A] **167,** 257 (1938).

[4] E. K. Plyler, R. Stair, and C. J. Humphreys, J. Research NBS **38,** 211 (1947).

[5] Infrared Spectrograms, No. 380, API Project, No. 44 (National Bureau of Standards).

[6] G. Herzberg, Infrared and Raman spectra of polyatomic molecules (D. Van Nostrand Co., Inc., New York, N. Y., 1945).

[7] F. Halverson and V. Z. Williams, J. Chem. Phys. **15,** 552 (1947).

[8] W. R. Harp, Jr., and R. S. Rasmussen, J. Chem. Phys. **15,** 778 (1947).

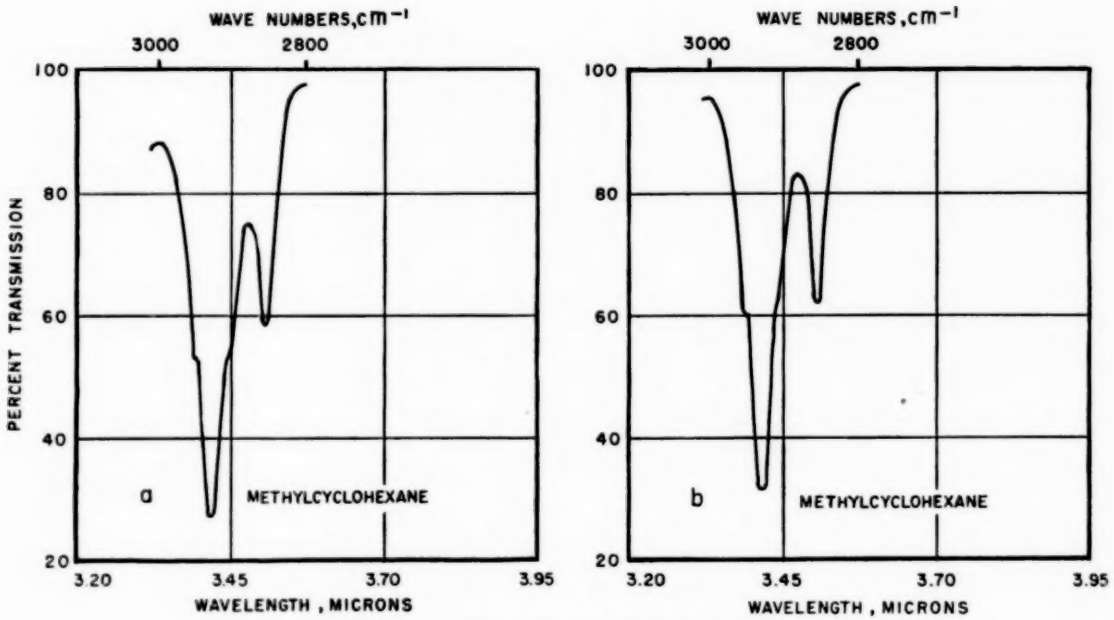

FIGURE 1. *Infrared absorption in the 3.4-μ region*

Curve a, Methylcyclohexane diluted in CCl_4 with an equivalent cell thickness of 0.0017 mm; b, the infrared absorption spectrum of methylcyclohexane for a liquid film on rock-salt windows.

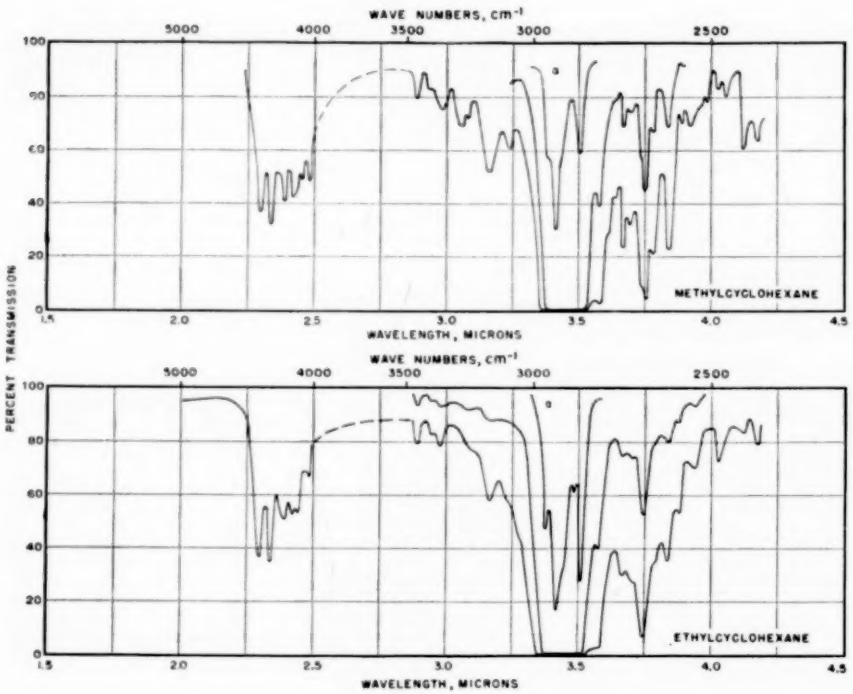

FIGURE 2. *Infrared absorption spectra of methylcyclohexane and ethylcyclohexane from 2 to 4.2 μ.*

The cell thicknesses for the liquids were 0.05 and 0.2 mm. Insert (a) represents the spectra when the substance is diluted in CCl_4. The equivalent cell thickness was 0.00.7 mm.

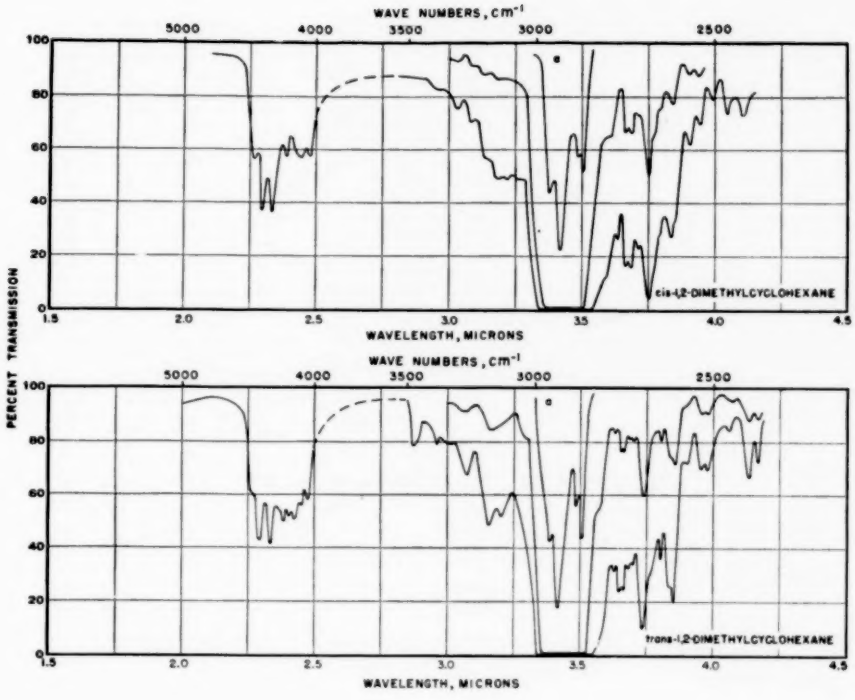

FIGURE 3. *Infrared absorption spectra of cis-1,2-dimethylcyclohexane and trans-1,2-dimethylcyclohexane.*

The cell thicknesses are the same as those in figure 2.

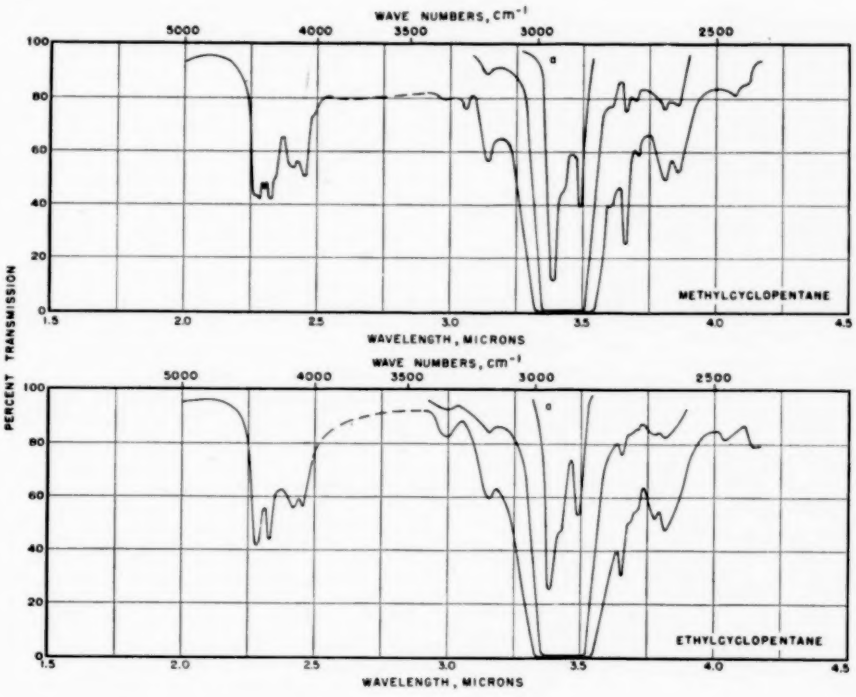

FIGURE 4. *Infrared absorption spectra of methylcyclopentane and ethylcyclopentane.*

The cell thicknesses are the same as those in figure 2.

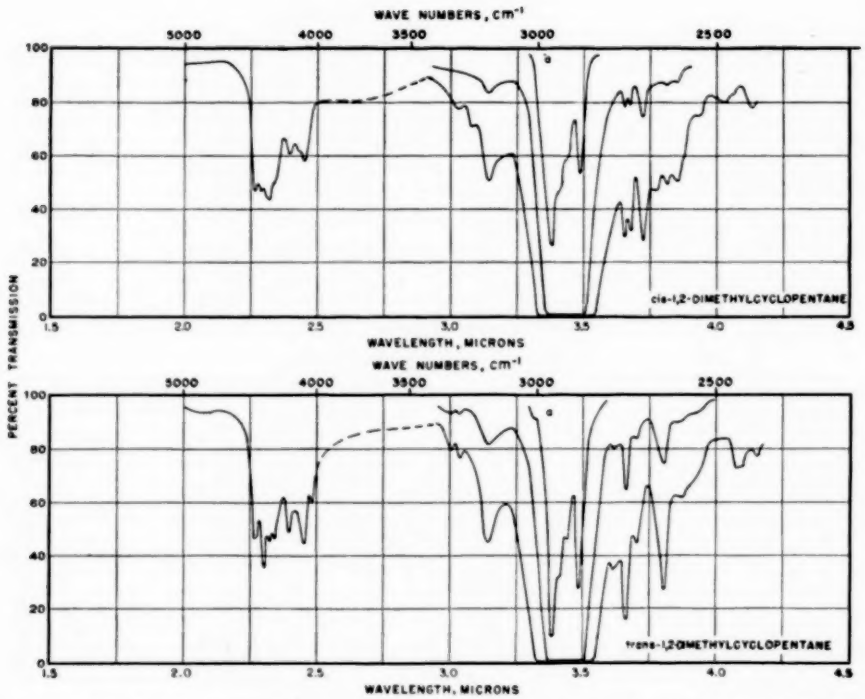

FIGURE 5. *Infrared absorption spectra of cis- 1,2-dimethylcyclopentane and trans-1,2-dimethylcyclopentane.*

The cell thicknesses are the same as those in figure 2.

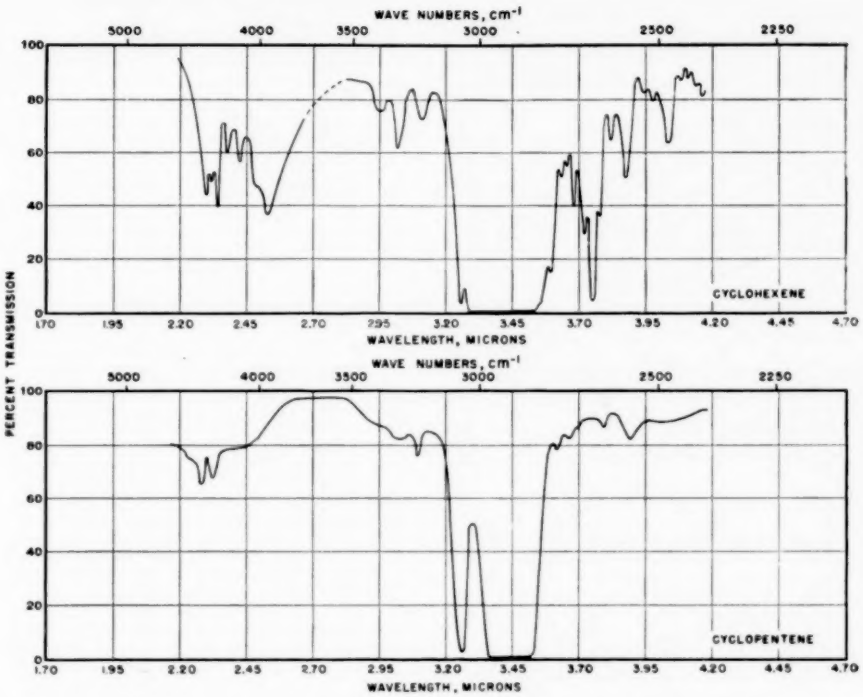

FIGURE 6. *Infrared absorption spectra of cyclohexene and cyclopentene.*

The cell thickness is 0.2 mm for cyclohexene and 0.05 mm for cyclopentene.

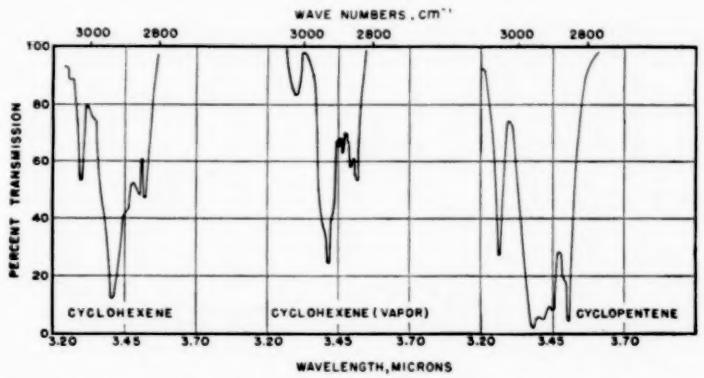

FIGURE 7. *Infrared absorption spectra of cyclohexene, cyclohexene vapor, and cyclopentene in the region of 3.4 μ.*

The two liquids were diluted in CCl_4. The equivalent cell thickness was 0.0017 mm.

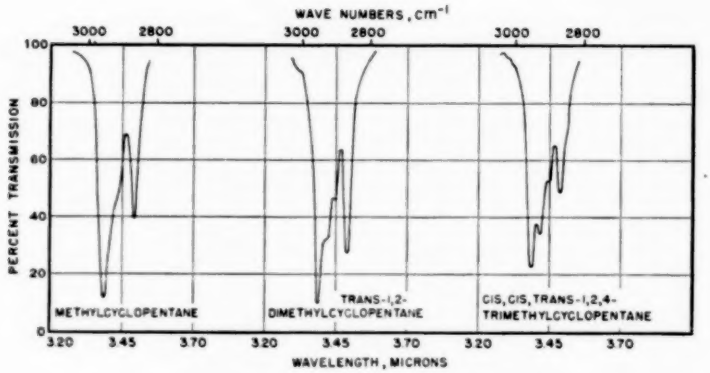

FIGURE 8. *A comparison of the infrared absorption spectra of methycyclopentane, trans-1,2-dimethylcyclopentane, and cis, cis, trans-1,2,4-trimethylcyclopentane in the 3.4-μ region.*

All three liquids were diluted in CCl_4 so that the equivalent cell thickness is 0.0017 mm.

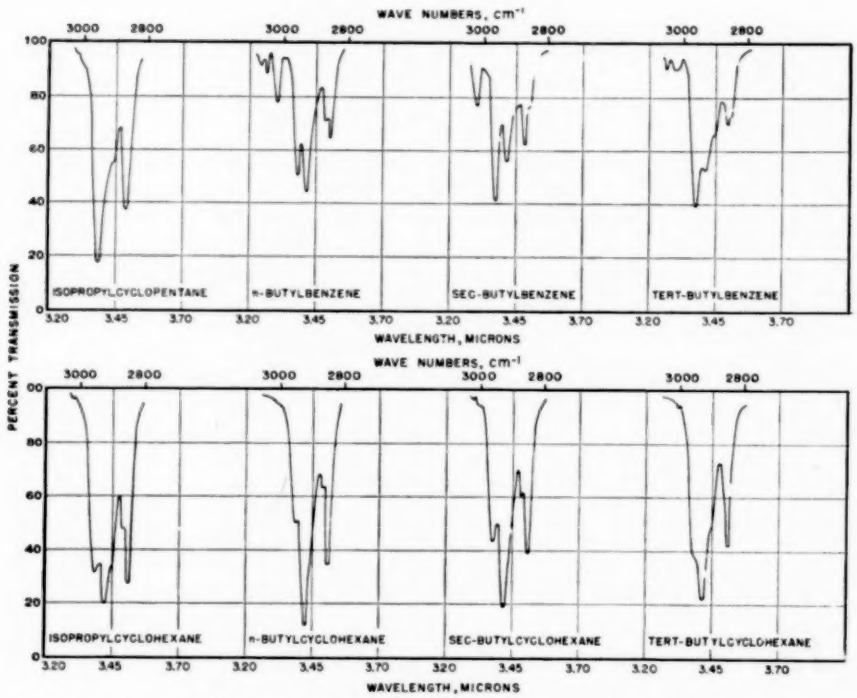

FIGURE 9. *A comparison of the infrared absorption spectra of some derivatives of cyclopentane, cyclohexane, and benzene in the 3.4-μ region.*

All of the liquids were diluted in CCl_4 so that the equivalent cell thickness is 0.0017 mm.

WASHINGTON, February 16, 1949.

U. S. Department of Commerce
National Bureau of Standards

Research Paper RP2003
Volume 43, July 1949

Part of the Journal of Research of the National Bureau of Standards

Low-Temperature Performance of Radiosonde Electric Hygrometer Elements[1]

By Arnold Wexler

The performance of radiosonde electric hygrometer elements was investigated in the temperature range from 0 to −40° C. It was found that an element indicated relative humidity with an average deviation of ±2.4-percent relative humidity from the average calibration for all of the elements tested. The maximum deviation in indication of any element did not exceed 10.5-percent relative humidity. The lag in response was found to increase markedly with decrease in temperature, to depend upon the magnitude and direction of relative humidity change, and the relative humidity from which the change was made.

I. Introduction

In the meteorological sounding of the upper atmosphere by means of the radiosonde, the device generally used in this country for humidity measurement is the electric hygrometer developed by Dunmore.[2] In a radiosonde flight in the temperate zone, temperatures below 0° C may be encountered from the ground up during the winter months, whereas during the summer months, freezing temperatures usually exist above 18,000 feet. Since a flight may reach an elevation of 80,000 feet, the greater proportion of the ascent will be at low temperatures. Information on the characteristics of the electric hygrometer at temperatures below 0° C is therefore important. Glückauf[3] has reported both calibration and lag data on the coil type of electric hygrometer at low temperatures. Data at low temperatures on the flat-strip hygrometer element used in radiosondes are very meager. An investigation was therefore undertaken to determine the performance of the flat-strip electric hygrometer at low temperatures.

II. Description of Hygrometer

The hygrometer most readily available, and therefore used in this study, was one in current manufacture. This element, which is a modification of the original Dunmore design, and which is used by the Weather Bureau, Navy, and Army, is made by coating a flat strip of polystyrene base, 4 in. long and $\frac{5}{16}$ in. wide, with an electrolytic film of lithium chloride dissolved in polyvinyl acetate or polyvinyl chloride, and sputtering tin electrodes on the two long edges. The resistance between the electrodes varies with relative humidity. This resistance, operating in the relaxation oscillator circuit of the radiosonde transmitter, controls the value of the audiofrequency to which the carrier wave is modulated.

III. Experimental Procedure

An experimental procedure was adopted that would subject the element as far as practical to conditions simulating those encountered in a radiosonde flight. Standard equipment was employed. A radiosonde was utilized to transmit the response of the element to humidity changes; a radio receiver to detect the intelligence from the radiosonde transmitter; an electronic frequency meter and a recorder to automatically record the data in terms of audio frequency or recorder divisions. One recorder division was equal to 2 c/s.

The temperature circuit of the radiosonde was modified to provide an additional humidity circuit. A sequence switch that automatically changed the transmitted signal from one humidity circuit to the second humidity circuit to a reference

[1] This investigation was financially supported by the Bureau of Ships, Department of the Navy.

[2] F. W. Dunmore, J. Research NBS **20,** 723 (1938) RP1102; F. W. Dunmore J. Research NBS **23,** 701 (1939) RP1265; H. Diamond, W. S. Hinman, F. W. Dunmore, and E. G. Lapham, J. Research NBS **25,** 327 (1940) RP1329.

[3] E. Glückauf, Proc. Phys. Soc. (London) **58,** 344 (1947).

frequency and back to the first humidity circuit was connected to the radiosonde. The radiosonde was permitted to transmit a signal continuously, the duration of which was 23 sec on one humidity circuit, 22 sec on the other humidity circuit, and 15 sec on the reference frequency, a complete cycle lasting 60 sec.

Known humidities at constant temperature were obtained by utilizing the divided flow, low temperature humidity apparatus.[4] This equipment produced an air atmosphere whose relative humidity, with respect to ice, was known to an accuracy of 3 percent.

The test procedure employed was to insert one or two elements into the test chamber of the humidity apparatus which had been brought to and maintained at a desired temperature. Each element was removed from its sealed vial immediately before test and inserted into the test chamber of the apparatus at as low a relative humidity as could be measured and recorded. The air velocity in the test chamber was adjusted to 525 ft/min. The element was tested with its length vertical and air flowing parallel to the length. The element was subjected in discrete steps of 16.7 percent to increasing values of relative humidity up to 100 percent, and back again to the lowest relative humidity. The change from one value of relative humidity to another took 1 to 2 sec. The element was exposed to a relative humidity long enough for the recorded reading to become constant. A total of 29 elements were used in this investigation.

IV. Data and Results

The hygrometer was subjected to a humidity calibration at nominal temperatures of −1°, −10°, −20°, −30°, and −40° C. Four or more units were tested at each temperature, and each unit supplied the data for one humidity cycle at one temperature. These data were in terms of relative humidity versus recorder divisions. By applying the standard frequency-resistance relationship for radiosondes, which was found to apply to the radiosonde used, the data were converted into relative humidity versus resistance for each humidity element. These are tabulated in table 1.

[4] A. Wexler, J. Research NBS **40**, 479 (1948) RP1894.

The logarithms of the average resistance values from table 1 are plotted against the logarithms of the relative humidity in figure 1. In this graph only the values of resistance measured for increasing changes of relative humidity, that is, from low relative humidity to 100 percent, were used in order to eliminate hysteresis effects and reduce polarization and exposure effects as much as possible. A family of straight lines was obtained for values of relative humidity of 50 percent and above. Below 50 percent, there is a slight bow in the curves for −1.1° and −9.9° C, in the direction of higher resistance.

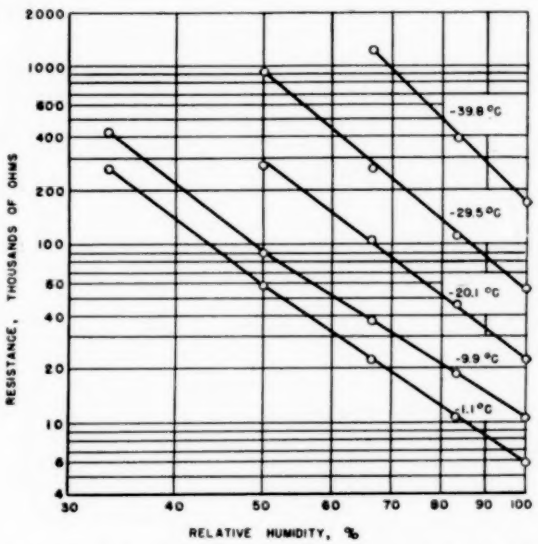

FIGURE 1. *Logarithm of average resistance of the electric hygrometer versus logarithm of relative humidity at low temperatures.*

By entering the curves of figure 1 with the resistances for each hygrometer element, as given in table 1, values of indicated relative humidity are obtained. The difference between this indicated relative humidity and the actual relative humidity may be considered a measure of the spread in indication to be expected from individual elements. The indicated relative humidity is the algebraic sum of the actual relative humidity and the difference. These differences are given in table 2 and show that the hygrometer at low temperatures will indicate the relative humidity with an average deviation of ±2.4-percent relative humidity from a mean calibration of all the

TABLE 1. *Low-temperature calibration—relative humidity versus resistance*

NBS No.	24	25	26	27	28	29	Average
Date of run	11-17-47	11-17-47	12-1-47	12-1-47	12-1-47	12-1-47	
Temperature, ° C.	−1.2	−1.2	−1.0	−1.0	−1.2	−1.2	−1.1
Relative humidity, %	Resistance, ohms						
33.3	177,000	387,000	177,000	280,000	282,000	279,000	262,000
50.0	52,300	70,500	53,000	57,500	.....	.....	58,300
66.7	20,700	27,000	20,700	22,500	.....	.....	22,700
83.3	11,500	11,500	10,400	11,200	.....	.....	11,100
100.0	6,100	6,200	5,600	6,450	6,450	6,400	6,200
83.3	11,300	11,200	9,900	10,700	.....	.....	10,800
66.7	20,900	27,000	20,000	23,200	.....	.....	22,800
50.0	54,300	74,000	51,000	60,500	.....	.....	60,000
33.3	180,000	394,000	158,000	334,000	271,000	269,000	268,000
NBS No.	1	2	3	4	.....	.....	.....
Date of run	6-19-47	6-19-47	6-23-47	6-23-47	.....	.....	.....
Temperature, ° C.	−9.4	−9.8	−19.2	−10.1	.....	.....	−9.9
33.3	272,000	455,000	520,000	455,000	.....	.....	425,000
50.0	65,000	99,000	102,000	94,000	.....	.....	90,200
66.7	31,200	38,000	44,000	39,900	.....	.....	38,300
83.3	17,700	18,200	21,500	19,900	.....	.....	19,300
100.0	9,800	10,300	11,900	10,800	.....	.....	10,500
83.3	14,800	17,000	20,100	18,700	.....	.....	17,600
66.7	28,000	38,800	42,500	39,000	.....	.....	37,300
50.0	61,000	103,000	101,000	93,000	.....	.....	89,500
33.3	250,000	500,000	520,000	430,000	.....	.....	425,000
NBS No	5	6	9	10	.....	.....	.....
Date of run	6-27-47	6-27-47	10-20-47	10-20-47	.....	.....	.....
Temperature, ° C	−19.7	−20.1	−20.4	−20.1	.....	.....	−20.1
50.0	210,000	192,000	226,000	500,000	.....	.....	282,000
66.7	94,000	91,000	93,000	149,000	.....	.....	107,000
83.3	42,000	42,500	43,000	57,000	.....	.....	46,100
100.0	21,200	23,200	22,900	26,200	.....	.....	23,400
83.3	40,000	41,500	56,000	53,500	.....	.....	47,700
66.7	93,000	88,500	156,000	139,000	.....	.....	119,000
50.0	255,000	175,000	510,000	465,000	.....	.....	351,000
NBS No	7	11	16	17	.....	.....	.....
Date of run	6-1-47	10-23-47	10-30-47	10-30-47	.....	.....	.....
Temperature, ° C	−29.7	−29.4	−29.2	−29.7	.....	.....	−29.5
50.0	880,000	950,000	1,400,000	500,000	.....	.....	935,000
66.7	275,000	310,000	293,000	197,000	.....	.....	269,000
83.3	103,000	125,000	111,000	106,000	.....	.....	111,000
100.0	51,000	60,000	54,500	52,500	.....	.....	54,000
83.3	107,000	117,000	162,000	117,000	.....	.....	126,000
66.7	279,000	271,000	570,000	260,000	.....	.....	345,000
50.0	770,000	830,000	2,000,000	710,000	.....	.....	1,080,000
NBS No.	8	12	13	14	15	.....	.....
Date of run	10-7-47	10-28-47	10-28-47	10-28-47	10-28-47	.....	.....
Temperature, ° C.	−40.2	−39.6	−39.6	−39.7	−39.7	.....	−39.8
66.7	1,130,000	930,000	880,000	1,100,000	930,000	.....	994,000
83.3	400,000	395,000	395,000	.....	.....	.....	397,000
100.0	182,000	170,000	159,000	162,000	192,000	.....	173,000
83.3	390,000	342,000	342,000	.....	.....	.....	358,000
66.7	1,130,000	780,000	725,000	700,000	770,000	.....	821,000

TABLE 2. *Difference between indicated and actual relative humidity at low temperature*

The indicated relative humidity is the algebraic sum of the actual relative humidity and the difference

NBS No. / Date of run / Temperature, ° C	24 11-17-47 −1.2	25 11-17-47 −1.2	26 12-1-47 −1.0	27 12-1-47 −1.0	28 12-1-47 −1.2	29 12-1-47 −1.2	Average −1.1
Actual relative humidity, %	Relative humidity difference, %						
33.3	+3.7	−3.7	+3.7	−0.7	−0.8	−0.7	±2.2
50.0	+1.7	−2.3	+1.5	+.2	.....	.....	±1.4
66.7	+2.0	−3.5	+2.0	+.3	.....	.....	±2.0
83.3	−1.0	−1.0	+1.5	−.3	.....	.....	±1.0
100.0	0.0	0.0	+3.0	−2.0	−2.0	−1.7	±1.4
83.3	−.8	−.3	+2.7	+0.9	.....	.....	±1.2
66.7	+1.8	−3.5	+3.2	−.5	.....	.....	±2.2
50.0	+1.0	−3.0	+2.1	−.2	.....	.....	±1.6
33.3	+3.6	−4.6	+4.9	−2.3	−0.5	−0.4	±2.7
NBS No. / Date of run / Temperature, ° C	1 6-19-47 −9.4	2 6-19-47 −9.8	3 6-23-47 −10.2	4 6-23-47 −10.1	.....	.....	..... / ..... / −9.9
33.3	+4.0	−0.8	−1.9	−0.7	.....	.....	±1.8
50.0	+5.7	−1.2	−1.4	−.8	.....	.....	±2.3
66.7	+3.8	−0.5	−1.5	−1.4	.....	.....	±1.8
83.3	+1.7	+.7	−3.5	−1.5	.....	.....	±1.8
100.0	+2.5	+1.0	−1.7	−0.5	.....	.....	±1.4
83.3	+6.5	+2.6	−1.8	+.2	.....	.....	±2.8
66.7	+6.6	−0.9	−2.7	−.9	.....	.....	±2.8
50.0	+6.9	−1.7	−1.3	−.5	.....	.....	±2.8
33.3	+4.9	−1.5	−1.9	−.3	.....	.....	±2.2
NBS No. / Date of run / Temperature, ° C	5 6-27-47 −19.7	6 6-27-47 −20.1	9 10-20-47 −20.4	10 10-20-47 −20.1	.....	.....	..... / ..... / −20.1
50.0	+4.2	+5.9	+3.2	−7.4	.....	.....	±5.2
66.7	+1.1	+1.8	+1.5	−6.7	.....	.....	±2.8
83.3	+1.6	+1.5	+0.7	−5.1	.....	.....	±2.2
100.0	+3.0	+0.2	+.7	−3.0	.....	.....	±1.7
83.3	+2.8	+2.2	−4.6	−3.5	.....	.....	±3.3
66.7	+1.3	+2.3	−7.7	−5.7	.....	.....	±4.2
50.0	+1.5	+7.5	−7.8	−3.5	.....	.....	±5.1
NBS No. / Date of run / Temperature, ° C	7 6-1-47 −29.7	11 10-23-47 −29.4	16 10-30-47 −29.2	17 10-30-47 −29.7	.....	.....	..... / ..... / −29.5
50.0	+0.4	−0.5	−4.8	+8.0	.....	.....	±3.4
66.7	+.6	−1.5	−0.5	+6.3	.....	.....	±2.2
83.3	+1.9	−2.0	+.2	+1.4	.....	.....	±1.4
100.0	+1.0	−3.0	−.7	0.0	.....	.....	±1.2
83.3	+0.9	−0.8	−7.0	−.6	.....	.....	±2.3
66.7	+.5	+1.0	−10.5	+1.3	.....	.....	±3.3
50.0	+2.3	+1.3	−8.6	+3.3	.....	.....	±3.9
NBS No. / Date of run / Temperature, ° C	8 10-7-47 −40.2	12 10-28-47 −39.6	13 10-28-47 −39.6	14 10-28-47 −39.7	15 10-28-47 −39.7	.....	..... / ..... / −39.8
66.7	−2.0	+1.3	+2.0	−1.4	+1.3	.....	±1.6
83.3	−1.3	−0.8	−0.8	.....	.....	.....	±1.0
100.0	−1.0	+.5	+2.0	+2.0	−2.2	.....	±1.5
83.3	−0.3	+2.1	+2.2	.....	.....	.....	±1.5
66.7	−2.0	+4.1	+5.3	+5.6	−4.1	.....	±4.2
.....	.....	.....	.....	.....	.....	.....	Mean ±2.4

elements tested. There is a tendency for these differences to be larger at the lower humidities and smaller at the higher humidities. The maximum difference did not exceed 10.5-percent relative humidity.

The dependence of the calibration upon temperature is given in tables 1 and 2 and figure 1. The curves in figure 1 essentially show that the primary effect of temperature is to produce a parallel displacement of the calibration, a higher humidity being indicated as the temperature is lowered. There also appears to be a small change in slope of calibration curve, but this is a secondary effect.

By interpolating values of resistance for relative humidities of 50, 60, 80, and 100 percent from figure 1, converting these into recorder divisions, and plotting them with curves redrawn from the manufacturer's calibration chart for the humidity element, a comparison between the calibration contained in this investigation and the manufacturer's calibration was obtained. This is shown in figure 2. From $-1°$ to $-40°$ C, the two calibrations agree within 5 to 7 percent.

In going through a cycle of increasing and then decreasing humidity, the elements, in general, exhibited hysteresis; the indicated relative humidities during the decreasing half of the cycle were sometimes greater and sometimes less than those measured during the increasing half of the cycle. See table 2 for the data. The magnitude of the differences between increasing and decreasing readings in some elements was 1-percent relative humidity or less; in other units it was observed to be considerably greater. One element (NBS No. 9) changed its indicated relative humidity reading by 11-percent relative humidity in going from an actual relative humidity of 50 to 100 percent and back to 50 percent. Several elements (NBS Nos. 10, 13, 14, 16, and 17) changed their readings by as much as 3- to 7-percent relative humidity.

The lag in response to changes in relative humidity was studied over the range of temperatures from -1 to $-40°$ C. The procedure followed was to shift from one relative humidity to another as rapidly as possible (1 to 2 sec), transmitting and recording a humidity signal for 23 sec during 1-min cycles. From the data thus obtained, the lag constant (the time required for 62 percent of the humidity change to occur) was computed.

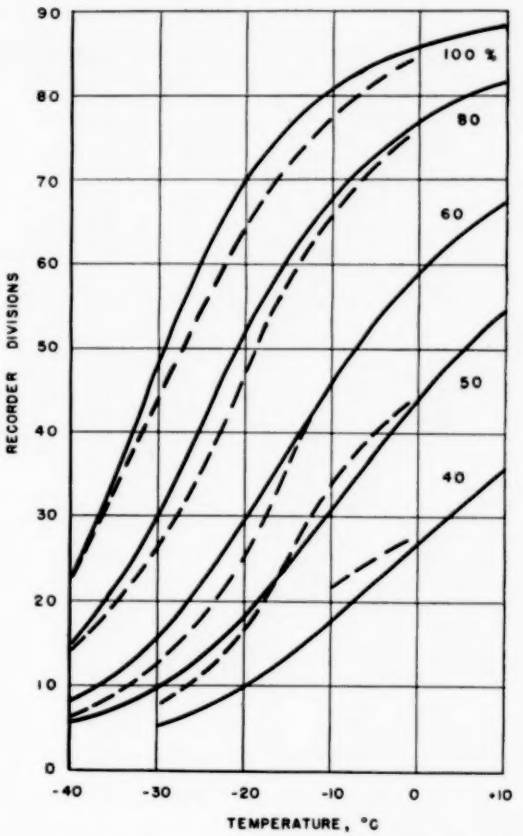

FIGURE 2. *Comparison of NBS and manufacturer's calibration of the electric hygrometer at low temperatures.*

Broken line is NBS calibration.

The time response of the hygrometer at low temperatures, although not a simple exponential function, still permitted the calculation of a lag constant with fair approximation. There was variation up to 30 percent in lag constant from element to element when subjected to the same relative humidity change at the same temperature. The lag was found to depend upon temperature, magnitude, and direction of the relative humidity change, and the relative humidity at which the change was made. Figure 3 shows the effect of these variables upon the lag constant. The lag constants used in figure 3 are the averages of two to eight values.

The lag constant was increased by (1) lowering the temperature, (2) increasing the magnitude of the humidity change, and (3) increasing the

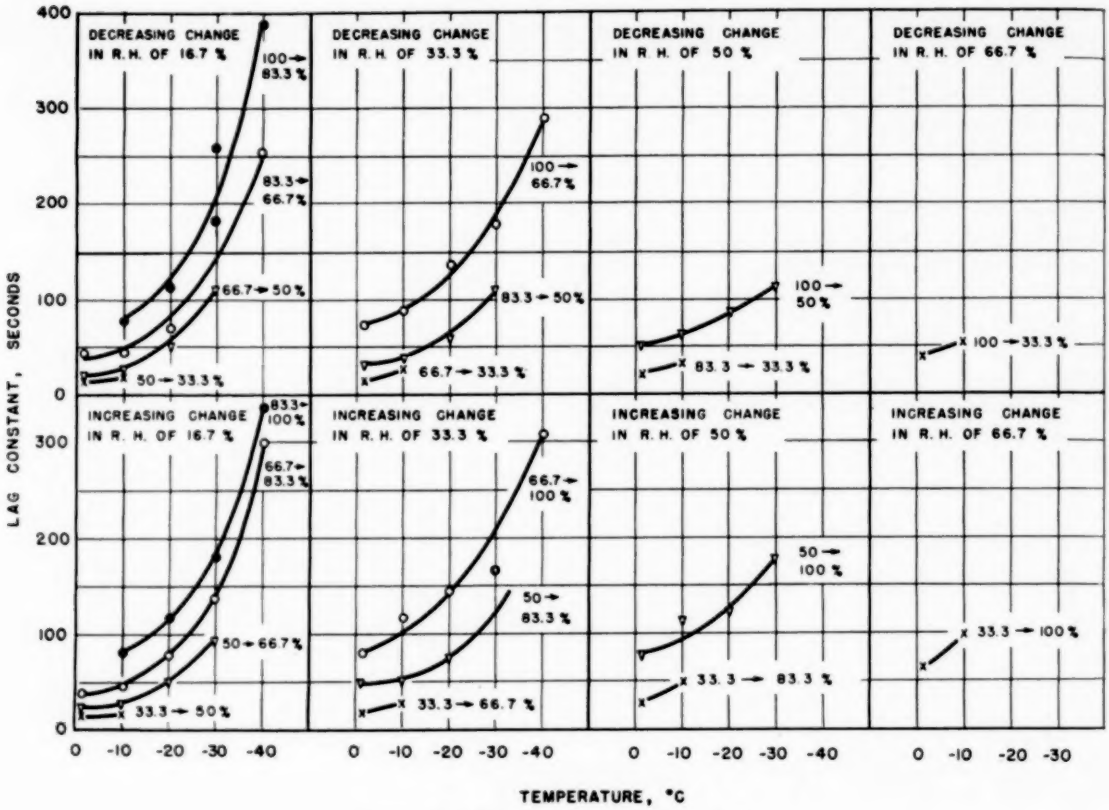

FIGURE 3. *Factors affecting the lag constant.*

The magnitude and direction of the change in relative humidity is shown on each curve.

initial value of the relative humidity from which the humidity change is made. For relative humidity changes of 16.7 and 33.3 percent, the lag constant was independent of direction, whereas for changes of 50 and 66.7 percent the lag constant in the increasing humidity direction was larger. The influence of these factors on the lag may also be demonstrated by time response curves for typical elements. In figure 4 is shown the time response of a single element at $-20°$ C to a sudden change in relative humidity of 16.7 percent at various initial relative humidities. The effect of magnitude of humidity change on the time response is shown in figure 5 for a typical element at $-20°$ C, in which discrete jumps of 16.7, 33.3, and 50 percent were made from an initial relative humidity of 50 percent. In figures 4 and 5, the humidity coordinate has been plotted on the basis of percentage change in relative humidity indication. Thus a total change of, say, 16.7-percent relative humidity is plotted on a scale of 100. An ordinate reading of 25 percent, therefore, represents 25 percent of the humidity change, that is, 25 percent of 16.7-percent or 4.2-percent relative humidity. The effect of temperature on the time responses is given in figure 6 for a relative humidity change of 66.7 to 83.3 percent. Each curve in this figure was obtained on a different unit.

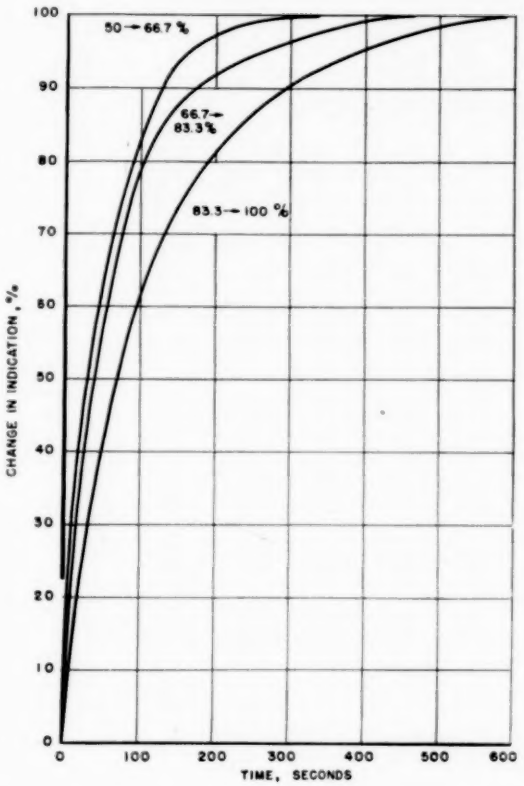

FIGURE 4. *Time response of a typical element at −20° C for a sudden change in relative humidity of 16.7 percent from various initial relative humidities.*

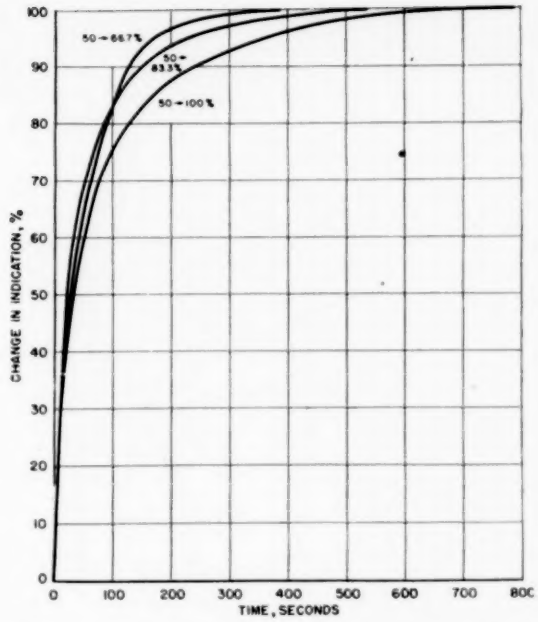

FIGURE 5. *Time response of a typical element at −20° C for discrete changes in relative humidity of 16.7, 33.3, and 50 percent made from an initial relative humidity of 50 percent.*

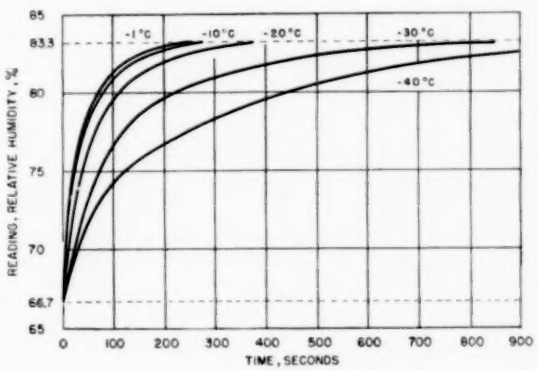

FIGURE 6. *Effect of temperature on the time response for a relative humidity change of 66.7 to 83.3 percent.*

V. Discussion and Summary

The continued subjection of the electric hygrometer element to the pulsating direct current of the radiosonde circuit has a deleterious effect on its life, primarily because of polarization. Hence in the tests described above, no unit was used more than once or for periods of time exceeding 2 hr. Under these conditions, exposure of a unit to a humidity of 100 percent did not appear to harm its performance. In general, the calibration and hysteresis characteristics of the hygrometer are satisfactory, except that the range does not extend to low humidities at the lower temperatures. The high lag and the complicated lag behavior of the hygrometer at low temperatures are its major limitations in radiosonde use. With the rates of balloon ascension now employed (1,000 ft/min) and the greater rates contemplated for future use, the lag of this hygrometer introduces a questionable factor in the interpretation of the humidity data.

U. S. Department of Commerce
National Bureau of Standards

Research Paper RP2004
Volume 43, July 1949

Part of the Journal of Research of the National Bureau of Standards

Refractive Index of Natural Rubber for Different Wavelengths [1]

By Lawrence A. Wood and Leroy W. Tilton

The refractive indices of a prism of natural rubber have been measured at five different wavelengths in the visible region by the use of a spectrometer. Values af the rate of change of index with temperature at each wavelength have been computed for the range 19.5° to 30.3° C. The Eykman equation in differential form is used to calculate the expansivity from the index and its rate of change with temperature. It is concluded that the two-constant Cauchy and Sellmeier dispersion equations are inadequate to represent the data. The dispersion observed for rubber is found to be essentially the same as that of hydrocarbons of similar structure but of low molecular weight.

I. Introduction

Published values of the refractive index of natural rubber, with very few exceptions, have been concerned with the value at the wavelength of the sodium *D*-lines (5,893 angstroms). This paper presents the results of measurements by the spectrometer method at this wavelength and four other wavelengths in the visible spectrum. Observations of the effect of temperature on index are also made. The constants of several different types of dispersion equations are evaluated in order to obtain an equation to represent the data. The dispersion observed for rubber is compared with that of hydrocarbons of low molecular weight.

The experimental portion of this work was conducted in 1939, and some of the results presented in graphical form in a general paper by one of the present authors [1].[2] The war prevented further work on this problem until recently.

II. Method of Measurement

The well-known and conventional method of measurement of refractive index by observations of the angle of minimum deviation produced by a prism of known angle does not seem to have been previously applied to rubber. This very direct method commonly yields results of higher precision and accuracy than can be obtained by available commercial refractometers since it is free from many of the complications and limitations inherent in comparison methods by critical-angle refractometry.

The rubber prisms required were made by molding the rubber between two plane glass plates inclined at an angle. A mold of 1-in., cold-rolled steel bars fastened together by bolts had an opening in which from one to six steel wedges could be placed, thereby fixing the angle of the prism at about 10° or some multiple of 10°. The rubber was molded against two glass plates 20 by 10 by 3.5 mm, which were left in position after the molding. The glass plates were special "plane parallels," that is, they had faces which were plane and parallel to each other to within a few wavelengths of light, as evidenced by comparison with optical flats and by examination of the interference phenomenon known as Haidinger's rings. Since their faces were parallel, the collimated light beam in its passage through the glass underwent no deviation or dispersion, and the observed refraction was due entirely to the wedge of rubber between the plates.

The pale crepe rubber was milled only very slightly, a few passages through the warm rolls

[1] This paper was presented on June 24, 1948, at the Rubber Technology Conference, London, England, sponsored by the Institution of the Rubber Industry. It has been published as paper No. 31, page 142, in the Proceedings of the Rubber Technology Conference; London 1948.

[2] Figures in brackets indicate the literature references at the end of this paper.

being found sufficient to make possible the production of a sheet about 1 cm in thickness and relatively free from entrapped air. A specimen was cut very roughly to shape and inserted in the mold just described. The molding was performed in a steam vulcanizing press at a temperature of 150° C for about 30 min.

When the prism was placed on the spectrometer table it was observed that the refracting angle showed a systematic change with time, a decrease of several minutes of angle a day being usually observed. This circumstance, arising no doubt from the plastic flow of the unvulcanized rubber, made it necessary to measure the prism angle before and after each set of measurements of the angle of deviation. The measurements of the refracting angle were made by means of reflections from the glass surfaces by the use of the spectrometer telescope, which was essentially autocollimating. As pointed out in a previous publication [2] the commonly used "split beam" method of measurement of refracting angle is never advisable. In the present instance additional difficulties would have arisen because of the finite thickness of the glass plates in contact with the rubber.

The spectrometer, which was manufactured by the Société Genevoise, has been described in detail in an earlier publication [3]. It has a circle 308 mm in diameter and is graduated to 5-min intervals. The use of micrometer microscopes allowed angles to be read to the nearest second.

The prism was set at the angle of minimum deviation in each case and the refractive index n computed from the usual spectrometer equation

$$n=\frac{\sin 1/2\ (A+D)}{\sin 1/2\ A}, \qquad (1)$$

where A is the refracting angle of the prism and D the angle of minimum deviation.

The light sources used were a sodium arc, a hydrogen discharge tube, and a mercury vapor lamp. The wavelengths of the spectral lines utilized are as follows:

Wavelength	Source	Designation
Angstroms		
6562.79	Hydrogen (alpha line)	*C*
5892.62	Sodium (weighted mean of two lines).	*D*
5460.74	Mercury	*e*
4861.33	Hydrogen (beta line)	*F*
4358.34	Mercury	*g*

The measurements with the *g*-line were made with more difficulty than those at longer wavelengths because of the greatly reduced transmission of light and the increased amount of light scattered by the sample in this region. Measurements of the transmission and scattering have been given in the earlier paper on the optical properties of rubber [1].

III. Results

Table 1 gives the results of the measurements made with prism 1, having a refracting angle near 20°. More measurements were made with this prism than with any of several others made since it appeared to possess the best optical properties. Measurements were made at all five wavelengths, and a stirred air-bath in a water-jacketed constant-temperature prism housing equipped with a thermostat was employed to obtain values at 19.5° and 39.3° C. The temperatures could be measured to the nearest hundredth of a degree. At least 1 hr at any given temperature was allowed to elapse before readings of index were made.

The data shown in table 1 for each wavelength were treated by the methods of linear regression, or "least squares," as outlined in books on statistical methods, for example, the text of Snedecor [4]. Inherent in this treatment is the usual assumption that there are no errors in the determination of the independent variable, the temperature in this case. By these methods values were obtained for the indices at 25° C, their standard deviations, and the rates of change of indices with temperature and their standard deviations.

TABLE 1. *Data obtained with prism 1*

1939	Angle			Temperature	n_C	n_D	n_s	n_F	n_g	$n_F - n_C$
	Degrees	Minutes	Seconds							
				°C						
July 17	20	55	25	28.7	1.51365	1.51737	.....	1.52679	.....	0.01314
18	20	52	15	28.0	1.51415	1.51793	.....	1.52732	.....	.01317
18	20	52	2	28.5	1.51409	1.51782	.....	.....	.....	.....
19	20	50	24	28.4	1.51390	1.51765	.....	1.52704	.....	.01314
19	20	50	26	28.5	1.51408	1.51773	.....	1.52725	.....	.01317
19	20	50	17	28.7	1.51411	1.51781	.....	1.52720	.....	.01309
Sept. 2	20	39	48	28.4	1.51407	1.51793	1.52121	1.52727	1.53510	.01320
5	20	39	30	26.5	1.51488	1.51868	1.52196	1.52809	1.53574	.01321
5	20	39	37	27.1	1.51475	1.51850	1.52179	1.52790	1.53557	.01315
6	20	39	31	26.9	1.51474	1.51847	1.52172	1.52791	1.53554	.01317
7	20	45	52	39.3	1.51013	1.51385	1.51707	1.52324	1.53088	.01311
7	20	45	52	39.3	1.51012	1.51382	1.51704	1.52318	1.53082	.01306
11	20	34	45	19.5	1.51737	1.52113	1.52440	1.53062	1.53835	.01325
11	20	34	45	19.5	1.51739	1.52111	1.52432	1.53066	1.53832	.01327
Computed from above data at.....				25.0	1.515345	1.519093	1.522415	1.528536	1.536292	.013193

Some observations were also made on prism 2, a prism of less satisfactory optical quality than prism 1. The results are shown in table 2. The second prism had a refracting angle near 10° and of course did not produce as large an angle of deviation as prism 1. Observations were made with this prism for the sodium *D*-lines, the hydrogen *C*-line, and the hydrogen *F*-line only. The temperature range covered was likewise much smaller than previously.

Table 3 presents a comparison of the results obtained on the two prisms. As would be expected, the standard deviations obtained with prism 2 are considerably larger than those found with prism 1. In the last column ($n_F - n_C$) is shown as calculated from the individual observations shown in tables 1 and 2. The desirability of computing the difference in this manner is demonstrated by the fact that the standard deviations for it are considerably smaller than those for the indices at the individual wavelengths.

The differences between the values of index at each wavelength for the two prisms can be seen to be of no significance when they are compared with

TABLE 2. *Data obtained with prism 2*

1939	Angle			Temperature	n_C	n_D	n_F	$n_F - n_C$
	Degrees	Minutes	Seconds					
				° C				
July 22	9	58	16	28.2	1.51420	1.51792	1.52735	0.01315
24	9	58	3	29.0	1.51408	1.51779	1.52722	.01314
25	9	57	59	29.0	1.51394	1.51766	1.52712	.01318
Aug. 17	10	4	35	32.3	1.51278	1.51647	1.52581	.01303
18	10	4	48	32.3	1.51286	1.51660	1.52601	.01315
18	10	4	47	32.3	1.51295	1.51659	1.52605	.01310
28	10	2	56	28.2	1.51438	1.51806	1.52743	.01305
30	10	2	36	27.2	1.51466	1.51836	1.52772	.01306
31	10	2	19	26.5	1.52482	1.51860	1.52794	.01312
Computed from above data at.....				25.0	1.515365	1.519095	1.528470	.013117

TABLE 3. *Comparison of results obtained with the two different prisms*

	C	D	e	F	g	(F−C)*
Index n^{25} for prism 1	1.515345	1.519093	1.522415	1.528536	1.536292	0.013193
Standard deviation of n^{25}	37.4×10^{-6}	35.2×10^{-6}	63.6×10^{-6}	43.2×10^{-6}	49.3×10^{-6}	10.5×10^{-6}
Index n^{25} for prism 2	1.515365	1.519095	.....	1.528470	.....	0.013117
Standard deviation of n^{25}	94.8×10^{-6}	152×10^{-6}	.....	147×10^{-6}	.....	42.5×10^{-6}
Difference between indices of prism 2 and prism 1	20×10^{-6}	2×10^{-6}	.....	-66×10^{-6}	.....	-76×10^{-6}
dn/dT for prism 1	-367.7×10^{-6}	-369.9×10^{-6}	-370.1×10^{-6}	-376.5×10^{-6}	-378.2×10^{-6}	-8.8×10^{-6}
Standard deviation of dn/dT for prism 1	5.90×10^{-6}	5.54×10^{-6}	8.11×10^{-6}	6.62×10^{-6}	6.29×10^{-6}	1.6×10^{-6}
dn/dT for prism 2	-341×10^{-6}	-345×10^{-6}	.....	-340×10^{-6}	.....	-1.8×10^{-6}
Standard deviation of dn/dT for prism 2	19.2×10^{-6}	30.7×10^{-6}	.....	29.7×10^{-6}	.....	8.6×10^{-6}
Difference between values of dn/dT of prism 2 and prism 1	$+26.7\times10^{-6}$	$+24.9\times10^{-6}$	.....	$+36.5\times10^{-6}$	.....	$+7.0\times10^{-6}$

* The values in this column have been calculated directly from the observations shown in tables 1 and 2, and are not obtained from differences of preceding columns of table 3.

the standard deviations. The differences are less than the standard deviation of prism 2 for each of the three spectral lines, and even for $(n_F - n_C)$ the difference is less than twice the standard deviation. Similarly, the differences in dn/dT are not significant, since they are less than twice the standard deviation.

Since the precision of the values obtained with prism 1 was much greater than that obtained with prism 2 and more observations were made with it, the remainder of the paper will be concerned only with the values obtained on prism 1.

It should be clearly recognized that the present work did not include a study of the dependence of refractive index on composition. The rubber used to make the second prism probably came from the same bale as that used to make the first. For simplicity the results have been treated as if the sample were pure rubber hydrocarbon, whereas it is only 93 to 94 percent hydrocarbon and is known to contain resins in solution and proteins, salts, and other foreign material dispersed in it. Hence the number of significant figures used here shows only the precision of the present measurements of a sample of given composition. Earlier work [5, 6] has shown little variation with composition in the fourth-place index values, but further studies would be required to show the effect of impurities on fifth-place and sixth-place values.

IV. Discussion

The results of measurements of refractive index for the *D*-line have been summarized in a paper presented at the Rubber Technology Conference in 1938 [7]. The most reliable value of n_D^{25} was judged to be 1.5190, found by McPherson and Cummings [6]. This is in very good agreement with that found in the present work, namely, 1.519093.

McPherson and Cummings also made measurements with a Pulfrich refractometer and reported an exceedingly large value for the dispersion, $n_F - n_C$. In the course of the present work the original data of McPherson and Cummings were reexamined and it was discovered that on account of a clerical error incorrect values were given for the refractive index of the *F*-line and consequently for the dispersion. The corrected results of McPherson and Cummings are as follows:

Temperature	24.5° C.	25.0° C.
n_C	1.5153	1.5151
n_D	1.5190	1.5188
n_F	1.5283	1.5281
$n_F - n_C$	0.0130	0.0130

These values are lower than those given in the present work by 2 to 4 units in the fourth decimal place.

A summary of previous values of the rate of change of index (*D*-line) with temperature is as follows:

Author	Year	dn/dT
McPherson [5]	1932	360×10^{-6}
Kirchof [8]	1932	369
McPherson and Cummings [6]	1935	350
Present work	.....	369.9

In a previous publication [7] it has been shown that the empirical Eykman equation, $(n^2-1)/(n+0.4)=Rd$, where d is the density and R a constant, can be differentiated to yield the following equation

$$\frac{dn}{dT}=-\frac{1}{\frac{2n}{n^2-1}-\frac{1}{n+0.4}}\left(\frac{1}{V}\frac{dV}{dT}\right). \quad (2)$$

Here V is the volume of a given mass of the material, so that $(1/V)\ (dV/dT)$ is its volume expansivity. It has now been found that the coefficient by which the expansivity is multiplied in the right-hand member of this equation can be represented to within about 0.2 percent over the complete range of normal refractive indices, namely from 1.33 to 1.7, by the expression $(1.10440n-1.12226)$. Thus the equation becomes

$$\frac{dn}{dT}=-(1.10440n-1.12226)\left(\frac{1}{V}\frac{dV}{dT}\right). \quad (3)$$

Of the three observable quantities involved in this equation it is considered that the experimental uncertainty is greatest in the value of the expansivity. Consequently, the expansivity has been calculated from the optical data by taking the ratio of (dn/dT) to $(1.10440n-1.12226)$ for each of the spectral lines. The following results were obtained

Spectral line	Calculated expansivity
C	667×10^{-6}
D	666
e	662
F	665
g	658

The mean value, 664×10^{-6} (deg. C)$^{-1}$, is in excellent agreement with values directly observed [7, 9].

By inserting this mean value for the expansivity and the value for n^{25} in eq 3 one then has

$$dn/dT=-(1.10440n^{25}-1.12226)(664\times10^{-6}). \quad (4)$$

The values of the right-hand member of this equation are compared with dn/dT as directly observed in the following tabulation

Spectral line	dn/dT		Difference
	Calculated	Observed	
C	366.1×10^{-6}	367.7×10^{-6}	-1.6×10^{-6}
D	368.8	369.9	−1.1
e	371.2	370.1	+1.1
F	375.7	376.5	−0.8
g	381.4	378.2	+3.2

The agreement is very satisfactory.

The molecular refractivity can be calculated by the Lorenz-Lorentz relation from the present data by taking the value 0.906 g/cm^3 for the density at 25° C. of purified natural rubber [5, 7]. As pointed out in the earlier paper [1] the result, 22.82, is in sufficiently good agreement with values obtained by taking the sum of atomic refractivities to afford optical confirmation of the existence of a C_5H_8 group containing one double bond as the unit group in rubber. It would be desirable to apply the methods outlined by Taylor, Pignocco, and Rossini [10] to a more detailed study of the data given in the present paper.

V. Comparison of Refractivity Intercept and Specific Dispersion With Values for Other Hydrocarbons

The refractivity intercept, $n_D-d/2$, and specific dispersion, $10^4\ (n_F-n_C)/d$, where d is the density, have been used for some years to distinguish between different classes of hydrocarbons [11]. Values for these quantities applicable to hydrocarbons with not more than nine carbon atoms are given in Circular C461 of the National Bureau of Standards, entitled Selected values of properties of hydrocarbons, by Rossini and coworkers [12]. The lowest and the highest values found for each class of hydrocarbon, together with the mean of the two, are listed in table 4 for comparison with the refractivity intercept and the specific dispersion for rubber. In these computations the value 0.906 g/cm^3 has again been used as the density at 25° C of purified natural rubber.

From the comparison shown in table 4 one can see that both the refractivity intercept and specific dispersion of rubber are somewhat above the corresponding values for the monoolefins but not nearly as high as those for the diolefins with

conjugated double bonds. This is exactly what would be expected from the structure of the rubber polymer. The double bonds in rubber are separated by four skeletal carbon atoms rather than by two carbon atoms as in a conjugated system. It has already been suggested [13] that this fact gives rise to a slight degree of double bond character in the single bond half-way between two double bonds.

TABLE 4. *Comparison of values of refractivity intercept and specific dispersion with those found in NBS Circular 461, Selected Values of Properties of Hydrocarbons, by Rossini and coworkers [12]*

	Refractivity intercept			Specific dispersion		
	$n_D^{25}-d/2$			$10^4(n_F^{25}-n_C^{25})/d$		
	Low	High	Mean[a]	Low	High	Mean[a]
Paraffins:						
C_5H_{12}	1.0436	1.0441	1.04385	98	99	98.5
C_6H_{14}	1.0437	1.0448	1.04425	97	100	98.5
C_7H_{16}	1.0439	1.0454	1.04465	96	100	98
C_8H_{18}	1.0437	1.0458	1.04475	96	100	98
C_9H_{20}	1.0420	1.0470	1.0445	94	101	97.5
Monoolefins:						
C_5H_{10}	1.050	1.056	1.053	128	135	131.5
C_6H_{12}	1.049	1.058	1.0535	122	132	127
C_7H_{14}	1.048	1.057	1.0525	118	130	124
C_8H_{16}	1.050	1.055	1.0525	116	127	121.5
Diolefins with conjugated double bonds:						
C_5H_8	1.080	1.091	1.0855	225	225	225
C_6H_{10}	1.075	1.091	1.083	225	225	225
Diolefins with adjacent double bonds:						
C_5H_8	1.06	1.074	1.067	--	--	----
C_6H_{10}	1.054	1.069	1.0615	--	--	----
Other diolefins:						
C_5H_8	1.057	1.057	1.057	--	--	----
C_6H_{10}	1.057	1.062	1.0595	--	--	----
Rubber[b]:						
$(C_5H_8)_p$	----	----	1.066	--	--	145.6

[a] Mean of low and high values.
[b] The number of (C_5H_8)-units, or degree of polymerization, is denoted by p.

VI. Dispersion Equations

From the data obtained in the present work it is possible to calculate the constants in a dispersion equation, which gives the relation between refractive index and wavelength. From a consideration of standard deviations one can draw conclusions regarding the validity of a particular form of dispersion equation. The present work shows that neither the Cauchy dispersion equation nor the Sellmeier dispersion equation is adequate to represent the observed data if the number of parameters is limited to two.

The two-constant Cauchy dispersion equation [11] is usually written

$$n=A_1+B_1/\lambda^2=A_1+B_1\nu^2. \tag{5}$$

Here n is the refractive index, λ is the wavelength, and ν its reciprocal, the wavenumber of the light. A_1 and B_1 are constants characteristic of the medium.

The constants in the Cauchy equation were evaluated at the five different wavelengths from the index for prism 1 by the usual methods of linear regression. The following equation was thus obtained

$$n=1{\cdot}498648+71{\cdot}16\times10^{-6}/\lambda^2. \tag{6}$$

A comparison of observed values with those calculated from this equation is given in table 5. It will be seen that the differences are considerably larger than the corresponding standard deviations of the observations. The observed variance in the Cauchy equation values yields a standard deviation of 176×10^{-6}, which can be compared with the average standard deviation of an observed value, namely, 46×10^{-6}. Consequently, it is concluded that the Cauchy dispersion equation with two parameters does not adequately represent the observations.

The single-term Sellmeier dispersion equation [11] is usually written

$$n^2-1=C/(\nu_0^2-\nu^2), \tag{7}$$

where C and ν_0 are constants. For purposes of calculation this equation may be written in the following form

$$1/(n^2-1)=A_2+B_2\nu^2. \tag{8}$$

The constants have been evaluated from the index values for prism 1, to yield the following equation

$$1/(n^2-1)=0{\cdot}800139-123{\cdot}09\times10^{-12}\nu^2. \tag{9}$$

Table 5 also shows the comparison of observed values with those calculated from this equation.

TABLE 5. *Comparison of dispersion equations*

	C	D	e	F	g	$F-C$
Observed value n^{25}	1.515345	1.519083	1.522415	1.528536	1.536292	0.013193
Standard deviation	37.4×10^{-6}	35.2×10^{-6}	63.6×10^{-6}	43.2×10^{-6}	49.3×10^{-6}	10.5×10^{-6}
Calculated from Cauchy equation	1.515169	1.519038	1.522510	1.528757	1.536108	0.013588
Difference between observed and calculated values	$+176\times10^{-6}$	-45×10^{-6}	-95×10^{-6}	-221×10^{-6}	$+184\times10^{-6}$	-395×10^{-6}
Calculated from Sellmeier equation	1.515281	1.519116	1.522420	1.528960	1.536202	0.013679
Difference between observed and calculated values	$+64\times10^{-6}$	-23×10^{-6}	-5×10^{-6}	-124×10^{-6}	$+90\times10^{-6}$	-186×10^{-6}

It will be noted that the representation of the data is still not adequate, although the differences and standard deviations associated with the Sellmeier equation are appreciably less than the corresponding values associated with the Cauchy equation. The standard deviation associated with the variance shown in the table is 84×10^{-6}.

The corresponding Lorenz dispersion equation, which is quite similar to the Sellmeier form, is as follows:—

$$\frac{n^2-1}{n^2+2}=\frac{C_2}{\nu_0^2-\nu^2} \tag{10}$$

Preliminary calculations indicated that it did not represent the data as well as the Sellmeier equation. Consequently, it was not considered further.

The equations thus far presented have been two-constant equations. In no previous case with which we are familiar has a two-constant equation been adequate to express the dispersion shown by fifth-place refractive index measurements. A three-constant equation may be successful for some materials, but most of them require a four-constant equation. However, it has not been found necessary to go beyond a four-constant equation. Such an equation, for example, has been shown to be quite adequate to represent the sixth-place index values obtained in the highest precision measurements on water [3, 14]. The Ketteler-Helmholtz equation has a theoretical justification more satisfactory than that behind the simpler equations, and probably should be used for the calculation of index at wavelengths other than those given here.

VII. Conclusions

The refractive index of natural rubber and its variation with temperature and wavelength are those which would be predicted for a similar hydrocarbon of low molecular weight. A two-constant equation of the Cauchy or Sellmeier type is inadequate to express the relation between refractive index and wavelength for rubber.

For convenient reference the best values resulting from the present investigation are recapitulated in table 6.

TABLE 6. *"Best" values resulting from present investigation*

	C	D	e	F	g	$F-C$
n^{25}	1.515345	1.519083	1.522415	1.528536	1.536292	0.013193
Standard deviation of n^{25}	37.4×10^{-6}	35.2×10^{-6}	63.6×10^{-6}	43.2×10^{-6}	49.3×10^{-6}	10.5×10^{-6}
dn/dT	-367.7×10^{-6}	-369.9×10^{-6}	-370.1×10^{-6}	-376.5×10^{-6}	-378.2×10^{-6}	-8.8×10^{-6}
Standard deviation of dn/dT	5.90×10^{-6}	5.54×10^{-6}	8.11×10^{-6}	6.62×10^{-6}	6.29×10^{-6}	1.6×10^{-6}

VIII. References

[1] L. A. Wood, The optical properties of rubber, J. Applied Phys. **12,** 119 (1941). Reprinted in Rubber Chem. Tech. **15,** 23 (1942).

[2] L. W. Tilton, Permissible curvature of prism surfaces and inaccuracy of collimation in precise minimum-deviation refractometry, BS J. Research **11,** 25 (1933).

[3] L. W. Tilton and J. K. Taylor, Refractive index and dispersion of distilled water for visible radiation at temperatures 0° to 60° C, J. Research NBS **20,** 419 (1938) RP1085.

[4] G. W. Snedecor, Statistical methods (Iowa State College Press, Ames, Iowa, 1946).

[5] A. T. McPherson, A method for the purification of rubber and properties of the purified rubber, BS J. Research **8,** 751 (1932) RP449. Reprinted in Rubber Chem. Tech. **5,** 523 (1932).

839743—49——5

[6] A. T. McPherson and A. D. Cummings, Refractive index of rubber, J. Research NBS **14,** 553 (1935) RP786. Reprinted in Rubber Chem. Tech. **8,** 421 (1935).

[7] L. A. Wood, Values of the physical constants of rubber, Proc. Rubber Technology Conference, London, p. 933 (W. Heffer and Sons, Cambridge, Eng., 1938). Reprinted in Rubber Chem. Tech. **12,** 130 (1939).

[8] F. Kirchhof, The refractometry of rubber and gutta percha hydrocarbons, Kautschuk **8,** 137 (1932). Translated in Rubber Chem. Tech. **6,** 92 (1933).

[9] N. Bekkedahl and L. A. Wood, Crystallization of vulcanized rubber, Ind. Eng. Chem. **33,** 381 (1941). Reprinted in Rubber Chem. Tech. **14,** 347 (1941).

[10] W. J. Taylor, J. M. Pignocco, and F. D. Rossini, Method for calculating the properties of hydrocarbons and its application to the refractive indices, densities, and boiling points of the paraffin and monoolefin hydrocarbons, J. Research NBS **34,** 413 (1945) RP1651.

[11] S. S. Kurtz and A. G. Ward, The refractivity intercept and the specific refraction equation of Newton, J. Franklin Inst. **222,** 563 (1936); **224,** 583, 697 (1937).

[12] F. D. Rossini, K. S. Pitzer, W. J. Taylor, J. R. Ebert, J. E. Kilpatrick, C. W. Beckett, M. G. Williams, and H. G. Werner, Selected values of properties of hydrocarbons, NBS Circular C461 (1947).

[13] G. A. Jeffrey, Structure of polyisoprenes, I. The crystal structure of geranylamine hydrochloride. VI. An investigation of the molecular structure of dibenzyl by X-ray analysis, Proc. Roy. Soc. **A183,** 388 (1945); **A188,** 222 (1947).

[14] L. W. Tilton, Accurate representation of refractive index of distilled water as a function of wave length, J. Research NBS **17,** 639 (1936) RP934.

WASHINGTON, March 11, 1949.

U. S. Department of Commerce
National Bureau of Standards

Research Paper RP2005
Volume 43, July 1949

Part of the Journal of Research of the National Bureau of Standards

Metastable Transitions in Mass Spectra of Hydrocarbons

By Evelyn G. Bloom, Fred L. Mohler, C. Edward Wise, and Edmund J. Wells

This paper gives a compilation of metastable transition peaks in mass spectra of about 170 hydrocarbons based on experimental data that have been published in the American Petroleum Institute Catalog of Mass Spectra Data. One hundred different transitions have been found and identified. These are tabulated according to the mass lost in the transition. Masses lost are 1, 2, 15, 16, 26, 27, 28, 29, 30, 40, 42, 43, 44, 56, 57, and 58. Nearly all transitions can be ascribed to breaking of one bond with or without the transfer of one hydrogen atom to the charged or to the neutral fragment. The data include those previously reported in Research Paper 1888 [1].[1]

I. Introduction

A previous paper has discussed the metastable transitions in mass spectra of 56 hydrocarbons [1]. The experimental data published by this laboratory in the American Petroleum Institute Catalog of Mass Spectral Data [2] now include nearly 170 hydrocarbons. All observable metastable transition peaks have been indicated in the tables, and the transitions giving rise to the peaks have been unambiguously identified in nearly all cases. This paper is a brief summary of the transitions observed to date, including and greatly extending the lists in the previous paper [1].

Metastable transition peaks are observed as small abnormally wide peaks that are in general at nonintegral mass positions. Hipple and Condon [3] have shown that these peaks arise from ions that dissociate after the ions have passed through the ion accelerating field. For this reason they have less than the full kinetic energy and an apparent mass, m_a, which is less than the true mass and given by the relation

$$m_a = m_f^2/m_i \qquad (1)$$

where m_i is the mass during passage through the electric field, and m_f is the mass after dissociation. m_i may be either the mass of the parent ion or the mass of a dissociation product formed in the ionization chamber before entering the ion accelerating field.

Theoretically the measured value of m_a is sufficient to determine both m_f and m_i, since m_f and m_i are integers. In practice a qualitative intensity rule is very helpful in the identification of the transition, namely that the height of the metastable peak depends on the intensity of both the peaks m_f and m_i and both will have an intensity of greater than 5 percent of the maximum peak if the metastable transition is observable. The experimental evidence for this rule has already been discussed [1].

The Socony Vacuum Laboratories and the Atlantic Refining Co. have published mass spectra of a number of the hydrocarbons included in the National Bureau of Standards study and have included metastable peaks [2]. There is usually good agreement between laboratories in spite of the fact that identification of these small peaks is sometimes a matter of personal judgment and experience.

The hydrocarbons covered in this study include 59 straight-chain saturated hydrocarbons, including n-decane, 18 nonanes and all lighter saturates; 34 olefins, including 1-decene, 1-nonene, 4 octenes, 3 heptenes, 13 hexenes and all lighter olefins; 21

[1] Figures in brackets indicate the literature references at the end of this paper.

839743—49——6

alkylcyclopentanes, 17 alkylcyclohexanes, 20 alkylbenzenes, 5 dienes, 3 acetylenes, 6 cyclopropanes and cyclobutanes, and 3 cycloolefins.

II. Experimental Results

The following tables list 100 different metastable transitions that have been observed in hydrocarbon mass spectra. Many of these recur in many different hydrocarbons, and over a thousand different instances of metastable transitions are noted in the API tables. Here the transitions are classified according to the mass lost in the metastable transition. The first column of each table gives the apparent mass and is the value computed from the initial and final masses listed in columns 2 and 3. In the last column is indicated the compounds, or class of compounds, showing the transition. When a transition occurs only in one or two compounds or one or two classes of compounds, these are indicated specifically. If it occurs in three or more compounds, only the class of compound is indicated, and if it occurs in three or more classes it is listed as common. The abbreviation *p* is used for the parent ion. The information on occurrence of metastable transitions must be evaluated with due regard to the above list of compounds studied. Data on diolefins, acetylenes, and cycloolefins are very incomplete.

Loss of mass 1 (table 1). The loss of H in a metastable transition is very rare in view of the fact that in every spectrum there are many large peaks differing by one mass unit. In addition to the four transitions listed in table 1, the Socony Vacuum Laboratories [4] list two such transitions in propylene; $42^+ \rightarrow 41^+ + 1$ and $40^+ \rightarrow 39^+ + 1$. Although the transitions were not observed in our work, there is no reason to doubt these observations. These metastable transition peaks coincide with large normal peaks and it requires careful study of the peak shape to prove that they exist. The second of these transitions gives an apparent mass of 38.0. An alternative explanation would be $42^+ \rightarrow 40^+ + 2$ with an apparent mass of 38.1.

It is of interest that the transition $68^+ \rightarrow 67^+$ occurs in nearly all the C_5H_8 isomers that have been studied, for these include a wide variety of compounds; spiropentane, cyclopentene, methylenecyclobutane, several pentadienes, and 1-pentyne. In all these spectra the loss of H from the parent ion is a very probable transition, often the maximum peak.

TABLE 1. *Transitions involving loss of mass 1*

m_a	m_i	m_f	Occurrence
66.0	68^+	67^+	From *p* of C_5H_8 isomers.
76.0	78^+	77^+	From *p* of benzene.
88.0	90^+	89^+	Alkyl benzenes.
90.0	92^+	91^+	From *p* of toluene.

Loss of mass 2 (table 2). This is by far the most common type of metastable transition and is observed in most cases where there are two strong peaks differing by two mass units.

TABLE 2. *Transitions involving loss of mass 2*

m_a	m_i	m_f	Occurrence
24.1	28^+	26^+	Common.
25.1	29^+	27^+	Do.
26.1	30^+	28^+	From *p* of ethane.
35.1	39^+	37^+	Common.
37.1	41^+	39^+	Do.
39.1	43^+	41^+	Do.
47.1	51^+	49^+	Vinylcyclohexene.
48.1	52^+	50^+	1,5-Hexadiene, benzene.
49.1	53^+	51^+	2,3,3-mey-1-butene, C_5H_8's.
51.1	55^+	53^+	Common.
63.1	67^+	65^+	Do.
65.1	69^+	67^+	Hexenes.
66.1	70^+	68^+	Cyclics.
74.1	78^+	76^+	From *p* of benzene.
75.1	79^+	77^+	Common.
77.1	81^+	79^+	C_6H_{10} isomers.
88.0	92^+	90^+	From *p* of toluene.
89.0	93^+	91^+	Alkyl benzenes.
101.0	105^+	103^+	Do.
110.0	114^+	112^+	From *p* of 2,5-me$_2$ hexane.

Loss of mass 15 (table 3). In the earlier work [1] all instances of loss of CH_3 in a metastable transition involved the parent ion, but cyclics and the heavier olefins were not included. As these molecule ions can dissociate into ions of lighter olefins (or ions isomeric with the lighter olefins), it is not surprising that this dissociation is followed by a metastable transition characteristic of the lighter olefin. In all instances of loss of CH_3, the initial state is a molecule ion or at least an isomer of a molecule ion.

TABLE 3. *Transitions involving loss of mass 15*

m_a	m_i	m_f	Occurrence
28.2	54°	39°	From *p* of C_4H_6's and from C_5H_{10}'s and vinylcyclohexene.
30.0	56°	41°	Cyclics and olefins.
31.9	58°	43°	From *p* of *n*-butane.
43.2	70°	55°	Cyclics and olefins.
54.7	82°	67°	From *p* of C_6H_{10}'s.
56.7	84°	69°	Cyclics and olefins.
58.6	86°	71°	From *p* of 2,3-me_2 butane.
70.3	98°	83°	Cyclics and olefins.
72.3	100°	85°	From *p* of 2-methylhexane.
78.1	106°	91°	From *p* of C_9H_{10} alkyl benzenes.
84.0	112°	97°	From *p* of C_8 cyclics and olefins.
86.0	114°	99°	From *p* of 2-me heptane and 2,5-me_2-hexane.
91.9	120°	105°	From *p* of C_9H_{12} alkyl benzenes.
105.7	134°	119°	From *p* of $C_{10}H_{14}$ alkyl benzenes.

Loss of mass 16 (*table 4*). The first two transitions listed in the table recur in many compounds, but other instances of losing CH_4 are obviously very rare and a specific property of a few molecules. The transition giving 82.3 is of interest because all eight of the C_8H_{16} cyclohexanes have been studied, and this is a conspicuous peak in *trans* 1,3-dimethylcyclohexane and *cis* 1,4-dimethylcyclohexane and is missing in all the others including the *cis* 1,3 and *trans* 1,4 isomers. The *cis* and *trans* isomers give mass spectra that are quite similar in other respects. The designation *trans* 1,3-dimethylcyclohexane is the revised designation for the compound of boiling point 124.45° C [5].

TABLE 4. *Transitions involving loss of mass 16*

m_a	m_i	m_f	Occurrence
27.7	55°	39°	Pentenes and hexenes.
29.5	57°	41°	Common.
30.4	58°	42°	From *p* of *n*-butane.
82.3	112°	96°	From *p* of *trans* 1,3-me_2 cyclohexane and *cis* 1,4-me_2 cyclohexane.

Loss of mass 26 (*table 5*). The second of these transitions has been listed [1]. The occurrence of transitions involving loss of C_2H_2 from benzene and alkyl benzenes is probably a consequence of a structure containing a ring of CH radicals dissociating by breaking carbon bonds.

TABLE 5. *Transitions involving loss of mass 26*

m_a	m_i	m_f	Occurrence
13.8	53°	27°	C_2H_3 isomers.
15.3	55°	29°	Common.
33.8	77°	51°	Alkyl benzenes.
34.7	78°	52°	Benzene and alkyl benzenes.
46.4	91°	65°	Alkyl benzenes.
59.4	105	79°	Do.

Loss of mass 27 (*table 6*). The first transition was reported in the earlier paper [1]. The second transition occurs in dimethyl and ethyl benzenes. The fact that the final mass is C_6H_6 suggests that radicals are replaced by H atoms in a rearrangement of H atoms during the dissociation process.

TABLE 6. *Transitions involving loss of mass 27*

m_a	m_i	m_f	Occurrence
13.5	54°	27°	From *p* of C_4H_6 isomers.
57.9	105°	78°	C_9H_{10} benzenes.

Loss of mass 28 (*table 7*). Loss of C_2H_4 is a common metastable transition reflecting the common occurrence of $CH_2.CH_2$ in molecular structure.

TABLE 7. *Transitions involving loss of mass 28*

m_a	m_i	m_f	Occurrence
24.4	69°	41°	Olefins and cyclics.
25.2	70°	42°	From *p* of cyclopentane and from other cyclics.
26.0	71°	43°	From straight-chain saturates.
36.4	83°	55°	Olefins and cyclics.
37.3	84°	56°	From *p* of C_6 cyclics and a few other molecules.
38.2	85°	57°	From straight-chain saturates.
43.6	91°	63°	Toluene.
49.1	97°	69°	Octenes and 1-nonene.
50.0	98°	70°	Olefins and cyclics.
56.5	105°	77°	Alkyl benzenes.
59.3	108°	80°	From *p* of vinylcyclohexene.
65.0	112°	84°	From *p* of C_8 cyclics and from olefins and 1-decene.
69.6	119°	91°	Alkyl benzenes.
76.2	126°	98°	From *p* of butyl cyclopentanes.
89.6	140°	112°	From *p* of 1-decene.

Loss of mass 29 (*table 8*). Loss of the ethyl radical, C_2H_5, always comes from a parent ion, and in nearly all cases it could come from simple

breaking of a carbon bond. Vinylcyclohexene does not contain a CH_3 radical in its structure, and a rearrangement or double dissociation must be involved.

TABLE 8. *Transitions involving loss of mass 29*

m_a	m_i	m_f	Occurrence
24.0	70°	41°	From p of pentenes.
48.6	98°	69°	From p of C_7H_{14} cyclopentanes.
50.4	100°	71°	From p of n-heptane.
57.8	108°	79°	From p of vinylcyclohexene.
61.5	112°	83°	From p of C_8H_{16} olefins and cyclics.
63.4	114°	85°	From p of n-octane and 3,4 me_2 hexane.
69.0	120°	91°	From p of propylbenzenes.
74.7	126°	97°	From p of n-butyl cyclopentane.
76.6	128°	99°	From p of n-nonane.
82.3	134°	105°	From p of $C_{10}H_{14}$ alkyl benzenes.
88.0	140°	111°	From p of sec. butyl cyclohexane and 1-decene.
89.9	142°	113°	From p of n-decene.

Loss of mass 30 (table 9). This is another metastable transition that always comes from parent ions. Loss of C_2H_6 from a hydrocarbon requires either a double dissociation or a rearrangement of hydrogen atoms in the dissociation process. In most of the C_8H_{16} isomers that give this and in the last two transitions listed, there is only one CH_3 radical in the structure; and in vinylcyclohexene there is no CH_3 radical so that rearrangements seem to be involved in these cases.

TABLE 9. *Transitions involving loss of mass 30*

m_a	m_i	m_f	Occurrence
24.5	72°	42°	From p of n-pentane.
36.5	86°	56°	From p of n-hexane.
49.0	100°	70°	From p of heptanes.
56.3	108°	78°	From p of vinylcyclohexene.
60.0	112°	82°	From p of C_8H_{16} isomers.
61.9	114°	84°	From p of octanes.
73.1	126°	96°	From p of n-butyl cyclopentane.
86.4	140°	110°	From p of sec. butyl cyclohexane.

Loss of mass 40 (table 10). There is only one instance of the loss of C_3H_4 in a metastable transition. It gives a conspicuous peak, and the initial and final states are abundant ions so the evidence is quite conclusive.

TABLE 10. *Transitions involving loss of mass 40*

m_a	m_i	m_f	Occurrence
33.5	97°	57°	2,4,4-mcy-2-pentene.

Loss of mass 42 (table 11). The loss of C_3H_6 is a fairly common type of metastable transition observed in a variety of compounds containing seven or more carbon atoms.

TABLE 11. *Transitions involving loss of mass 42*

m_a	m_i	m_f	Occurrence
21.7	85°	43°	Heptanes, octanes and nonanes.
31.2	97°	55°	Olefins and cyclics above C_7.
32.0	98°	56°	From p of C_7H_{14} isomers and 1-decene.
32.8	99°	57°	Octanes and nonanes.
40.3	108°	66°	From p of vinylcyclohexene.
43.8	112°	70°	From p of C_8 cyclics.
44.6	113°	71°	Nonanes.

Loss of mass 43 (table 12). There are only three instances in which the propyl radical C_3H_7 is lost, and these all involve parent ions.

TABLE 12. *Transitions involving loss of mass 43*

m_a	m_i	m_f	Occurrence
54.7	126°	83°	From p of propylcyclohexanes.
67.2	140°	97°	From p of i-butylcyclohexane.

Loss of mass 44 (table 13). Loss of C_3H_8, like the loss of C_2H_6, requires a double dissociation or a rearrangement of atoms in the dissociation process.

TABLE 13. *Transitions involving loss of mass 44*

m_a	m_i	m_f	Occurrence
31.4	100°	56°	From p of heptanes.
53.4	126°	82°	From p of n-propylcyclohexane.

Loss of masses 56, 57, and 58 (table 14). There are only a few instances of metastable transitions involving the loss of four carbon atoms and all these occur from parent ions of $C_{10}H_{20}$ isomers losing C_4H_8, C_4H_9, and C_4H_{10}. Loss of a butyl

radical, C_4H_9, from these molecules involves simple breaking of a carbon bond. Loss of C_4H_8 or C_4H_{10} would involve a rearrangement or double dissociation.

TABLE 14. *Loss of masses 56, 57, and 58*

m_*	Transition	Occurrence
50.4	$140^+ \rightarrow 84^+ + 56$	From *p* of 1-decene.
49.2	$140^+ \rightarrow 83^+ + 57$	From *p* of 1-decene and butylcyclohexanes.
48.0	$140^+ \rightarrow 82^+ + 58$	From *p* of butylcyclohexanes.

III. Discussion

The interest in compiling data on occurrence of metastable transitions is that the transitions give some evidence as to the mechanism by which molecule ions dissociate. In the case of dissociations that give normal peaks, the dissociation takes place within the ionization chamber in less than 10^{-7} sec. If, however, the half-life for the dissociation transition is of the order of 10^{-6} sec, then some of the transitions take place after the ion has traversed the ion accelerating field, and metastable transition peaks are observed. Because of this delay the different kinds of transitions are sorted out and distinguished from each other. If the initial mass is the parent ion, then a single dissociation is involved. If it is not, then there are at least two stages involved in the dissociation process, one within the ionization chamber and one delayed transition. This multiple dissociation occurs more frequently than single dissociation. The above results show that often the metastable transition is not a simple dissociation but involves either a rearrangement of atoms or a multiple dissociation. The following considerations show that a rearrangement involving transfer of one hydrogen atom can explain most of the cases other than simple dissociation.

By far the most common type of metastable transition is the loss of two hydrogen atoms. It is known from appearance potential measurements that hydrogen atoms are commonly lost from the molecule ion as H_2 and not 2H [6]. This suggests that in all metastable transitions involving loss of mass 2 there is a rearrangement to form H_2 in the dissociation process. As the loss of H in a metastable transition is very rare, it is not attractive to assume that loss of 2H in two separate processes is common. It seems more probable to assume that the affinity between H atoms favors removal of pairs of atoms in the form H_2.

Appearance potential measurements also give some evidence as to transitions involving loss of CH_4 (table 4). Stevenson and Hipple [7] find that in the butanes the transition $58^+ \rightarrow 42^+ + 16$ gives CH_4 and not $CH_3 + H$. This suggests that all metastable transitions involving loss of CH_4 involve a similar process. The affinity of the methyl radical for H removes an additional atom in the dissociation process. Transitions involving loss of mass 30 (table 9), 44 (table 13), and 58 (table 14) probably involve the same mechanism. All except one of these transitions can be explained by transfer of only one H atom in the dissociation process. Removal of mass 30 from vinylcyclohexene involves more complicated rearrangements.

The losses of CH_3 (table 3), C_2H_5 (table 8), C_3H_7 (table 12), and C_4H_9 (table 14) from parent ions can in most cases be ascribed to simple breaking of a carbon bond. Two exceptions are the loss of CH_3 from cyclopentane and cyclohexane. The mass spectra of these are much like 1-pentene and 1-hexene, and it seems probable that in the cyclics the ring breaks with a rearrangement of H atoms to give CH_3 at one end and CH at the other and that the metastable transition follows this. Loss of CH_3 from 1,3-butadiene and loss of C_2H_5 from vinylcyclohexene also involve rearrangements.

The losses of C_2H_2 (table 5), C_2H_4 (table 7), and C_3H_6 (table 11) can come from simple breaking of a carbon bond in cases where the initial ion is not a parent ion. In cases where it is a parent ion, a rearrangement of hydrogen atoms or a double dissociation is required since breaking one bond in a hydrocarbon gives radicals with an odd number of H atoms, except in the case of breaking a ring.

Nearly all the observed metastable transitions can be accounted for as single dissociation processes. In this dissociation one additional hydrogen atom may be transferred to either the charged or uncharged fraction of the dissociating ion. This transfer of a hydrogen atom is very common. Only a few of all the observed transitions require more complicated rearrangements, and in these

cases an isomerization of the initial ion probably precedes the dissociation.

The results show that ions dissociate in a great variety of ways, either in several successive stages or by loss of a rather large fragment in one step, but loss of more than three carbon atoms in one metastable transition is rare and only observed in a few C_{10} hydrocarbons.

The intensity rule relating height of the metastable peak to the intensity of the initial and final ions is quite general, and there are only a few instances where metastable transitions are distinctive of a given compound when the normal spectra are similar. That the peak at 28.2 (table 3) is missing in 1,2-butadiene and present in other C_4H_6 isomers has been noted [1]. The discussion of table 4 mentions another distinctive difference found in two C_8 cyclohexanes. In general metastable transition peaks are not useful in identification of unknown compounds in a chemical analysis, but it is essential to include them in a careful description of the spectrum.

IV. References

[1] Evelyn G. Bloom, Fred L. Mohler, J. H. Lengel, and C. Edward Wise, J. Research NBS **40,** 437 (1948) RP1888.

[2] American Petroleum Institute Catalog of Mass Spectral Data. Research Project 44, National Bureau of Standards.

[3] J. A. Hipple and E. U. Condon, Phys. Rev. **68,** 54 (1945).

[4] API Catalog of Mass Spectral Data, Table No. 120.

[5] K. S. Pitzer and C. W. Beckett, J. Chem. Soc. **69,** 977 (1947).

[6] J. A. Hipple, Phys. Rev. **53,** 530 (1938).

[7] D. P. Stevenson and J. A. Hipple, J. Am. Chem. Soc. **64,** 1588 (1942).

Washington, March 16, 1949.

U. S. Department of Commerce
National Bureau of Standards

Research Paper RP2006
Volume 43, July 1949

Part of the Journal of Research of the National Bureau of Standards

Impedance Characteristics of Some Experimental Broad-Band Antennas for Vertical Incidence Ionosphere Sounding

By H. N. Cones

This paper presents the results of measurements of the modulus of input impedance of a number of nonresonant antennas over a continuous frequency range from 1 to 25 megacycles per second. These antennas were constructed as part of a design problem of developing an effective radiating system for vertical-incidence ionospheric sounding equipment. The data are in the form of curves, and the antennas are compared with each other from the standpoint of uniformity of impedance over the frequency range. The use of multiple-wire construction to lower the average input impedance, to minimize impedance variations, and to increase radiation efficiency is discussed.

I. General

The delta antenna (illustrated in figs. 2 and 4) has a number of characteristics that make it attractive as an antenna for vertical-incidence ionospheric work. It is fairly compact, requires only a single large mast, and is easy to erect. However, its input impedance, even when properly terminated, may vary from as low as 300 ohms to as much as 1,200 or 1,400 ohms over the frequency range of 1 to 25 Mc/s, and the use of a transmission line to feed the antenna causes an even greater impedance variation. Furthermore, the radiation efficiency at the lower frequencies of the operating range is quite small.

The vertical rhombic antenna, which is another form of nonresonant antenna frequently used for ionospheric measurements, is somewhat more difficult to construct than the delta, requiring one large mast and two smaller ones. Theoretical considerations lead to the conclusion that the impedance characteristics of a vertical rhombic antenna should be somewhat more uniform than that of a delta. However, the tests performed thus far were limited to existing rhombic antennas that were not designed for optimum impedance characteristics. Theoretical considerations would also lead one to believe that the radiating efficiency of a vertical rhombic antenna, which is small compared to the wavelength used, would be lower than a delta or vee antenna designed for the same frequency range.

Elementary considerations indicate that the radiated field of a nonresonant antenna would be proportional to the product of the current flowing through the antenna and the length of the antenna, and is some function of the configuration of the antenna. Because physical limitations restrict the height and, therefore, the length of the antenna, the most promising approach to a more efficient radiator is a multiple wire antenna. Effectively, this lowers the impedance of the antenna, permitting increased current for a given input power. A qualitative analysis indicates that increased radiation efficiency may be thus obtained. Furthermore, because a multiple-wire antenna permits adjustment of wire spacing along its length, it appears to offer a possibility of also securing a more uniform impedance characteristic over the entire frequency range.

The remainder of this report describes the techniques and results of experimental impedance measurements of the following types of antennas:

1. Single-wire delta antennas.
2. A series of multiple-wire delta antennas.
3. A vertical W antenna.
4. A vertical double-W antenna.

II. Instrumentation

For measurement of antenna impedance, a balanced recording impedance meter developed at this Bureau was used. A description of this instrument was presented at the winter 1946–47 IRE convention in New York City.[1] Figure 1 presents the block diagrams of the instrument.

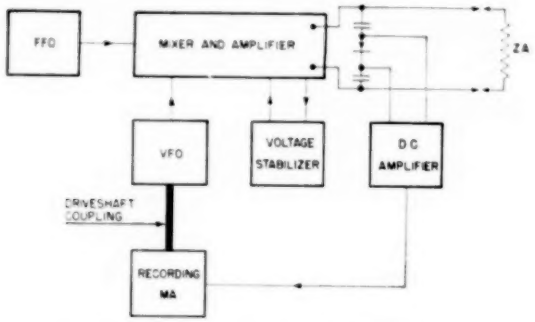

FIGURE 1. *Block diagram of impedance meter.*

Briefly, it consists of a 57-Mc/s fixed-frequency oscillator heating with a variable frequency oscillator covering the frequency band from 57 to 82 Mc/s. The difference frequency of 0 to 25 Mc/s is passed through a wide-band amplifier designed to have a constant current output. The output voltage is therefore directly proportional to the absolute magnitude of impedance connected across the output terminals; no direct indication of the phase angle of the impedance has thus far been provided. This voltage is rectified, amplified, and applied to a recording milliammeter. The recording milliammeter and the variable frequency oscillator are mechanically coupled, so that the impedance is plotted as a function of frequency. A voltage stabilizer is incorporated to insure constant output current. The instrument is calibrated by substituting noninductive resistors for the unknown impedance.

III. Results of Measurements

Figure 2 shows the construction of a simple form of single-wire delta antenna. The principle of a delta antenna is similar to that of a terminated vertical vee in the higher portion of its frequency range; at lower frequencies it behaves somewhat like a loop. The delta construction minimizes the number of supports required and serves to solve the problem of termination. Measurements of the impedance of the antenna shown in figure 2 were made for values of terminating resistance, R_T, equal to 800, 1,000, 1,200, 1,400, and 1,600 ohms. Figure 3 shows the impedance of the antenna over the frequency range of 1 through 25 Mc/s, using a terminating resistance of 1,000 ohms, which was found to be optimum for minimum variation of input impedance. The range of input impedance in this case was from 300 to 1,200 ohms. The value of R_T was not particularly critical, since the range of input impedance for the 800-ohm termination was 300 to 1,300 ohms, and for the 1,600-ohm termination was 300 to 1,200 ohms. The impedance at frequencies from 16 to 25 Mc/s was only slightly affected by changes in terminating resistance. At frequencies below 8 Mc/s, the impedance characteristics were influenced to a

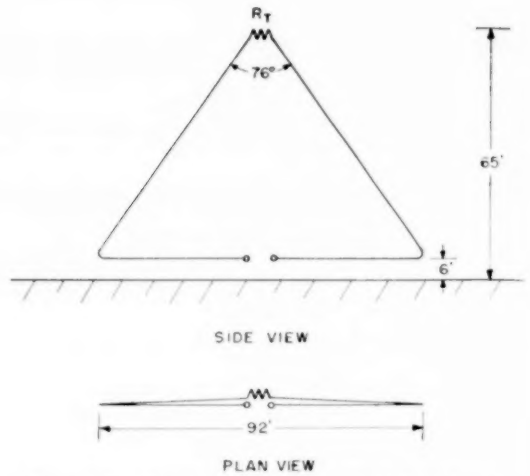

FIGURE 2. *Construction of single-wire delta antenna.*

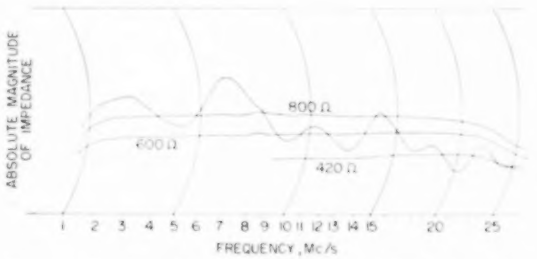

FIGURE 3. *Impedance of single-wire delta antenna for optimum termination of 1,000 ohms.*

[1] H. V. Cottony, A method of rapid continuous measurement of antenna impedance over a wide frequency range. Paper presented before IRE Convention, March 6, 1947, New York, N. Y.

much greater degree by different values of terminating resistance, the number and location of the peaks being changed, although the maximum and minimum values of impedance remained about the same.

Figure 4 shows the construction of a variation of the delta antenna designed by J. W. Cox of the Great Baddow Research Laboratories of the British Marconi Co. It is distinguished from the simpler delta by the presence of corkscrew turns at the lower corners of the antenna. These turns are intended to improve the performance of the antenna. Figure 5 shows the impedance characteristics of this antenna. It can be seen that with optimum terminating resistor (R_T equal to 1,200 ohms), the impedance varied from less than 400 ohms to approximately 1,100 ohms, and it appears that the impedance characteristics of the antenna were not appreciably improved by the addition of the corkscrew turns.

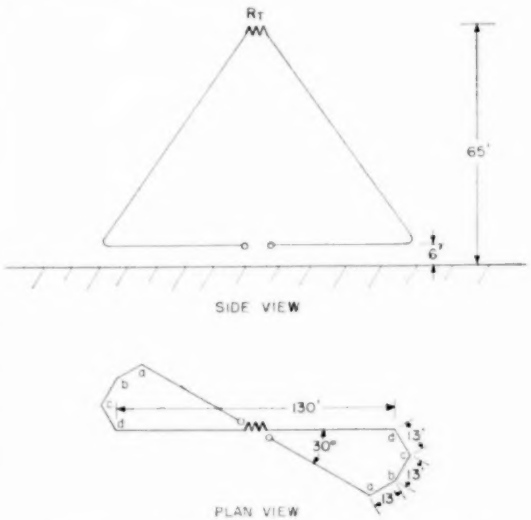

FIGURE 4. *Construction of modified delta antenna.*

Point a, 6 ft. above ground; point b, 8 ft. above ground; point c, 10 ft. above ground; point d, 14 ft. above ground.

The first multiple-wire delta constructed was identical in size shape to the antenna shown in figure 2, except that it was constructed by using two parallel wires spaced 15 in. apart in place of the single wire. Measurements were made by using a number of different terminations. Figure 6 shows the impedance characteristics of this antenna for an optimum termination of 600 ohms.

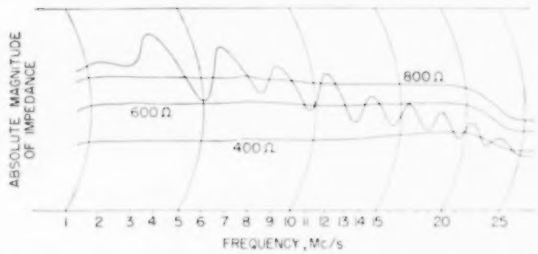

FIGURE 5. *Impedance of modified delta antenna for optimum termination of 1,200 ohms.*

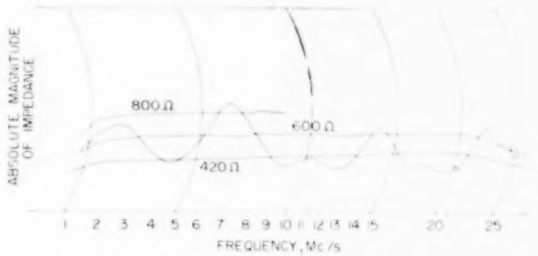

FIGURE 6. *Impedance of parallel-wire delta antenna.*

Construction identical to that of figure 2, except that two parallel wires spaced 15 in. apart are used. R_T=600 ohms.

The impedance in this case varied from 300 to 850 ohms. It should be noted that the parallel-wire delta terminated with 600 ohms was superior from the standpoint of uniformity of impedance to the single-wire delta terminated with 1,000 ohms. The impedance is lower and the variation small enough so that it would be practical to use a 600-ohm line to feed it.

Several other types of multiple-wire deltas were constructed. The best results were obtained when the oblique wires had the configuration shown in figure 7. Each leg consisted of two wires joined at the apex and the lower corners and flayed 36 in. apart at a point 18 ft. from the lower corner. The exact position of the spreaders is not critical nor is the plane of the wires. The horizontal wires, however, have a very significant effect on the impedance characteristics of the antenna. Tests were, therefore, made in which the arrangement of oblique wires shown in figure 7 remained unchanged and with the various arrangements of horizontal wires shown in the same figure. Referring to figure 8, curve A shows the impedance when only a single No. 12 wire was used on each side. Curve B shows the results obtained by replacing the single wire by two No. 18 wires spaced

839743—49——7

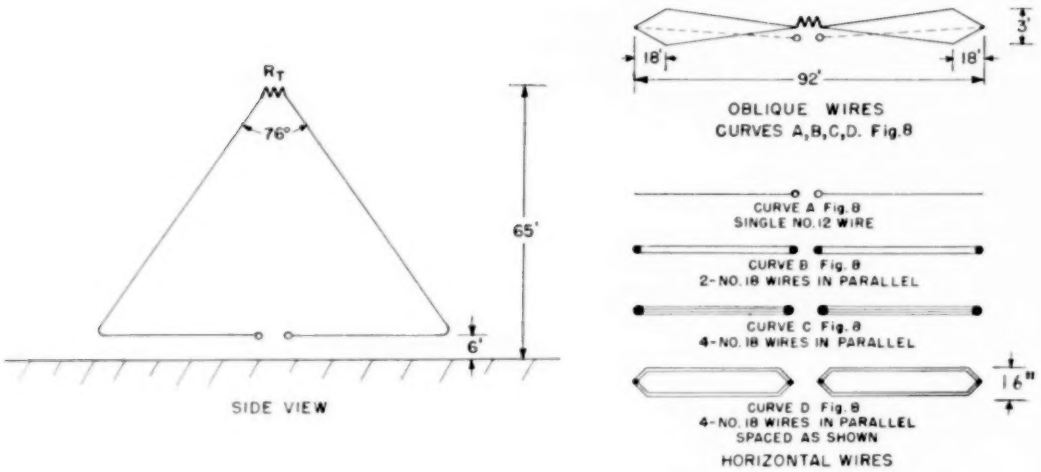

FIGURE 7. *Configuration of oblique and horizontal wires of multiple-wire delta antennas.*

Impedance curves shown in figure 8.

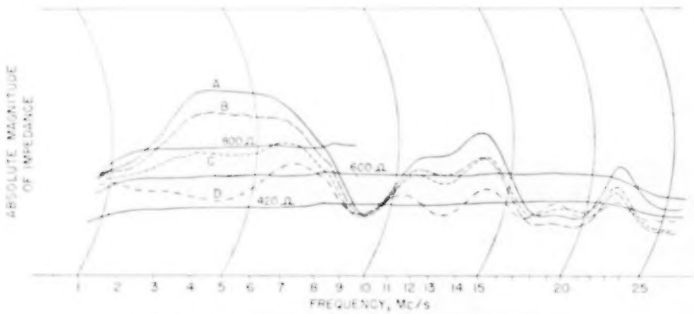

FIGURE 8. *Impedance of multiple-wire delta antennas.*

Each antenna terminated with 800-ohm resistor. Constructional details are shown in figure 7.

0.3 in. apart and connected in parallel. Curve C shows the results when four No. 18 wires were connected in parallel, and curve D the results when the bottom wires consisted of two pairs of No. 18 wires connected in parallel and spaced 16 in. between pairs, as shown in figure 7.

Figure 9 shows that the high-frequency impedance characteristics can be improved at the expense of the low-frequency characteristic by changing the terminating resistance from 800 to 600 ohms.

The W antenna, the construction of which is shown in figure 10, is essentially two vertical-vee antennas excited in phase. One side of each vee terminates in a common resistor, R_T, and the other sides are grounded by means of vertical wires connected to ground by another resistor equal to one-half the value of R_T. The vees are fed by 800-ohm lines, which join to form a 400-ohm line. The impedance characteristic of the transmission-line system with the 800-ohm lines

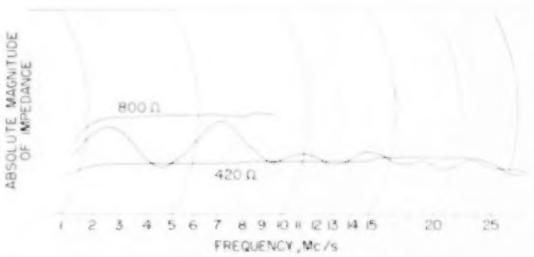

FIGURE 9. *Impedance of multiple-wire delta antenna.*

Same as curve D, figure 8, except that value of terminating resistor is 600 ohms.

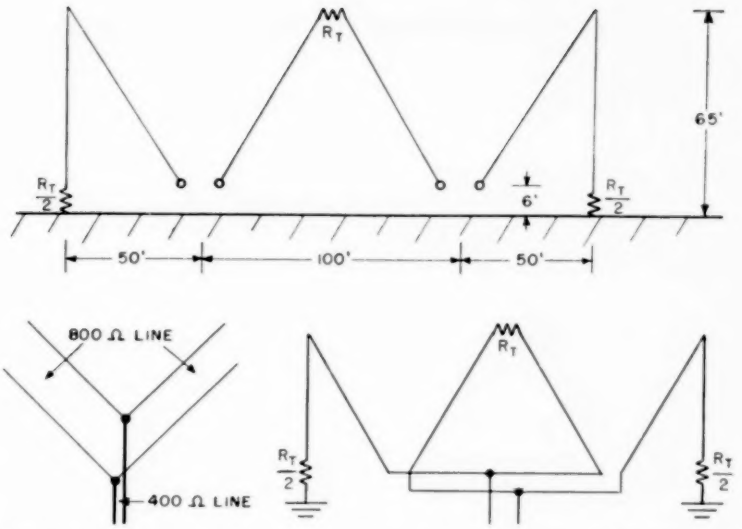

FIGURE 10. *Construction of W antenna and associated transmission line system.*

being terminated by 800-ohm resistors is shown in figure 11. Impedance measurements of the antenna were made for values of R_T equal to 600, 800, 1,000, 1,200, and 1,400 ohms. Figure 12 shows the impedance characteristics of this antenna with the optimum termination of 1,000 ohms between the two vee antennas and with 500 ohms on each side. For R_T equal to 600 ohms, the impedance variation was between 200 and 800 ohms over the entire range. Over most of the range, however, the impedance variation was only about 2:1. For R_T equal to 1,400 ohms, the impedance variation is only slightly greater than for the 1,000-ohm termination.

Another section of the *W* antenna was constructed to make a double-*W* antenna (four vertical vees all excited in phase). This antenna system is shown in figure 13. Each vee was fed with an 800-ohm line, pairs of 800-ohm lines being paralleled and fed with 400-ohm lines. The two resulting 400-ohm lines also were fed in parallel. The impedance looking into the transmission-line system was, therefore, 200 ohms. Since 200 ohms is not a suitable load for current designs of multifrequency ionosphere recorders, it was necessary to introduce an impedance transformer. The design of an rf transformer aperiodic over a frequency range of 1 to 25 Mc and capable of handling

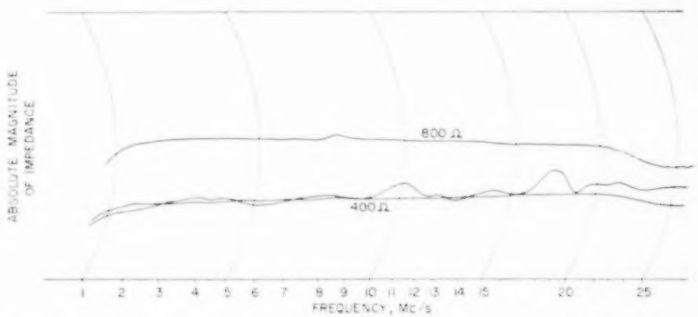

FIGURE 11. *Impedance of transmission line system used with W antenna.*

800-ohm lines terminated with 800-ohm resistors.

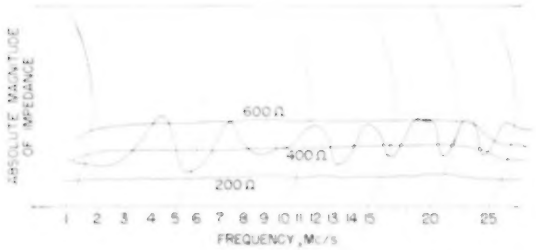

FIGURE 12. *Impedance of W antenna for optimum termination of 1,000 ohms.*

with a pure resistance of 200 ohms is shown in figure 14. Figure 15 shows the impedance characteristic of the entire transmission-line system used with the double-W antenna, including the exponential-line transformer, the 800-ohm lines being terminated with resistance of 800 ohms. Impedance measurements were made of the antenna for values of R_T equal to 800, 1,000, and 1,200 ohms. Figure 16 shows the best results obtained with this antenna, which were secured using a 1,000-ohm termination. Over most of

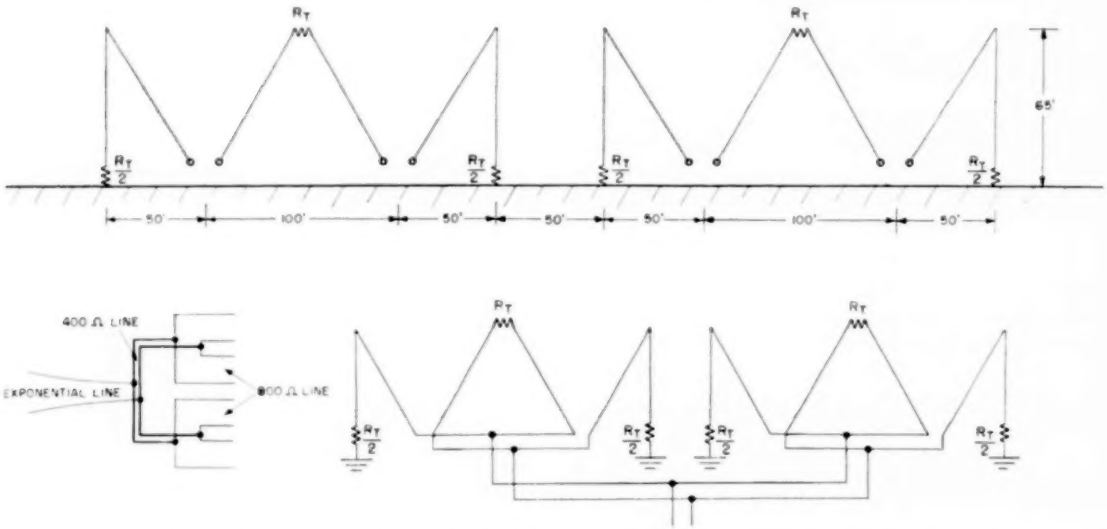

FIGURE 13. *Construction of double-W antenna and associated transmission line system.*

10-kw power is quite complicated. The most promising solution appeared to be an exponential-line transformer.[2] Such a line is reasonably flat at all frequencies substantially greater than the cut-off frequency. Since, for this application, a frequency range of 1 to 25 Mc/s was desired, the cut-off frequency of the line should be considerably below 1 Mc/s if impedance variations at the lower frequencies were to be minimized. However, if the cut-off frequency was too low, the line would be inconveniently long.

An exponential line transformer was therefore designed for an impedance transformation of 200 to 600 ohms and for a cut-off frequency of 300 kc. The resulting line was 88 m long. The performance of this line as a transformer when terminated the range the impedance varied between about 400 and 825 ohms. The impedance variation for a value of R_T equal to 1,200 ohms was 300 to 1,100 ohms and for a value of R_T equal to 800 ohms was from 400 to 900 ohms.

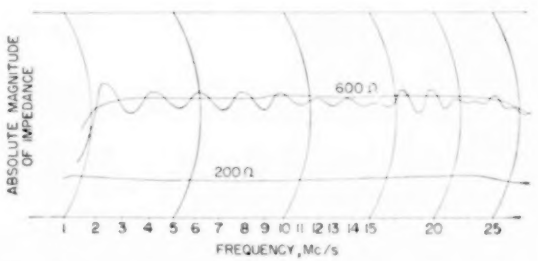

FIGURE 14. *Impedance of exponential transmission line.*
Line terminated with 200-ohm resistor.

[2] H. A. Wheeler, IRE **27**, 65 (Jan. 1939); C. R. Burrows, Bell Sys. Tech. J. **17**, 555 (Oct. 1938); W. N. Christiansen, Proc. IRE **34**, 576 (June 1947).

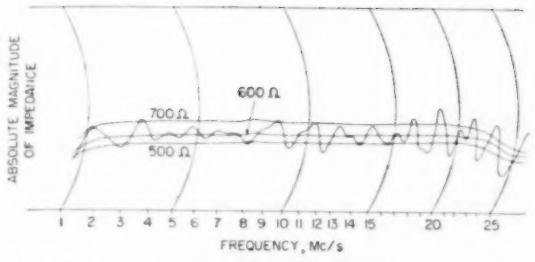

FIGURE 15. *Impedance of entire transmission line system used with double W antenna.*

800-ohm lines terminated with 800-ohm resistors.

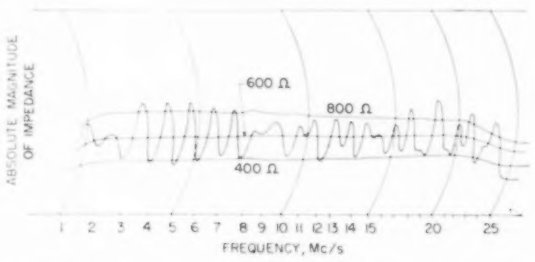

FIGURE 16. *Impedance of double-W antenna for optimum termination of 1,000 ohms.*

An attempt was made to determine the approximate radiation efficiency of the antenna system by measuring the power absorbed by the antenna and its associated transmission-line system and the power dissipated in the terminal resistors. This measurement is possible at frequencies at which the impedance of the antenna is a pure resistance. These are the frequencies at which the impedance of the antenna is a maximum of a minimum. The power input to the antenna system is given by the expression

$$\frac{E_a^2}{R_a}.$$

The power input to the terminating resistors is given by the sum of

$$\frac{E_1^2}{R_1}+\frac{E_2^2}{R_2}+\frac{E_3^2}{R_3}+\cdots\frac{E_r^2}{R_r}+\cdots\frac{E_n^2}{R_n}.$$

In these expressions R_a is the value of the input impedance (resistive) of the antenna; R_1, R_2, . . . R_r . . . R_n are the values of the various terminating resistors, E_a is the rms input voltage to the antenna; and E_1, E_2, . . . E_r, . . . E_n are the rms voltages across the respective terminating resistors.

Then the efficiency of the antenna as a radiator is given by the relationship:

$$EFF=\frac{\dfrac{E_a^2}{R_a}-\sum_{r=1}^{r=n}\dfrac{E_r^2}{R_r}}{\dfrac{E_a^2}{R_a}}$$

$$=1-\frac{R_a}{E_a^2}\sum_{r=1}^{r=n}\frac{E_r^2}{R_r}.$$

It should be noted that the copper, dielectric, and ground losses are all included in the power radiated, and hence the efficiency of the antenna thus obtained is somewhat higher than the true radiation efficiency.

At 3.6 Mc/s, the radiation efficiency of the antenna as measured by this method was found to be approximately 39 percent.

Measurements were made that indicated that each vee had an average input impedance somewhat higher than 800 ohms. An attempt was made to reduce this impedance by constructing the vees with spaced parallel wires, 6-in. spacing being used. The results are shown in figure 17. Comparing figures 16 and 17, it can be seen that, considering the entire frequency range, the single-wire double-W antenna is more desirable. However, for certain limited frequency ranges, the parallel-wave antenna has smaller impedance variations.

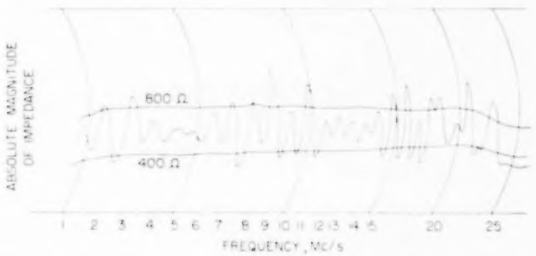

FIGURE 17. *Impedance of parallel wire double-W antenna.*

IV. Conclusions

1. The input impedance of the delta antenna over the frequency range 1 to 25 Mc/s can be lowered and variations minimized, to the point where it is practical to use a transmission line to feed it, by the use of multiple wires in its construction.

2. The size and spacing of the wires parallel to the ground have a decided effect on the input impedance of the multiple-wire delta antenna.

3. The input impedance variations of the experimental double-*W* antenna were of the same order of magnitude as those obtained with the single-wire delta. However, preliminary measurements indicate that the radiation efficiency of the double-*W* antenna is somewhat higher than that of the single-wire delta antenna, particularly at the lower frequencies. The double-*W* antenna is, however, physically large, and its radiation pattern has not yet been determined.

WASHINGTON, March 31, 1949.

U. S. Department of Commerce
National Bureau of Standards

Research Paper RP2007
Volume 43, July 1949

Part of the Journal of Research of the National Bureau of Standards

Formulas for the Percentage Points of the Distribution of the Arithmetic Mean in Random Samples from Certain Symmetrical Universes [1]

By Uttam Chand

Using the method of Fisher and Cornish, the $100\epsilon\%$ point of the distribution of the arithmetic mean in random samples of size N from any universe having finite cumulants, $K_1, K_2, K_3, \ldots$, is expressed to order $1/N^2$ as a function of (*i*), the first five positive integral powers of the $100\epsilon\%$ point of a standardized normal variable, and (*ii*) the quantities K_1, $(K_2)^{\frac{1}{2}}$, and $K_r/(K_2)^{r/2}$ for $r=3$, 4, 5, and 6. The numerical coefficients involved are evaluated for the case of sampling from the normal, rectangular, double-exponential, sech, and sech^2 distributions, and the accuracy of the resulting formulas illustrated by numerical examples.

Consider $y_1 \ldots y_N$ a random sample of size N from a population having finite cumulants $K_r = K_r(y)$, $(r=1,2, \ldots)$. Let $a_r = a_r(y) = K_r/K_2^{r/2}$ be the relative cumulants, $(r=1,2, \ldots)$, and let λ and σ specify the location and scale parameters of the population distribution, respectively.

Let $\bar{y}$ denote the sample mean and consider the standardized variate

$$t=\frac{\bar{y}-K_1(\bar{y})}{\sqrt{K_2(\bar{y})}}.$$

Applying the formulas of Fisher and Cornish [1, 2] [2] and utilizing the relations

$$K_1(\bar{y})=K_1(y)$$

$$K_2(\bar{y})=K_2(y)/N$$

$$a_1(t)=0$$

$$a_2(t)=1$$

and

$$a_r(t)=a_r(\bar{y})=a_r(y)/N^{\frac{r-2}{2}}, (r=3, 4, \ldots),$$

the one-tail ϵ-probability point, t_ϵ, of the standardized variate t can be expressed to order of $1/N^2$ as

$$t_\epsilon = x + \frac{a_3}{6N^{\frac{1}{2}}}(x^2-1) - \frac{a_3^2}{36N}(2x^3-5x) + \frac{a_4}{24N}(x^3-3x)$$
$$+ \frac{a_5}{120N^{\frac{3}{2}}}(x^4-6x^2+3) - \frac{a_3a_4}{24N^{\frac{3}{2}}}(x^4-5x^2+2)$$
$$+ \frac{a_3^3}{324N^{\frac{3}{2}}}(12x^4-53x^2+17)$$
$$+ \frac{a_6}{720N^2}(x^5-10x^3+15x)$$
$$+ \frac{a_3^2a_4}{288N^2}(14x^5-103x^3+107x)$$
$$- \frac{a_4^2}{384N^2}(3x^5-24x^3+29x)$$
$$- \frac{a_3a_5}{180N^2}(2x^5-17x^3+21x)$$
$$- \frac{a_3^4}{7776N^2}(252x^5-1688x^3+1511x)$$

where $x=x_\epsilon$ is a normal deviate exceeded with probability ϵ.[3]

In particular for a *symmetrical universe* we have

$$a_r(y)=0 \text{ for } r=3, 5, 7, \ldots,$$

whence

$$t_\epsilon = x + \frac{a_4}{24N}(x^3-3x) + \frac{1}{N^2}\left[\frac{a_6}{720}(x^5-10x^3+15x) - \frac{a_4^2}{384}(3x^5-24x^3+29x)\right].$$

[1] Revision of a paper written during the summer of 1947 when the author was a guest worker at the National Bureau of Standards, and which was read by title at the Eleventh Summer Meeting of the Institute of Mathematical Statistics, held in Madison, Wis., Sept. 7 to 10, 1948.

[2] Figures in brackets indicate the literature references at the end of this paper.

[3] Miriam L. Yevick has drawn to my attention the fact that comparison of the above expression for t_ϵ with the corresponding expression given by Simaika [3], which includes terms involving $\gamma_1(=a_3)$ and $\gamma_2(=a_4)$ only, reveals two errors in his numerical coefficients: the coefficient of γ_2^2 given as "$-29/381$" should read "$-29/384$", and the coefficient of $\gamma_1^2\gamma_2$ given as "$-107/288$" should read "$+107/288$".

It is interesting to note that for the one-tail 0.04163-probability point, for which $x_\epsilon^2=3$, we have

$$t_\epsilon = x_\epsilon + 0(N^{-2})$$

as $N \to \infty$.

The density functions and the requisite cumulants of five symmetrical distributions considered explicitly are listed in table 1, and the values of t_ϵ computed for $N=10$ from 1-term (normal approximation), 2-terms, and 3-terms of the immediately preceding formula are compared with the corresponding true values in table 2.

TABLE 1. *Five symmetrical distributions and some of their cumulants*

Distribution	Density function	K_2 (variance)	$a_4(=\gamma_2)$	a_6
Normal	$\frac{1}{\sigma\sqrt{2\pi}} e^{\frac{-(y-\lambda)^2}{2\sigma^2}}$	σ^2	0	0
Rectangular	$\frac{1}{\sigma}$ for $-\frac{1}{2} \leq \frac{y-\lambda}{\sigma} \leq \frac{1}{2}$	$\frac{\sigma^2}{12}$	$-\frac{6}{5}$	$\frac{48}{7}$
Double exponential	$\frac{1}{2} e^{\frac{-\lvert y-\lambda \rvert}{\sigma}}$	$2\sigma^2$	3	30
Sech	$\frac{1}{\pi\sigma} \operatorname{sech}\left(\frac{y-\lambda}{\sigma}\right)$	$\frac{\pi^2\sigma^2}{4}$	2	16
Sech^2	$\frac{1}{2\sigma} \operatorname{sech}^2\left(\frac{y-\lambda}{\sigma}\right)$	$\frac{\pi^2\sigma^2}{12}$	$\frac{6}{5}$	$\frac{16}{7}$

TABLE 2. *Comparison of various approximate and exact values of probability points, t_ϵ, of the standardized variate t $N=10$*

Distribution [a]	One-tail probability levels						
	0.001	0.005	0.010	0.025	0.050	0.100	0.250
Normal:							
1 term (exact)	3.0902	2.5758	2.3263	1.9600	1.6449	1.2816	0.6745
Rectangular:							
2 terms	2.9860	2.5280	2.2983	1.9517	1.6473	1.2803	.6831
3 terms	2.9837	2.5270	2.2973	1.9515	1.6474	1.2805	.6833
exact	2.9825	2.5269	2.2971	1.9515	1.6474	1.2805	.6833
Double exponential:							
2 terms	3.3432	2.6829	2.3865	1.9806	1.6388	1.2598	.6530
3 terms	3.3038	2.6839	2.3941	1.9822	1.6409	1.2612	.6531
exact	3.3114	2.6839	2.3932	1.9814	1.6406	1.2612	.6531
Sech:							
2 terms	3.2589	2.6539	2.3731	1.9737	1.6408	1.2671	.6602
3 terms	3.2426	2.6492	2.3712	1.9738	1.6415	1.2677	.6605
exact	3.2449	2.6494	2.3711	1.9736	1.6414	1.2677	.6605
Sech^2:							
2 terms	3.1914	2.6226	2.3544	1.9682	1.6424	1.2729	.6659
3 terms	3.1840	2.6219	2.3548	1.9691	1.6439	1.2739	.6657
exact	3.1646	2.6207	2.3540	1.9681	1.6426	1.2732	.6661

[a] The exact values of t_ϵ for the normal distribution were taken from Kelley [4]; for the rectangular and double-exponential distributions, from an unpublished table prepared in connection with [5]. The exact values of t_ϵ for the sech and sech^2 distributions were computed under the supervision of Irene A. Stegun of the National Bureau of Standards Computation Laboratory from formulas prepared by Julius Lieblein of the National Bureau of Standards Statistical Engineering Laboratory.

The author expresses appreciation to Churchill Eisenhart for suggesting this problem and to Lola S. Deming and Celia S. Martin of the Statistical Engineering Laboratory, National Bureau of Standards, for the numerical computations.

References

[1] E. A. Cornish and R. A. Fisher, Moments and cumulants in the specification of distributions, Rev. Inst. Intl. Stat. **4**, 1 to 14 (1937).

[2] Maurice G. Kendall, The advanced theory of statistics, **I**, p. 156 to 158 (Charles Griffin & Co., Ltd., London; 1st ed., 1943; 3d ed., 1947).

[3] J. B. Simaika, Interpolation for fresh probability levels between the standard table levels of a function, Biometrika **XXXII**, parts III and IV, p. 263 to 276 (April 1942).

[4] T. L. Kelley, The Kelley statistical tables, revised 1948 (Harvard University Press, Cambridge, Mass.).

[5] Churchill Eisenhart, Lola S. Deming, Celia S. Martin, On the arithmetic mean and median in small samples from the normal and certain nonnormal populations, presented at the Summer Meeting of the Institute of Mathematical Statistics, held in Madison, Wis., Sept. 7 to 10, 1948.

WASHINGTON, March 22, 1949.

U. S. Department of Commerce
National Bureau of Standards

Research Paper RP2008
Volume 43, July 1949

Part of the Journal of Research of the National Bureau of Standards

Refractive Indices of Thallium Bromide-Iodide Crystals for Visible and Infrared Radiant Energy [1]

By Leroy W. Tilton, Earle K. Plyler, and Robert E. Stephens

The refractive indices of two specimens of thallium bromide-iodide (KRS$_5$) were measured at a constant room temperature of 27° C from 0.577 to 39 microns by use of a minimum-deviation spectrometer and a Perkin-Elmer infrared spectrometer equipped with a calibrated screw for operation of the Littrow mirror. In order to cover the entire region over which the prisms are transparent, many known wavelengths were used, including lines of mercury, sodium, hydrogen, and helium for the visible region. A cadmium-mercury lamp was the source from 1 to 2 microns. From 2 to 39 μ various absorption bands of carbondioxide, water, methylcyclohexane, polystyrene, and polyethylene were used, with a Globar as source, for the identification of wavelengths.

Mixed crystalline thallium bromide-iodide, a material known as KRS–5, has a very high refractive index, 2.63 for sodium light, and also a high density. It is opaque to wavelengths shorter than about 0.5 μ but very transparent in the infrared to about 40 μ. The material is a solid solution of thallium bromide and thallium iodide. That is, it is truly a mixed crystal of the cubic system and therefore not double refracting when free from strain. Interferometer photographs indicate that some of the material is produced in a reasonably homogeneous state, although certainly not as uniform as good optical glass.

For growing these crystals, commercially obtainable chemicals of reagent quality are further purified by crystallization, and then proper mixtures are melted and well stirred. The Germans report that a crystal nucleus is introduced at the top and that the whole is cooled from the upper surface, but it is also successfully grown from the bottom in this country. Crystalline KRS–5 was of great importance to the Germans in the design of optical systems transmitting infrared energy. Incidentally, thallium bromide and iodide have been more or less known to petrographers for 15 or 20 yr as powders that could be mixed and melted for producing a series of solid immersion media having sodium-lines indices ranging from about 2.40 to 2.65 accordingly as the proportion of thallium iodide is varied from 0 to 75 percent. Solid solutions with more than 75 percent of the iodide component are not stable in the cubic system but invert into a birefringent orthorhombic modification.[2]

Crystals of KRS–5 have been grown by a number of investigators in the United States and are now grown by the Harshaw Chemical Co. of Cleveland. The measurements of refractive index herein reported were made on a 25° prism with faces about 6 by 6.2 cm, from a crystal grown by Harshaw, and on a 12° prism with faces about 4 by 6.5 cm, from a crystal grown by Francis P. Phelps at this Bureau. These prisms were made in the Bureau's Optical Shop, and the surfaces were flat within a few wavelengths over about 80 percent of their apertures. Both these prisms were designed to contain approximately 58 percent of thallium iodide. The Phelps prism was analyzed by Howard B. Knowles of this Bureau and found to contain 58.3 percent of thallium iodide

[1] The work described in this paper was carried out in 1947 in part under contract S & A 2858 between the Bureau of Ships and the National Bureau of Standards, in order to confirm and extend our knowledge of the optical properties of this medium.

[2] Tom. Barth, Am. Mineral. **14,** 358 (1929). The curves of refractive index for the visible region versus composition by weight, figure 2 of Barth's paper, seem too low in the neighborhood of 60% thallium iodide by about 0.03 in index, as judged by the data of this paper on the Phelps prism which, by analysis, contains 58.3% thallium iodide. Similarly, Barth's curves would seem too low by 0.05 if judged by the Hettner and Leisegang data on a prism said to contain 50% thallium iodide. (See footnote 4.)

and 41.7 percent of thallium bromide. The Harshaw prism has not been analysed, because it is in almost constant use on a long program of investigations in the infrared. Moreover, since this material is very susceptible to deformation by stress or shock, it seems unwise to jeopardize the homogeneity of this uniquely valuable optical component by the mechanical operations necessary in removing a sample for analysis. Later it is hoped that an analysis can be made in order to confirm the reasonable inference that this prism is about 0.5 percent higher in thallium iodide content than is the Phelps prism, which has refractive indices only 0.002 lower than those of the Harshaw prism.

The refractive indices of these prisms were first measured in the visible region for eight wavelengths in the yellow and red. This was done by use of a minimum-deviation spectrometer, chiefly at room temperatures near 23° C. The results for each prism were expressed by a Ketteler-Helmholtz dispersion formula of the form

$$n^2=a^2-k\lambda^2+\frac{m}{\lambda^2-\lambda_r^2}, \qquad (1)$$

in which the parameters a^2, k, m, and λ_r^2 were adjusted by the method of averages. The average residual of 7×10^{-5}, somewhat larger than anticipated, may be ascribed in part to somewhat imperfect surfaces and some inhomogeneity, but also it is due in large part to lack of careful temperature control and observation for these preliminary data with visible energy. Also, since this material is practically opaque to visible radiation shorter than about 5,000 A, the indices measured in the yellow region are affected to some extent by the fact that the yellow light is more predominantly transmitted near the apex and perhaps not at all through the thicker portions of the prism near its base. Therefore, the effective apertures for yellow and for red light do not exactly coincide. The resulting error in index measurement is probably appreciable in the yellow region but of little importance in the red and beyond.

Subsequent measurements for $\lambda=5{,}876$ and $\lambda=6{,}678$ at 30° C were much lower than those near 23°, and a temperature coefficient of -16×10^{-5}/deg C was found for light of approximately 6,000 A. This optical sensitivity to temperature is over four times that of rock salt.

The method to be described for the index measurements in the infrared is not self-sufficient. For each prism the adjusted index (computed by eq 1) for the cadmium red line, $\lambda=6{,}438$, is taken as the basis with respect to which the infrared indices are to be computed. The use of eq 1 for adjusting the data in the visible region probably compensates in large part for the inadequate knowledge of temperatures of the KRS–5 during individual observations. These basic indices for cadmium red at an average temperature of 23° were then reduced to 27° C, the temperature of the room in which the infrared observations were made.

In the infrared region use was made of a Perkin-Elmer infrared spectrometer equipped with a calibrated screw for operation of the Littrow mirror, M of figure 1. The concave collimating mirror, C, focal length 27.5 cm, approximately 18° off axis, has an aperture of about 7.5 cm but was stopped down to a rectangular aperture of about 5×5 cm to reduce stray energy. The angular separation of the entrance and exit slits is 1.9636° at the face of the Littrow mirror. The angular equivalent of the screw was found to be 27.05′ or 1623″ per turn, averaged over almost its total length. This was done by means of 64 successive steps with two mirrors that were set at an angle of 5′ of arc. A collimator and telescope were used for precision in making the steps. Evidence was found that seemed to indicate that the periodic errors of a single turn may be ±10 sec, and that progressive corrections to the average equivalent of the screw may sometimes exceed 30 sec, but it is possible that this was merely evidence of distortion of the Littrow mirror, introduced by clamping.

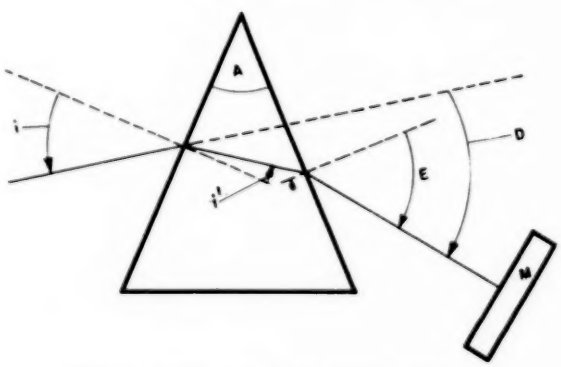

FIGURE 1. *Prism installed on infrared spectrometer.*

The detector was of the Golay type with a KRS–5 window, the incident beam being interrupted about 10 times per sec. Slit widths as wide as 0.35 to 0.43 mm were necessary for visible radiation and for the region where the water vapor absorption was utilized. Widths of from 0.03 to 0.20-mm were sufficient in the intermediate region. A measure of the energy received by the detector is automatically recorded on a Leeds & Northrup Speedomax recording potentiometer.

This spectrometer was used, not because it is particularly favorable for this work, but because it was available and index values were required. An objection is the return passage of energy through the prism, which causes additional losses by reflection and absorption. This is particularly disadvantageous in that the energy does not exactly retrace its path because of the angular separation of entrance and exit slits.

Since on the infrared spectrometer the prism is stationary, and only the rotation of the Littrow mirror may be observed, it is necessary to use the method of known incidence angle for refractive-index measurements with a spectrometer of this type. This method of known incidence was used by Rydberg [3] over a century ago, and Martens [4] found it useful in measuring indices in the ultraviolet. Martens recommended the computation of indices by the equations

$$\tan\left(i'-\frac{A}{2}\right)=\tan\frac{A}{2}\cot\frac{A+D}{2}\tan\left(i-\frac{A+D}{2}\right), \tag{2}$$

and

$$n=\frac{\sin i}{\sin i'}$$

especially when logarithms are used. For use with computing machines it is preferable to use the equivalent forms

$$\cot i'=\cot A+\frac{\sin E}{\sin A\sin i}, \tag{3}$$

and

$$n=\sin i\,(1+\cot^2 i')^{1/2},$$

where the symbols have the meanings designated in figure 2.

[3] F. Rydberg, Poggendorf's Annalen **14**, 45 (1828).
[4] F. F. Martens, Verhandl. deut. physik. Ges. **3**, 10 (1901).

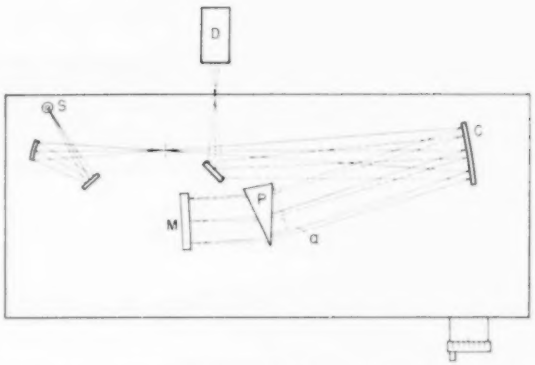

FIGURE 2. *Simplified relation of Littrow mirror to deviation produced by prism.*

In order to install each prism of KRS–5 with suitable known incidence angle, i, on an infrared spectrometer of this type, small auxiliary prisms of glass were made with angle, A_x, approximately equal, in each case, to $(A+D)/2$ for the minimum-deviation condition and some wavelength of visible radiant energy traversing the KRS–5 prism. Although there is nothing very precise about the selection of a favorable incidence angle, i, it is necessary to know the i that is actually used. Consequently, the angles of the auxiliary glass prisms are carefully measured, and they are used in the installation of the corresponding prisms of KRS–5 on the spectrometer as shown at A in figure 1. With any intense visible radiation focused on the entrance slit, the prism pair is so oriented that light reflected from the outer polished face of the auxiliary prism is returned to the entrance slit. After removal of the auxiliary prism, any energy from the entrance slit will be incident on the unknown sample prism at an angle $i=A_x$, where A_x is the measured refracting angle of the auxiliary glass prism.

For any prism, starting with the refracting angle, A, the index, n, as adjusted for $\lambda_0=6{,}438$, $t=27°$, and incidental angle, i, it is possible to trace rays through the prism, as indicated in figure 2, and find E_0, angle of emergence for these basic or initial conditions. If the Littrow mirror were normal to the emergent ray (zero angle between entrance and emergence slits), or even if the incidence angle of $\delta E/2$ on the Littrow mirror remained constant for the different wavelengths to be used, then the observable angular increments for the Littrow mirror, as determined from the

drum readings of the screw, would be the exact increments applicable to E_0 to give E_λ.

Fortunately, $\delta E/2$, the incidence angle on the Littrow mirror, varies rather slowly as n changes, and it is not difficult to trace a series of pairs of rays (for i and for $i-1.9636°$) for arbitrarily selected evenly spaced values of n, as 2.60, 2.50, 2.40, 2.30, and form an interpolation table of $\delta E/2$ as a function of n. Then when computing n by means of eq 1, it is found that correct preestimation of n within 1 or 2×10^{-3} will enable one to select a satisfactory value for the small correction to the observed angular increment in E, for use in computing n correctly within ±1 or 2×10^{-5}.

In order to cover the entire infrared region over which these prisms are transparent, many wavelengths were used, including those for various absorption bands of carbondioxide, water, methylcyclohexane, polystyrene, and polyethylene, with a Globar as source. The ordinarily sharp zero branches of the absorption curves for various vapors could not be used, because the recorded contours of these branches are not sharp at the center when the dispersion is low as is the case for these prisms from 3.4 to 14.3 μ. Here, however, the recordings of the ordinarily broad bands of absorption of polystyrene, polyethylene, and methylcyclohexane become usefully narrow.

Equation 1 was found definitely inadequate for accurately representing the index of refraction, even to four decimal places, over so long a spectral range as that covered in this investigation. Also, the four-constant Sellmeier formula with two terms, namely,

$$n^2=1+\frac{M'\lambda^2}{\lambda^2-\lambda_r^2}+\frac{m'\lambda^2}{\lambda^2-\lambda_s^2}, \tag{4}$$

exactly equivalent to one form of the Kettler-Helmholtz formula (as strictly limited to two resonance frequencies), namely,

$$n^2=a^2-\frac{M}{\lambda_r^2-\lambda^2}+\frac{m}{\lambda^2-\lambda_s^2}, \tag{5}$$

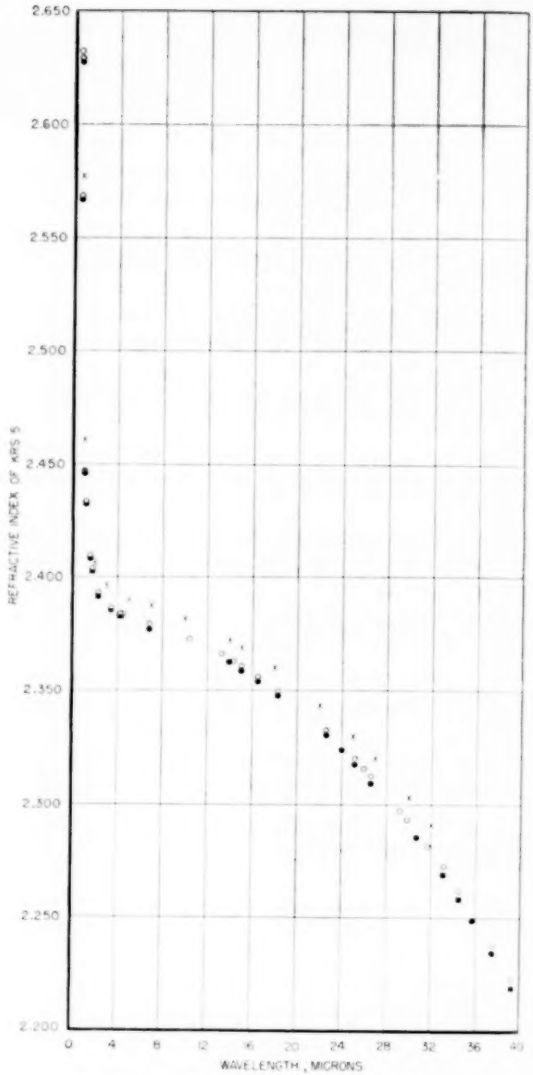

FIGURE 3. *Index of refraction of* KRS–5.

The raw observed values for the Harshaw and the Phelps prisms are used here, this graph being identical with that shown at the New York meeting of the Optical Society of America, March 1948.

where

$$a^2=1+\frac{M}{\lambda_r^2}+\frac{m}{\lambda_v^2}=1+M'+m',$$

was found to be considerably worse than eq 1, which is merely a partially expanded, and therefore an approximate, form of eq 4 or 5. Equation 4 or 5 can, however, account for the effect of only one absorption band in the infrared and one in the ultraviolet, whereas their expanded forms can, with the same number of constants, approximate the effects of multiple bands, and these prisms of KRS–5 are known to have two prominent infrared bands, one each for the bromide and iodide constituents. By retaining in the expansion a term in $-\lambda^4$, however, and adjusting the five parameters by least squares, the equation

$$n^2=5.676\,927-0.000\,452\,226\,4\lambda^2-0.000\,000\,018\,019\,7\lambda^4+\frac{0.287\,301\,7}{\lambda^2-0.102\,773\,4}, \quad (6)$$

was found to represent the indices of the 25° Harshaw prism.

The same equation with $a^2=5.667\ 927$ serves so well (see residuals in table 1) for the 12° Phelps prism that a betterment by least squares is unnecessary.

Equation 5 with five constants, that is one in which

$$a^2=1+\frac{M}{\lambda_r^2}+\frac{m}{\lambda_v^2}+\ \ldots,$$

was not tried because if five constants are to be used, it appears much better to try the expanded form as in eq 6, where not only the constant, but certain other additional terms relating to any other pertinent absorption bands are automatically taken into account.

Table 1 gives, according to eq 6 and 7, the indices and the residuals, observed minus computed, for each of these prisms for the wavelengths that were used. The agreement between observed and computed indices for each prism is entirely satisfactory, and the computed indices for these prisms are probably typical for this material. The differences in index from wavelength to wavelength, easily obtainable from table 2, are probably accurate to a few units in the fifth decimal. The

TABLE 1. *Observed and computed data on index of refraction of* KRS–5 *(27° C)*

Wavelength	Source or absorbing media	Computed index Harshaw prism	(o−c)×10⁴	Computed index Phelps prism	(o−c)×10⁴
μ					
.5770	Hg yellow	2.6316	+1		
.5780	Mean Hg yellow			2.6286	−14
.5791	Hg yellow	2.6291	+1		
.6438	Cd red	2.5987	−6	2.5970	−6
1.0142	Hg	2.4408	+3	2.4450	+13
1.1289	Hg	2.4334	+2	2.4316	+11
1.5208	Hg	2.4092	+3	2.4073	+12
1.700	Hg	2.4039	+2	2.4020	+11
2.26	Polyethylene abs	2.3942	−5	2.3923	−5
3.42	Polystyrene abs	2.3867	+2	2.3848	+10
4.24	CO_2 abs. in air	2.3843	−1	2.3824	+8
4.4	CO_2 flame emission	2.3839	−4		
6.86	Methylcyclohexane abs.	2.3794	+1	2.3775	−4
10.34	do	2.3730	+0		
13.23	Polystyrene abs	2.3692	+3		
13.90	Polyethylene abs			2.3625	+6
14.32	Polystyrene abs	2.3632	+1		
14.98	CO_2 abs. in air	2.3613	−1	2.3594	−2
16.48	Methylcyclohexane abs.	2.3567	−2	2.3547	−1
18.29	do	2.3504	−4	2.3485	−3
22.60	do	2.3328	+1	2.3308	+3
23.92	Water vapor abs.[a]	2.3265	+3	2.3246	+1
25.16	do.[a]	2.3203	+0	2.3184	−4
25.97	do.[a]	2.3160	−1		
26.60	do.[a]	2.3127	−3	2.3107	−7
28.33	do.[a]			2.3008	−2
29.15	do.[a]	2.2978	−6		
29.81	do.[a]	2.2937	−1		
30.69	do.[a]			2.2861	+2
31.70	do.[a]	2.2814	−0		
33.11	do.[a]	2.2715	+10	2.2695	0
34.48	do.[a]	2.2614	+1	2.2594	−7
35.7	do.[a]			2.2500	−7
37.45	do.[a]	2.2377	−3	2.2357	−6
39.22	do.[a]	2.2224	−1	2.2204	−6

[a] For the wavelengths of the absorption bands of water vapor, see H. M. Randall, D. M. Dennison, N. Ginsburg, and L. R. Weber, Phys Rev. **52**, 160 (1937).

index residuals for the Phelps prism are larger, because the effects on index of accidental errors in deviation measurement are fully twice as large for the prism of 12° angle. Moreover, since the resolution is much lower, the angular errors themselves are larger. The average difference in raw observed index between the two prisms varies from 13×10^{-4} in the visible region to 28×10^{-4} at 39 μ, figure 3, whereas the corresponding differences are 17 to 20×10^{-4} in the computed indices. In other

TABLE 2. *Refractivity of* KRS–5 *at 27° C for use in computing partial dispersions*

This table is an average for two samples of KRS–5 grown independently in different laboratories in the United States in efforts to produce solid solutions of minimum melting point. One, by analysis, contains 58.3 percent thallium iodide and the other, by inference from its indices, contains 58.8 percent thallium iodide. The measurements were made at 35 wavelengths well distributed over the range of 40 μ. The table is computed by means of equation 6, except that a^2 has the value 5.672427. It is estimated that differences taken from this table are reliable to $\pm 2\times10^{-5}$.

Wavelength	Tenths of microns									
	.0	.1	.2	.3	.4	.5	.6	.7	.8	.9
	Values of $(n-2)\times10^5$									
μ										
0	.....	.....	.....	.....	.....	.....	60561	53262	49137	46542
1	44789	43544	42623	41923	41376	40940	40586	40296	40053	39848
2	39673	39523	39393	39279	39178	39089	39009	38937	38873	38814
3	38760	38711	38666	38623	38584	38548	38514	38482	38452	38423

Wavelength	$(n-2)\times10^5$	Wavelength	$(n-2)\times10^5$	Wavelength	$(n-2)\times10^5$	Wavelength	$(n-2)\times10^5$
μ		μ		μ		μ	
1	44789	11	37062	21	33883	31	28306
1.5	40940	11.5	36949	21.5	33670	31.5	28172
2	39673	12	36832	22	33451	32	27832
2.5	38989	12.5	36710	22.5	33226	32.5	27485
3	38760	13	36584	23	32996	33	27131
3.5	38548	13.5	36453	23.5	32760	33.5	26770
4	38396	14	36317	24	32518	34	26403
4.5	38276	14.5	36176	24.5	32271	34.5	26028
5	38173	15	36030	25	32017	35	25647
5.5	38081	15.5	35880	25.5	31758	35.5	25258
6	37994	16	35724	26	31493	36	24862
6.5	37910	16.5	35564	26.5	31222	36.5	24459
7	37826	17	35398	27	30945	37	24048
7.5	37740	17.5	35227	27.5	30662	37.5	23630
8	37653	18	35051	28	30373	38	23205
8.5	37563	18.5	34870	28.5	30078	38.5	22772
9	37471	19	34683	29	29776	39	22331
9.5	37374	19.5	34491	29.5	29468	39.5	21882
10	37274	20	34294	30	29154		
10.5	37170	20.5	34092	30.5	28833		

words, there is little if any difference in dispersion between these two prisms. The corresponding difference, if any, in the proportions in which the bromide and the iodide are present would be about 0.5 percent, the Harshaw prism to have the slightly higher iodide content.

Figure 3 shows by open circles the (observed) indices of the 25° prism grown by Harshaw and by black dots the indices of the 12° prism grown by Phelps. Some indices of a sample of KRS–5 according to "Hettner",[5] as read from a curve obtained from Germany, are entered on this figure as crosses. They extend, however, only to 32 μ. At the long wavelengths that sample of KRS–5 averaged fully 100×10^{-4} higher in index than the Phelps prism even allowing for a possible difference of 10 deg C. This indicates, according to the index curves published by Barth, that the Hettner sample contained about 2.5 percent *more* thallium iodide than the Phelps prism.[6]

[5] Possibly based on the data published later by G. Hettner and Gertrud Leisegang, Optik **3**, 305 (1948).

[6] The Hettner and Leisegang prism (footnote 4) is said, however, to contain 50% of thallium iodide, which is about 2.3% *less* than that in the Phelps prism. With reference to index stability, it may be added that check measurements for λ=6438 were made on the Phelps prism after a 15-month interval, using a different spectrometer, and no change was found in the fourth decimal place.

U. S. Department of Commerce
National Bureau of Standards

Research Paper RP2009
Volume 43, July 1949

Part of the Journal of Research of the National Bureau of Standards

Fundamental Aspects of the Reaction of Oxygen With Carbon Adsorbents[1]

By William V. Loebenstein[2] and Neil L. Pennington

The kinetics for the oxidation of the carbon in a coconut-shell charcoal, a new bone char, two service bone chars, and a spent bone char was found to be retarded first-order in character. The experimental data were obtained in a flow system with nitrogen-oxygen gas mixtures at temperatures below 400° C. Using the initial fractional rate of oxidation of the carbon as the criterion of evaluation, a linear plot against oxygen concentration was obtained for each temperature at which the combustion was studied. The influence of temperature was expressed as the sum of two exponential Arrhenius-type terms. A single relationship was derived by combining the effects of these two variables. This relationship proved equally valid when applied to all carbon adsorbents investigated. Some reaction mechanisms were proposed that were consistent with the experimental findings of the investigation.

I. Introduction

The study of the kinetics of combustion of carbon was initiated about 85 yr ago [1, 2],[3] and it was early appreciated that the subject was highly complex. Oxygen was found to react with carbon at temperatures much lower than those associated with ordinary burning, and the reaction was explained by the postulation of the formation of stable surface complexes. Rhead and Wheeler [3] in 1912 to 1913 found that it was not possible to break down these complexes by evacuating at the same temperatures at which they were formed. McLean [4] confirmed these findings years later and observed that above 200° C none of the oxygen is recovered in the uncombined state. Later, different forms of surface oxide complexes were suggested to explain the results of measurements of heats of adsorption of oxygen on a charcoal. Very high values were identified with the initial uptake of oxygen, and these values dropped off rapidly with the addition of more oxygen [5, 6].

In 1932 Kolthoff [7] demonstrated the existence of different specific oxide complexes on charcoals by observing either predominantly acidic or basic properties, depending upon the conditions under which the sample had been heated. A few years later Klemenc, Wechsberg, and Wagner [8] proposed carbon suboxide (C_3O_2) as the intermediate complex formed during the combustion of carbon. They pointed out that the ratio of carbon dioxide to carbon monoxide, which could be predicted from the decomposition of carbon suboxide at 400° C, was of the same magnitude as that observed in the combustion of carbon at that temperature. Rhead and Wheeler [3] believed the oxide complex to have a variable composition C_xO_y, with x and y having different values, depending upon the temperature so as to break down into carbon monoxide and carbon dioxide in varying relative amounts. This view was shared by Haslam [9], Shah [10], and also Oshima [11].

Chukhanov and Karzhavina [12] believed that the intermediate complex existed in the form C_3O_4, which might decompose directly or combine with more carbon and oxygen so as to yield

[1] This investigation is sponsored by a joint research project undertaken by the United States Cane Sugar Refiners and Bone Char Manufacturers, a greater part of the refining industry of the British Commonwealth, and the National Bureau of Standards.

[2] Research Associate at the National Bureau of Standards, representing the cooperating manufacturers.

[3] Figures in brackets indicate the literature references at the end of this paper.

different relative amounts of carbon dioxide and carbon monoxide. Strickland-Constable [13] cited data supporting the simultaneous existence of two types of surface oxide, to which he assigned the names "Labile" and "Stable".

The apparent order of the oxidation reaction has also been subjected to considerable study. The results have varied, depending upon the source and history of the type of carbon studied, the temperature, pressures, oxygen concentration, and in some cases upon the rate of flow of the reactant gases. A wide range of activation energies also have been reported in the literature. Values as high as 100,000 [14] and as low as 20,000 [15] calories have been obtained in the same temperature range and for similar types of carbon. Mayer [16] in a review article in 1934 concluded that no complete formulation of the rates or mechanism of the combustion of carbon was yet possible.

In spite of the variety of experimental methods employed, most of the recorded investigations agree on one of several important factors: the relative quantity of gaseous carbon dioxide compared to carbon monoxide increases with the time of contact of the reactant gases with the carbon sample. This effect was noted by Meyer [17] in the oxidation of a carbon filament at high-flow velocities; by Lambert [18] using a granular bed of charcoal; and by Tsukhanova [19] during the passage of air through a hollow carbon cylinder. Recently, the effect was observed by Deitz [20] in a plant-scale oxidation of bone char by passage through a rotary decarbonizer. Samples of gas were collected from various positions within the decarbonizer for analysis. The ratio of carbon dioxide to carbon monoxide increased to as high as 40:1 as the gases moved from the hotter region toward the cooler end from which they were withdrawn. These examples point to a possible secondary oxidation of the carbon monoxide that is formed as one of the primary products during the combustion.

II. Status of Present Investigation

In a previous article [22] the rate of combustion of bone char and other carbon adsorbents was followed with respect to carbon. The data for bone char satisfied the requirements of a retarded first-order reaction. The equation, in its integrated form, which lent itself most readily to a direct evaluation of the reaction rate constant was stated as follows:

$$\frac{1}{t}\ln\left[\frac{1}{1-f}\right]=k-b\,\frac{1}{t}\left[\left(\ln\frac{1}{1-f}\right)-f\right]. \qquad (1)$$

where

t = time (hours) measured from steady-state conditions;
f = fraction of the original carbon present in the sample that had burned in t hours;
k = reaction-rate constant (reciprocal hours);
b = a constant whose numerical value is related to the extent of retardation.

The reaction-rate constant was determined for one bone char (char 2) at different oxygen concentrations, but at the same temperature and flow rate. Under these conditions it was found that a plot of k against percentage of oxygen gave a straight line. This line, when extrapolated to zero percent of oxygen, intercepted the k axis at a value greater than zero. The same situation was found to exist for an activated carbon (char 6) where the retardation was so slight that a simple (unretarded) first-order relationship fitted the data satisfactorily. When ln k was plotted against $1/T$ for a new bone char, the resultant graph deviated markedly from linearity.

In the present paper a more detailed study is presented of the effects of oxygen concentration and temperature for a coconut-shell charcoal (char 1) and number of different bone chars. Plausible mechanisms are suggested for the combustion process that are consistent with the observed dependence of the initial reaction rate upon these variables.

III. Procedure

The apparatus and procedure have been described earlier [22]. Oxygen-nitrogen mixtures of known composition were passed downward through a vertically supported reaction tube containing the sample. The reaction products were then determined gravimetrically. The temperature, oxygen concentration, and rate of flow were held constant for a given combustion experiment; and the resultant carbon dioxide and carbon monoxide were measured at known intervals of time. The amount of carbon burned during each time inter-

val was computed from these quantities and expressed as a fraction of the total carbon originally present in the sample. In every case, measurements were corrected to steady-state conditions. Equation 1 was employed for the evaluation of the rate constant k by plotting the function

$$\frac{1}{t}\ln\left[\frac{1}{1-f}\right],$$

against

$$\frac{1}{t}\left[\ln\left(\frac{1}{1-f}\right)-f\right],$$

and determining the intercept of the resultant straight line.

IV. Independence of k and Dependence of CO_2/CO Upon Sample Weight

Several combustion experiments were conducted with new bone char (char 2) at 280° C, 4.8-percent oxygen in nitrogen and three separate flow rates: 270, 330, and 465 ml/min. The samples varied in weight from about 0.5 to 6.0 g. The results are listed in table 1 in the order of increasing weight of sample within a group of a given flowrate. A comparison of the second and fifth columns shows no dependence of rate constant upon sample weight at a flowrate of either 270 or 465 ml/min. An examination of the fifth column discloses only a slight effect of flow-rate upon k.

TABLE 1. *Comparison of the rate constants and the ratios CO_2/CO with sample weights for char 2 (a new bone char) at three different rates of flow*

All measurements were made at 280° C and 4.8 percent oxygen in nitrogen

Experiment	Weight of sample (W)	Flow rate (V)	CO_2/CO	Rate constant (k)
	g	*ml/min*		*1/hr*
15	0.484	270	2.1	0.126
18	.601	270	2.7	.094
17	.727	270	2.5	.101
16	.972	270	4.1	.118
21	.987	330	3.3	.080
13	.485	465	1.4	.18 (?)
14	.730	465	1.9	.087
12	.986	465	2.6	.084
3	.988	465	2.6	.080
11	1.936	465	4.0	.102
1	1.996	465	3.3	.063(?)
20	3.392	465	5.5	.091
4	4.824	465	6.5	.091
2	4.983	465	6.2	.081
19	5.856	465	6.1	.096

It may be seen from the fourth column of table 1 that the ratio of carbon dioxide to carbon monoxide definitely increases with increasing weight of sample within each group of flow rates.[4] Furthermore, higher ratios are seen to be associated with lower flow rates. This is demonstrated by comparing the ratio of carbon dioxide to carbon monoxide for experiments 16, 21, 12, and 3, all of which are based on sample weights close to 1 g. These ratios at 270, 330, and 465 ml/min are 4.1, 3.3, and 2.6, respectively. Moreover, when each of the ratios mentioned is multiplied by the corresponding flow rate, the values 1,100, 1,100, and 1,200, respectively, are obtained. Since velocity of flow is inversely proportional to the time of contact, this demonstrates clearly that for the same weight of sample the CO_2/CO ratio is directly proportional to the time of contact of the reaction mixture with the char sample.

V. Influence of Oxygen Concentration and Temperature on the Reaction Rate Constant

Equation 1 is the integrated form of the equation:

$$\frac{df}{dt}=k\,\frac{1-f}{1+bf}, \qquad (2)$$

where both k and b may be considered to be functions of oxygen concentration and temperature, and df/dt is the fractional rate of combustion of the carbon in the sample. It may be seen from eq 2 that k is the limiting value of df/dt as t tends toward zero. An alternative definition of k is, therefore, the initial rate of combustion. A plot of k against mole fraction of oxygen is given in figure 1 for a coconut-shell charcoal (char 1) at a flow of 270 ml/min at the indicated temperatures. The values of k were obtained from the experimental data by use of eq 1. These values are given in columns 3 and 5 of table 2.

The results for a new bone char, 2; service char, 35; service char, 3; and spent char, 27 also gave linear dependences of k upon oxygen concentration, as may be seen from the unbroken lines in

[4] It is felt that the tapering off of the last two figures in column 4 (i. e., 6.2 and 6.1) is not a real effect. It is possible that the capacity of the carbon dioxide absorption tube in the analysis train was slightly exceeded when the highest weight samples were used. This would have allowed a small amount of CO_2 to pass through and be included later with the CO.

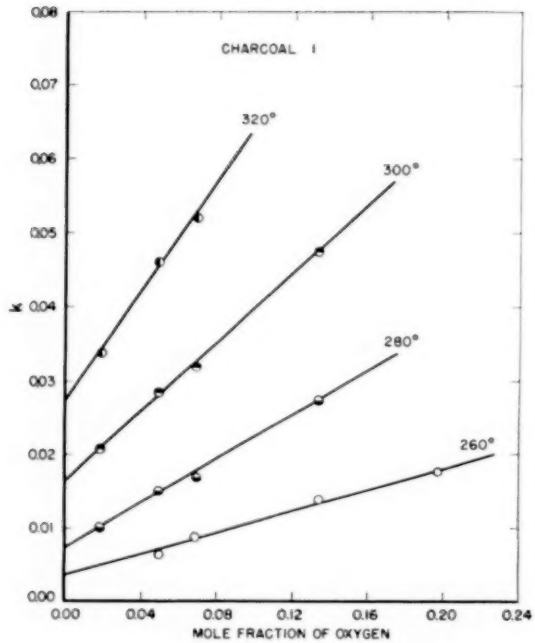

FIGURE 1. *Rate constant k as a function of oxygen concentration for char 1 (a coconut-shell charcoal) at 260°, 280°, 300°, and 320° C and a flow rate of 270 ml/min (see also table 2).*

TABLE 2. *Rate constants for the combustion of char 1 (a coconut-shell charcoal) at a flow rate of 270 ml/min for various percentages of oxygen in nitrogen and at the four temperatures indicated (see also fig. 1)*

Experiment	Temperature	Oxygen	Weight of sample	k (observed)
	°C	*Percent*	*g*	1/*hr*
141	260	4.92	0.6477	0.0064
139	260	6.93	.8365	.0080
140	260	13.29	.3915	.0158
142	260	19.71	.2839	.0176
133	280	1.83	.4742	.0102
134	280	4.92	.5820	.0151
131	280	6.93	.5231	.019
132	280	13.29	.3744	.0275
128	300	1.83	.5300	.0206
130	300	4.92	.4912	.029
126	300	6.93	1.2025	.032
129	300	13.29	.3779	.0475
137	320	1.83	.3204	.0337
138	320	4.92	.5203	.0474
135	320	6.93	.4995	.062

figures 2, 3, 4, and 5. The values are given in columns 3 and 5 of tables 3, 4, 5, and 6, respectively.

TABLE 3. *Rate constants for the combustion of char 2 (a new bone char) at a flow rate of 270 ml/min for various percentages of oxygen in nitrogen and at the four temperatures indicated*

The figures in the last column were calculated from equations of the broken lines shown in figure 2

Experiment	Temperature	Oxygen	Weight of sample	k (observed)	k (calculated)
	°C	*Percent*	*g*	1/*hr*	1/*hr*
111	260	1.83	1.9686	0.058	
112	260	4.92	1.9435	.0698	
68	260	11.3	1.1963	.086	
73	260	11.3	1.3264	.089	
110	260	20.56	1.9388	.117	
109	280	1.83	1.9527	.080	
15	280	4.8	0.1835	.101	
18	280	4.8	.6007	.094	
17	280	4.8	.7268	.101	
16	280	4.8	.9716	.104	
107	280	6.93	1.9487	.116	
103	280	6.93	1.9632	.112	
23	280	11.3	0.7339	.145	
69	280	11.3	1.1966	.115	
70	300	11.3	1.0874	.27	0.25
72	300	11.3	1.0961	.25	.25
65	320	1.9	2.4335	.203	.16

It is immediately evident from figure 1 that k exhibits a linear dependence upon the mole fraction of oxygen, regardless of the temperature at which the combustion was carried out. An extrapolation to zero mole fraction yields a positive intercept greater than zero on the k axis. Both the intercept, I_T, and the slope, S_T, increase as the temperature increases. The initial rate of combustion may then be written in the form

$$k = I_T + [O_2]S_T, \tag{3}$$

where $[O_2]$ is the mole fraction of oxygen, I_T and S_T being functions of the temperature and independent of one another.

The numerical values of I_T and S_T may be computed graphically from the data of table 2 and figure 1 corresponding to each of the four temperatures indicated. If, now, ln I_T and ln S_T are each plotted against the reciprocal of the absolute

TABLE 4. *Rate constants for the combustion of char 35 (a service bone char) at a flow rate of 270 ml/min for various percentages of oxygen in nitrogen and at the six temperatures indicated*

The figures in the last column were calculated from equations of the broken lines shown in figure 3

Experiment	Temperature	Oxygen	Weight of sample	k (observed)	k (calculated)
	°C	*Percent*	*g*	1/*hr*	1/*hr*
92	280	1.83	2.4917	0.0136	.....
60	280	1.9	2.4807	.0141	.....
62	280	1.9	2.4861	.0142	.....
89	280	4.92	1.9868	.0192	.....
99	280	4.92	2.0076	.0194	.....
91	280	4.92	2.4996	.0195	.....
88	280	6.93	1.9882	.021	.....
87	280	6.93	2.4773	.018	.....
93	280	6.93	2.5009	.022	.....
97	280	13.29	2.0075	.027	.....
96	280	13.29	2.4752	.027	.....
100	280	19.71	2.0211	.031	.....
98	280	19.71	2.4875	.033	.....
95	280	20.56	1.9865	.036	.....
94	280	20.56	2.4978	.032	.....
59	300	1.9	2.4876	.027	0.030
63	300	1.9	2.4888	.029	.030
54	320	1.9	2.4896	.066	.....
117	320	4.92	1.9889	.095	.....
118	320	6.93	2.0131	.1345	.....
55	340	1.9	2.4946	.16	.16
56	360	1.9	1.3501	.46	.35
64	360	1.9	2.4878	.42	.35
57	380	1.9	1.1457	.88	.88

TABLE 5. *Rate constants for the combustion of char 3 (a service bone char) at a flow rate of 270 ml/min for various percentages of oxygen in nitrogen and at the five temperatures indicated*

The figures in the last column were calculated from equations of the broken lines shown in figure 4

Experiment	Temperature	Oxygen	Weight of sample	k (observed)	k (calculated)
	°C	*Percent*	*g*	1/*hr*	1/*hr*
27	260	4.8	1.4969	0.018	0.015
26	260	4.8	2.4873	.018	.015
121	280	1.83	2.0562	.023	.....
24	280	4.8	1.9994	.035	.....
25	280	4.8	2.9852	.036	.....
119	280	13.29	1.9878	.058	.....
31	300	4.8	.7477	.085	.081
30	300	4.8	1.4948	.069	.081
124	320	1.83	2.0174	.100	.....
33	320	4.8	1.4911	.193	.....
32	320	4.8	2.4848	.194	.....
125	320	6.93	2.0085	.23	.....
34	340	4.8	1.9024	.44	.44

TABLE 6. *Rate constants for the combustion of char 27 (a spent bone char) at a flow rate of 270 ml/min for various percentages of oxygen in nitrogen and at the five temperatures indicated*

The figures in the last column were calculated from equations of the broken lines shown in figure 5

Experiment	Temperature	Oxygen	Weight of sample	k (observed)	k (calculated)
	°C	*Percent*	*g*	1/*hr*	1/*hr*
47	280	1.9	2.4903	0.042	.....
104	280	6.93	1.9973	.071	.....
105	280	13.29	1.9984	.089	.....
106	280	20.56	1.9941	.127	.....
48	300	1.9	2.2428	.089	0.086
49	320	1.9	0.9965	.173	.....
44	320	1.9	2.4934	.157	.....
114	320	6.93	1.9989	.227	.....
108	320	13.29	1.9965	.43	.....
116	320	19.71	1.9898	.44	.....
113	320	20.56	2.0073	.445	.....
42	340	1.9	0.9979	.38	.31
43	340	1.9	1.4948	.34	.31
38	360	1.9	1.0575	.77	.56
39	360	1.9	1.4850	.70	.56

temperature, a linear relationship is obtained in both cases, as is borne out by figure 6.

$$I_T = Ae^{-\frac{E_1}{RT}}, \tag{4}$$

and

$$S_T = Be^{-\frac{E_2}{RT}}, \tag{5}$$

where the constants A, E_1, B, and E_2 may be evaluated from the linear plots of figure 6. Upon substitution of eq 4 and 5 in eq 3, the dependency of k upon temperature as well as oxygen concentration is obtained as given in eq 6:

$$k = Ae^{-\frac{E_1}{RT}} + B[O_2]e^{-\frac{E_2}{RT}}, \tag{6}$$

A test of the experimental validity of eq 6 was next applied to the other carbonaceous adsorbents (i. e., bone chars) studied in this investigation. A similar treatment was made only for those data that show no entries in the last column in tables 3, 4, 5, and 6. This corresponds to the two unbroken lines in each of the figures 2, 3, 4, and 5.[5]

A numerical evaluation of the four parameters of eq 6 was thus obtained for each of the four bone chars, since only two lines are necessary for this

[5] These particular choices were made when three or more points were available for determination of the unbroken lines.

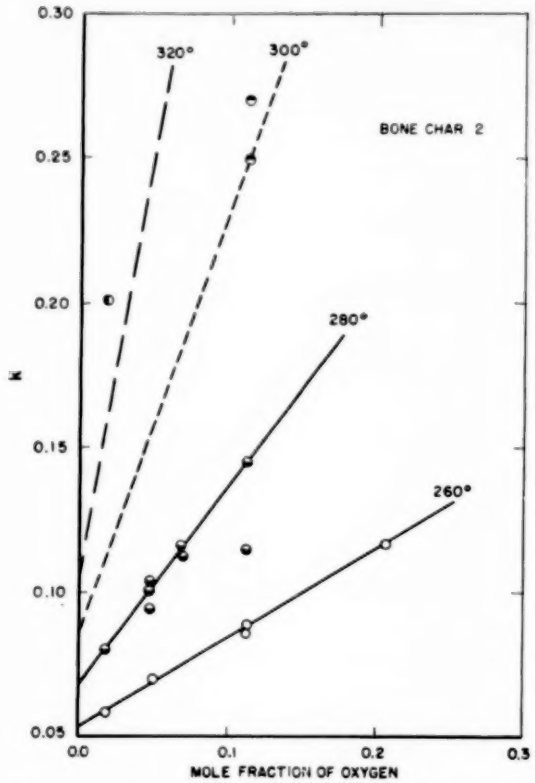

FIGURE 2. *Rate constant k as a function of oxygen concentration for char 2 (a new bone char) at 260°, 280°, 300°, and 320° C and a flow rate of 270 ml/min.*

The broken lines were constructed by using eq 6 with appropriate parameters computed from equations of the continuous lines at 260° and 280° C. (See also table 3.) The continuous lines are drawn through experimental points.

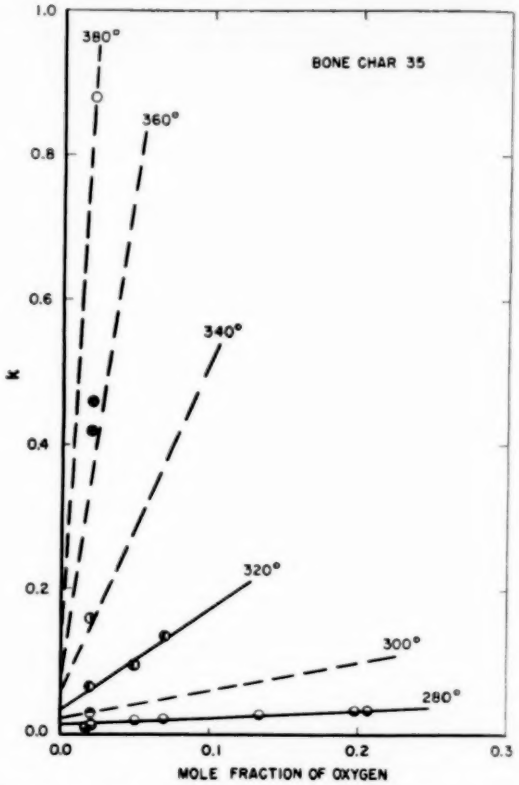

FIGURE 3. *Rate constant k as a function of oxygen concentration for char 35 (a service bone char) at 280°, 300°, 320°, 340°, 360°, and 380° C and a flow rate of 270 ml/min.*

The broken lines were constructed by using eq 6 with appropriate parameters computed from equations of the continuous lines at 280° and 320° C. (See also table 4.) The continuous lines are drawn through experimental points.

type of determination. The broken lines in figures 2, 3, 4, and 5 were then constructed from eq 6 by using values of T at which other measurements had been made. The closeness of fit of these points with the predicted lines so constructed is evidenced from an examination of the figures. A numerical comparison of observed and calculated values of k is available between the last two columns of tables 3, 4, 5, and 6. The numerical values of the parameters A, B, E_1, and E_2 for each of the materials investigated in this paper are given in table 7.

VI. Theoretical Considerations

Any mechanism, in addition to predicting the observed results, must be consistent with accepted thermodynamic concepts. To be of real value the mechanism should predict unknown facts concerning the reaction and thus point the way for further investigations.

One reaction that is known to take place in connection with the combustion of solid carbonaceous adsorbents is the catalytic oxidation of CO to form CO_2. Evidence in support of this may be gained from the data contained in table 1 by

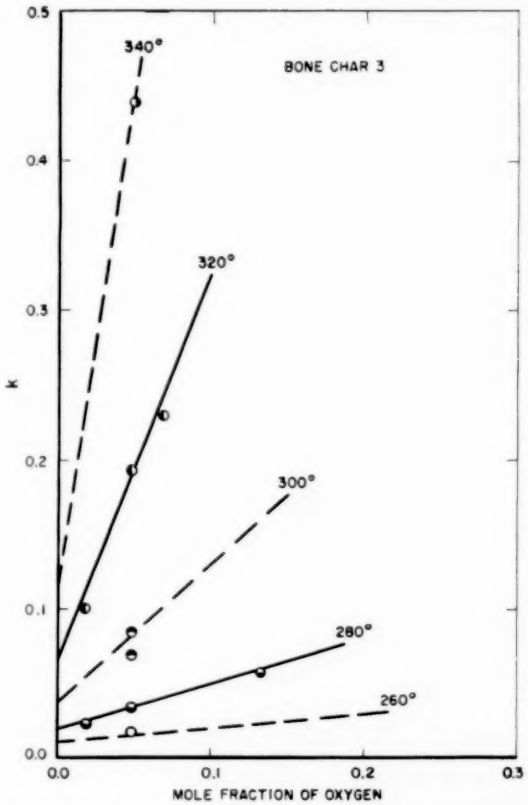

FIGURE 4. *Rate constant k as a function of oxygen concentration for char 3 (a service bone char) at 260°, 280°, 300°, 320°, and 340° C and a flow rate of 270 ml/min.*

The broken lines were constructed by using eq 6 with appropriate parameters computed from equations of the continuous lines at 280° and 320° C. (See also table 5.) The continuous lines are drawn through experimental points.

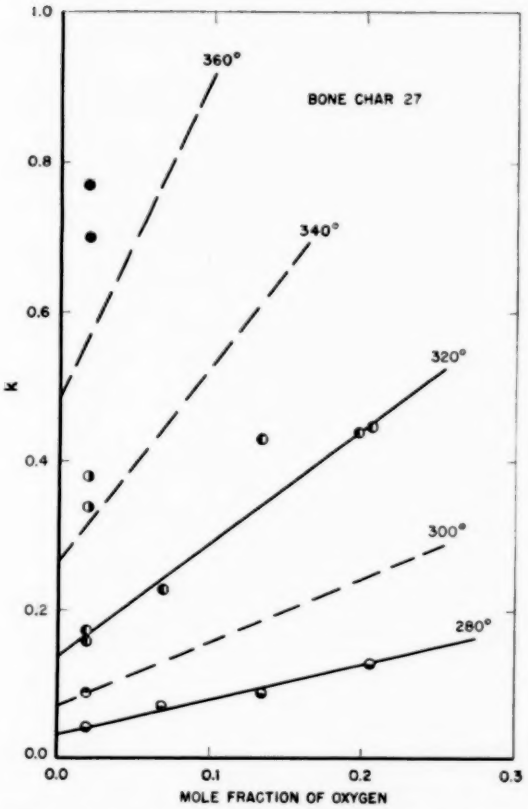

FIGURE 5. *Rate constant k as a function of oxygen concentration for char 27 (a spent bone char) at 280°, 300°, 320°, 340°, and 360° C and a flow rate of 270 ml/min.*

The broken lines were constructed by using eq 6 with appropriate parameters computed from equations of the continuous lines at 280° and 320° C. (See also table 6.) The continuous lines are drawn through experimental points.

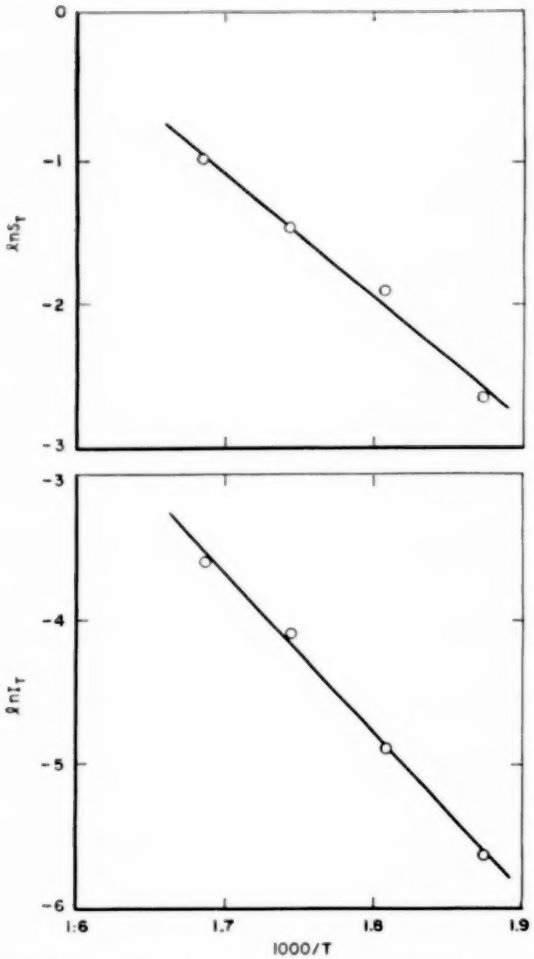

FIGURE 6. *Logarithms of the slopes and intercepts, respectively, of the lines in figure 1 for char 1 (a coconut-shell charcoal) expressed as a function of the reciprocal absolute temperatures.*

TABLE 7. *Calculated values for the parameters of the relationship (eq 6), which expresses the rate constant as a function of oxygen concentration and temperature*

	E_1	E_2	A	B
Char 1 (coconut-shell charcoal)	*cal* 21,880	*cal* 16,900	*1/hr* 2.93×10^6	*1/hr* 6.09×10^5
Char 2 (new bone char)	7,000	23,500	4.10×10^1	1.25×10^9
Char 35 (service bone char)	16,200	43,200	3.45×10^3	1.09×10^{18}
Char 3 (service bone char)	19,700	34,800	1.16×10^5	1.63×10^{13}
Char 27 (spent bone char)	23,300	19,200	5.37×10^7	1.70×10^7

considering the change in the ratio of CO_2 to CO with time of contact of the gases with the sample. The catalytic oxidation is not concerned with the consumption of carbon from the solid state; hence, the variation in the CO_2 to CO ratio can not be expected to have any effect upon k. This point was also brought out earlier in the paper. The catalytic reaction may thus be eliminated in connection with the initial steps involved in the combustion process.

Of the many mechanisms that have been proposed in the past for the low temperature combustion of carbon, only a few are consistent with the experimental findings of this paper. Equation 6 contains two terms, both of which increase exponentially with the reciprocal of the absolute temperature; but only one depends upon oxygen concentration. This requires that two processes must be taking place independently. Furthermore, some, if not all, of the primary product must be CO, since CO is one of the products. A recent article by Strickland-Constable [25] reviewed the various mechanisms that have been proposed for the combustion of carbon at temperatures above and below 1,000° C. One mechanism contained in that paper applicable in the range of 400° C could easily be expanded to fit the experimental findings of this present investigation. It states: "Since the (surface oxygen) complex appears to be neither an intermediate product, nor reversibly adsorbed product, a remaining possibility is to consider it to be a by-product of the main reaction, which is only formed at certain favourable points on the surface. When once formed, the complex remains on the surface as a relatively stable body that is decomposed to the product only on raising the temperature." Insofar as the rest of the surface is concerned, the reaction could be first order with respect to oxygen. The decomposition of the stable complex need not be caused solely by raising the temperature. It could depend upon the acquisition of sufficient energy to decompose it at the reaction temperature and, hence, could very well be independent of oxygen concentration.

Another possibility is that the entire surface is covered with a single type of complex. This could then decompose to products in two ways, both taking place simultaneously. In the first way, the decomposition would be spontaneous depending upon the absorption of sufficient energy to decompose the complex at the reaction temperature

and thus be independent of the oxygen concentration. In the second way, the complex would combine with additional oxygen before decomposing to products such that this step would be proportional to the oxygen concentration.

A third possibility is that two distinct surface complexes are formed independently of one another. In the one case, the rate of decomposition of the complex (assumed to be much slower than its rate of formation) would be rate determining and, thus, be independent of oxygen concentration. In the other case, the rate of formation of the complex would be the slower and, hence, could very likely be proportional to oxygen concentration.

In any of the above processes the total reaction rate would, of necessity, be given by the sum of the two individual steps and lead to an expression of the form of eq 6. Whether one, if any, of these mechanisms is to be preferred depends upon additional experimental work beyond the scope of this paper. The existence of one, or more than one, species of complex taking part in the combustion process is a problem that might be answered from X-Ray diffraction measurements.

Surface-area studies may not be expected to throw any light on the extent of complex covering the surface. On the other hand, heats of adsorption of nitrogen for surfaces covered with complex as compared with surfaces partially denuded of complex might afford a means of estimating the extent of complex coverage.

A positive intercept on the k axis has been treated as though a finite initial reaction rate existed as the oxygen concentration approached zero. This may or may not be so. If, as shown in figures 1 through 5, the extrapolation below the lowest measured value of 0.02 is valid, it would imply the prior presence of chemisorbed oxygen. On the other hand, if the linear relationship breaks sharply as zero oxygen concentration is approached such that the reaction rate also goes to zero, this would imply an initial induction period. Such an initial process could be interpreted as the rapid formation of a chemisorbed oxygen layer. Further experimental work at very low oxygen concentration is required under conditions where the amount of chemisorbed oxygen were known and could be altered deliberately.

A possible reaction that has not been considered elsewhere in this paper is the reduction of carbon by CO_2 and its converse, the autooxidation of CO. At 360° C the equilibrium constant for the CO_2 reduction of graphitic carbon is of the order of magnitude of 10^{-6} [24]. No similar figure is available for the carbonaceous residues such as exist in carbon adsorbents. One may assume that it is about the same magnitude, since no measurable loss of carbon in bone char by reaction with pure CO_2 was observed in independent experiments until temperatures in excess of around 600° C were used. The converse reaction would cause the formation of carbon brought about by the simultaneous oxidation and reduction of CO. No evidence exists as to whether this reaction takes place to any measurable degree under the conditions of this investigation. This point could be established, however, by treating carbon adsorbents with CO and testing for the presence of CO_2 in the products. Radioactive tracer technique might also be employed to advantage in determining whether carbon is deposited.

VII. Summary

1. A study was made of the rate of combustion with respect to carbon of carbon adsorbents below 400° C as a function of oxygen concentration and temperature.

2. Experimental results confirm the beliefs of earlier investigators that some of the carbon monoxide formed is oxidized catalytically to carbon dioxide as a secondary process. The extent of this secondary conversion is inversely proportional to the velocity of flow, other factors remaining constant.

3. The initial combustion rate at constant temperature depended linearly upon oxygen concentration.

4. The temperature dependence of initial combustion rate at constant oxygen concentration was expressed as the sum of two Arrhenius-type terms.

5. By combining the influence of oxygen concentration with that of temperature, a single relationship was obtained in terms of the initial reaction rate.

6. Activation energies (or free energies) of the Arrhenius-type terms were evaluated for the combustion of each of the five carbon adsorbents investigated.

7. Possible reaction mechanisms consistent with the experimental results were postulated.

VIII. References

[1] R. A. Smith, Phil. Mag. [4] **26,** 311 (1863); Proc. Roy. Soc. (London) **12,** 424 (1863).
[2] C. J. Baker, J. Chem. Soc. **51,** 249 (1887).
[3] T. F. E. Rhead and R. V. Wheeler, J. Chem. Soc. **101,** 846 (1912); **103,** 461 (1913).
[4] Stuart McLean, Trans. Roy. Soc. Canada **15,** 73 (1921).
[5] W. E. Garner and E. A. Blench, J. Chem. Soc. **125,** 1288 (1924).
[6] F. G. Keyes and M. J. Marshall, J. Am. Chem. Soc. **49,** 156 (1927).
[7] I. M. Kolthoff, J. Am. Chem. Soc. **54,** 4473 (1932).
[8] A. Klemenc, R. Wechsberg, and G. Wagner, Z. physik. Chem. **A170,** 97 (1934).
[9] R. T. Haslam, Proc. Inst. Fuel Tech. **1927,** 8.
[10] M. S. Shah, J. Chem. Soc. **1929,** 2661.
[11] Y. Oshima, Y. Fukuda, and S. Takashima, J. Soc. Chem. Ind. Japan **36,** 148 (1933).
[12] Z. F. Chukhanov and N. A. Karzhavina, J. Tech. Phys. (USSR) **9,** 1932 (1939); Fuel **20,** 44, 73 (1941).
[13] R. F. Strickland-Constable, Trans. Faraday Soc. **34,** 1074 (1938).
[14] Ts. M. Klibanova and D. A. Frank-Kamenetskii, Acta Physiocochim (USSR) **18,** 387 (1943).
[15] Lothar Meyer, Trans. Faraday Soc. **34,** 1056 (1938).
[16] M. A. Mayers, Chem. Rev. **14,** 31 (1934).
[17] Lothar Meyer, Z. physik Chem. **B17,** 385 (1932).
[18] J. D. Lambert, Trans. Faraday Soc. **32,** 1584 (1936).
[19] O. A. Tsukhanova, J. Tech. Phys. (USSR) **9,** 295 (1939).
[20] V. R. Deitz, Preliminary survey of bone char revivification and filtration, Chap. II, 132 (1947). (Available from Publications Section, National Bureau of Standards, Washington 25, D. C.)
[21] G. W. Bridger, Nature **158,** 236 (1946).
[22] W. V. Loebenstein, L. F. Gleysteen, and V. R. Deitz, J. Research NBS **42,** 33 (1949) RP1948.
[23] C. N. Hinshelwood, The kinetics of chemical change, p. 198 (Reprinted from the 1st edition 1942, 1945; Oxford Univ. Press).
[24] D. D. Wagman, J. E. Kilpatrick, W. J. Taylor, S. Pitzer, and F. D. Rossini, J. Research NBS **34,** 143 (1945) RP1634.
[25] R. F. Strickland-Constable, Chem. & Ind. **49,** 771 (1948).

WASHINGTON, March 18, 1949.